

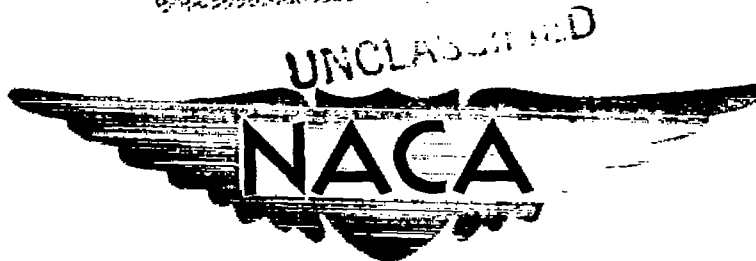
JAN 24 1958

CONFIDENTIAL

RM A57H19

C.1

NACA RM A57H19



UNCLASSIFIED

# RESEARCH MEMORANDUM

EFFECTS OF A LEADING-EDGE SLAT AND A TRAILING-EDGE SPLIT FLAP ON THE AERODYNAMIC CHARACTERISTICS OF A WING-FUSELAGE COMBINATION HAVING A NEARLY TRIANGULAR WING OF ASPECT RATIO 2.9 AT MACH NUMBERS FROM 0.60 TO 0.92

By Fred A. Demele ✓

Ames Aeronautical Laboratory  
Moffett Field, Calif.

**LIBRARY COPY**

JAN 27 1958

CLASSIFICATION CHANGED

UNCLASSIFIED

LANGLEY AERONAUTICAL LABORATORY  
LIBRARY, NACA  
LANGLEY FIELD, VIRGINIA

To \_\_\_\_\_

By authority of TPA #39 CLASSIFIED DOCUMENT DATE Jan 17, 1941

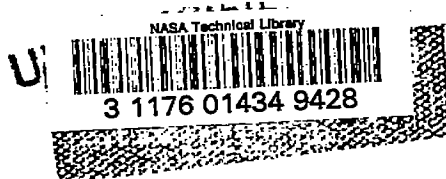
This material contains information affecting the National Defense of the United States within the meaning of the espionage laws, Title 18, U.S.C., Secs. 793 and 794, the transmission or revelation of which in any manner to an unauthorized person is prohibited by law.

## NATIONAL ADVISORY COMMITTEE FOR AERONAUTICS

WASHINGTON  
January 24, 1958

CONFIDENTIAL

UNCLASSIFIED



## NATIONAL ADVISORY COMMITTEE FOR AERONAUTICS

RESEARCH MEMORANDUM

EFFECTS OF A LEADING-EDGE SLAT AND A TRAILING-EDGE SPLIT FLAP  
ON THE AERODYNAMIC CHARACTERISTICS OF A WING-FUSELAGE  
COMBINATION HAVING A NEARLY TRIANGULAR WING OF  
ASPECT RATIO 2.9 AT MACH NUMBERS FROM  
0.60 TO 0.92

By Fred A. Demele

## SUMMARY

An investigation has been made to determine the effectiveness of a leading-edge slat and a trailing-edge split flap in improving the high subsonic speed aerodynamic characteristics of a model representing the wing-fuselage portion of an airplane having a nearly triangular wing. The wing had an aspect ratio of 2.9, a leading-edge sweepback of  $41.1^\circ$ , and a rounded tip.

Slat angles of  $0^\circ$ ,  $5^\circ$ ,  $10^\circ$ ,  $15^\circ$ , and  $20^\circ$  and flap angles of  $0^\circ$ ,  $2.5^\circ$ ,  $5^\circ$ ,  $7.5^\circ$ , and  $10^\circ$  were tested throughout a Mach number range from 0.60 to 0.92 and at a Reynolds number of approximately  $3.5 \times 10^6$ .

Deflection of the slat resulted in increased lift at high angles of attack throughout the Mach number range. The slat was effective in promoting substantial increases in lift-drag ratio at high lift coefficients, although reductions in maximum lift-drag ratio occurred with all slat angles. It was also generally found that extension of the slat resulted in more nearly linear pitching-moment curves and in shifting of the region of abrupt stability change to higher lift coefficients.

Deflection of the split flap resulted in large negative moment shifts, but generally caused no adverse effects on static longitudinal stability. Although slight improvement in maximum lift-drag ratio was indicated at the highest Mach numbers, the primary result of deflecting the flap was an increase in lift-drag ratio at high lift coefficients.

A large, rectangular stamp with a textured, grainy appearance. The word "UNCLASSIFIED" is printed in a bold, sans-serif font across the bottom of the stamp.

UNCLASSIFIED

## INTRODUCTION

Devices such as leading-edge slats and trailing-edge flaps have been used quite extensively to promote favorable high-lift characteristics during take-off and landing for many types of airplanes. It has also been found that such devices can be used to improve the high-speed characteristics of airplanes. For example, it was shown in reference 1 that the use of slats on a  $45^\circ$  sweptback wing-fuselage combination generally reduced the severity of the unstable pitching-moment break and extended the lift coefficient at which it occurred to higher values, and increased the lift-drag ratio at high lift coefficients in the high subsonic speed regime.

The present investigation was undertaken to determine the effectiveness of a leading-edge slat and a trailing-edge split flap in improving the aerodynamic characteristics at high subsonic speeds of a model of an airplane having a nearly triangular wing. Of primary concern was the reduction of drag at high lift coefficients in order to improve the maneuverability of the airplane at high subsonic speeds. The wing had an aspect ratio of 2.9,  $41.1^\circ$  sweepback of the leading edge, and the tip was rounded in plan form. The tests were conducted in the Ames 12-foot pressure wind tunnel at Mach numbers up to 0.92 and, for the most part, at a Reynolds number of about  $3.5 \times 10^6$ .

## NOTATION

A	aspect ratio
$\bar{c}$	wing mean aerodynamic chord
$C_D$	drag coefficient, $\frac{\text{drag}}{qS}$
$C_L$	lift coefficient, $\frac{\text{lift}}{qS}$
$C_m$	pitching-moment coefficient, $\frac{\text{pitching moment}}{qS\bar{c}}$ , referred to quarter point of the mean aerodynamic chord
D	drag
L	lift
M	free-stream Mach number
q	free-stream dynamic pressure
R	Reynolds number, based on the wing mean aerodynamic chord

- S area of the semispan wing
- $\alpha$  angle of attack, measured with respect to the wing chord at the plane of symmetry
- $\delta_f$  flap deflection angle (see fig. 1(b))
- $\delta_s$  slat deflection angle (see fig. 1(b))

#### Subscripts

- max maximum
- o zero lift

#### MODEL

The investigation was made with a wing-fuselage combination which represented the left half of an airplane. The steel wing had  $41.1^\circ$  sweep-back of the leading edge, an aspect ratio of 2.9, and an effective taper ratio of 0.23. The thickness form was essentially the NACA 0008 at the root and the NACA 0005 at the tip; the camber was approximately half that of an NACA 230 mean line. Geometry of the model is given in figure 1 and in table I, coordinates of the root and tip sections are given in table II, and photographs of the model are shown as figure 2.

The wing was equipped with a leading-edge slat, a split flap of constant chord, and an aileron which was sealed along its leading edge. In addition, a fairing which represented the wheel fairing was affixed to the lower surface of the wing at 25 percent of the wing semispan and extended from the leading edge to the trailing edge (see fig. 2(c)). The slat was mounted on continuous-arc support brackets and could be set at any angle up to  $24^\circ$  (see fig. 1(b)). The area of the slat was about 7-1/2 percent that of the wing, and the flap area was approximately 10 percent that of the wing.

The wood fuselage contained an inlet duct through which air flowed at an estimated mass-flow ratio of 0.85 at a free-stream Mach number of 0.80.

The model was mounted on a turntable in the tunnel floor, and the aerodynamic forces and moments were transmitted directly to the force-measuring apparatus.

## TESTS

The major portion of the investigation was conducted over a Mach number range from 0.60 to 0.92 at a Reynolds number of about  $3.5 \times 10^6$ ; however, a few tests were made at approximately double this Reynolds number at a Mach number of 0.60. Longitudinal force and moment data were obtained for slat deflection angles of  $0^\circ$ ,  $5^\circ$ ,  $10^\circ$ ,  $15^\circ$ , and  $20^\circ$  with the split flap in the undeflected position, and for split-flap deflection angles of  $5^\circ$  and  $10^\circ$  with the slat in the retracted position. Data were also obtained with the slat extended  $10^\circ$  and the flap deflected  $2.5^\circ$ ,  $5^\circ$ ,  $7.5^\circ$ , and  $10^\circ$ . The maximum angle of attack of the investigation was  $30^\circ$ ; however, because of tunnel power limitations, the maximum attainable angle at high Mach numbers was about  $12^\circ$ .

Static pressures were measured at the tunnel wall in the region of the model to determine the test conditions for which the data may have been affected by local choking.

## CORRECTIONS

The data have been corrected for tunnel-wall interference associated with lift on the wing, for blockage due to the presence of the tunnel walls, for buoyancy effects due to a streamwise static-pressure gradient, and for longitudinal force tares of the turntable on which the model was mounted.

The method of reference 2 was used to evaluate the magnitude of the wall interference effects. The resulting corrections which were added to the angles and coefficients are as follows:

$$\Delta\alpha = 0.659 C_L$$

$$\Delta C_D = 0.0088 C_L^2$$

$$\Delta C_m = 0.0032 C_L$$

Corrections to the data to take account of the effects of constriction due to the tunnel walls were determined by the method of reference 3. The magnitudes of the corrections to Mach number and dynamic pressure are shown in the following table:

$M_{\text{corrected}}$	$M_{\text{uncorrected}}$	$\frac{q_{\text{corrected}}}{q_{\text{uncorrected}}}$
0.60	0.596	1.009
.80	.789	1.018
.85	.834	1.022
.88	.859	1.026
.90	.875	1.030
.92	.890	1.035

A buoyancy correction was applied to the drag to take account of the drag force on the model resulting from the tunnel streamwise static pressure gradient. The value of this drag coefficient correction varied approximately linearly from 0.0013 at a Mach number of 0.92 to 0.0003 at a Mach number of 0.80; at a Mach number of 0.60 there was no correction.

The corrections associated with drag tare force due to aerodynamic forces on the exposed surface of the turntable are given in the following table. No attempt has been made to evaluate possible drag forces due to interference between the model and turntable.

$M$	$C_{D_{\text{tare}}}$
0.60	0.0025
.80	.0028
.85	.0029
.88	.0030
.90	.0032
.92	.0033

## RESULTS AND DISCUSSION

The results of the tests are presented in figures 3 through 20. The basic longitudinal characteristics of the model with the slat and flap both in the open and closed positions, are presented in figures 3 through 12. Figures 13 through 16 show the effect of Mach number on the lift, pitching-moment, drag due to lift, and lift-drag characteristics of the model with the slat in various positions. The effects of Mach number on the lift, pitching-moment, and lift-drag characteristics of the model with the split flap in various positions are shown in figures 17 through 20. It should be noted that the model with the slat and the flap in the retracted positions is referred to hereinafter as the basic configuration.

Measurements of static pressures at the tunnel wall in the region of the model were made to define the conditions at which local sonic velocities occurred at the tunnel wall, indicating partial choking of the wind tunnel. The extent to which the data are affected by this phenomenon is

not known quantitatively, although on the basis of continuity in the data it is assumed to be small. The following table indicates the angles of attack at which partial choking first occurred:

<u>M</u>	<u><math>\alpha</math>, deg</u>
0.88	14
.90	10
.92	6

Data obtained at these Mach numbers during conditions of partial choking are represented in the figures by flagged symbols.

#### Effects of Reynolds Number

The effects at a Mach number of 0.60 of increasing Reynolds number from  $3.5 \times 10^6$  to about  $8 \times 10^6$  on the aerodynamic characteristics of the model both with the slat retracted and with the slat extended  $10^\circ$  are shown in figure 3. The data indicate that this change in Reynolds number resulted in only small changes in the lift and pitching-moment characteristics. The effect of increasing Reynolds number on drag was evidenced primarily as a reduction in minimum drag coefficient, although for the basic configuration there were further drag reductions at high lift conditions.

#### Effects of Slats

Lift characteristics.- Comparison of the data in figure 4 indicates that up to a Mach number of 0.85, increasing the slat angle apparently increased the angle of attack at which flow separation occurred on the wing and resulted in increased lift at high angles of attack. The improvement in lift prevailed throughout the Mach number range, as indicated by the variation of lift with Mach number at an angle of attack of  $12^\circ$  as shown in figure 13. It can also be seen from figures 4 and 13 that deflecting the slat increased the average lift curve slope (measured between  $0^\circ$  and  $4^\circ$ ) slightly up to a Mach number of 0.84, whereas above 0.84 there was a reduction in slope due to deflecting the slat.

Pitching-moment characteristics.- The data of figure 4 show that for Mach numbers less than 0.90, deflection of the slat resulted in more nearly linear pitching-moment curves and shifted the region of abrupt moment change to higher lift coefficients. These effects are also present at Mach numbers of 0.90 and 0.92 for small deflection angles; however, at slat angles greater than about  $10^\circ$ , a sudden reduction in stability occurred between lift coefficients of about 0.2 and 0.3. At Mach numbers

less than 0.90, a slat deflection of  $20^\circ$  resulted in an increase of about 0.25 in the lift coefficient at which abrupt stability changes occur (fig. 4).

At Mach numbers less than 0.90 and at lift coefficients less than about 0.5 or 0.6, deflection of the slat caused a rearward movement of center of pressure and a reduction in the static longitudinal stability (see figs. 4 and 14).

Drag characteristics.- As shown by the lift and pitching-moment results, deflection of the slat resulted in improvements in the flow conditions over the wing at high angles of attack. This improvement is reflected in substantial drag reductions due to slat deflection. As noted from figure 5, above a lift coefficient of about 0.6, all of the slat angles resulted in lower drag than that for the basic configuration throughout the Mach number range.

A further indication of the effectiveness of the slat in providing drag reductions is shown in figure 15, wherein the drag parameter,  $C_D - (C_{D_0})_{\delta_S = 0}$  (drag coefficient minus the zero-lift drag coefficient for the basic configuration), is presented as a function of the square of lift coefficient for Mach numbers of 0.60 and 0.80. Also included in the figure is the theoretical induced drag for a wing of the same aspect ratio and having an elliptic load distribution. If the assumption is made that the rapid rate of drag rise is indicative of flow separation, it is seen that deflecting the slat to  $20^\circ$  resulted in a delay in separation to a lift coefficient about 65 percent higher than that for the basic configuration at a Mach number of 0.60. Since, at a Mach number of 0.80, the drag departed rather rapidly from the ideal curve even at low lift coefficients, the slat effectiveness is better measured by drag comparisons at constant lift coefficient. Thus it is seen that at a lift coefficient of 0.6, a 30-percent reduction in  $C_D - (C_{D_0})_{\delta_S = 0}$  accompanied a slat deflection of  $10^\circ$ , which was the most effective angle at this particular lift coefficient.

Lift-drag ratio.- The curves of lift-drag ratio presented in figure 6 further illustrate the aerodynamic gains that are possible through the use of a slat. In all cases the improvements in lift-drag ratio resulting from slat deflection occurred beyond the lift coefficients for which the lift-drag ratios were maximum. Although the data are for an untrimmed condition, it is likely that these improvements will prevail for the trimmed condition since the pitching-moment shifts due to slat deflection are small and, in fact, positive compared to the basic configuration at high lift coefficients.



The variation of maximum lift-drag ratio with Mach number is seen in figure 16 to be similar for all slat angles, there being a reduction in maximum lift-drag ratio with increasing Mach number and with increasing slat deflection. At a lift coefficient of 0.6, the lift-drag ratio was improved by slat deflection although the increase diminished somewhat at the highest Mach numbers. At still higher lift coefficients, for example, 0.8, the improvements due to slat deflection were largest at a Mach number of 0.60 and disappeared at a Mach number of 0.92. Examination of these data reveals that maximum benefits in the high-lift regime were achieved through the use of the slat deflected  $10^\circ$ .

### Effects of Flaps

Lift and pitching-moment characteristics.- The effects of deflection of the split flap on the lift and pitching moment of the model are shown in figure 7 for the condition of slat retracted and in figure 10 for the slat extended  $10^\circ$ . The lift effectiveness of the flap at low lift coefficients was essentially constant throughout the range of Mach numbers investigated and generally increased with increasing angle of attack for Mach numbers greater than 0.60. As seen in figure 17 for the condition of slat retracted and in figure 18 for the condition of slat extended  $10^\circ$ , the effect of Mach number on the average lift-curve slope of the model was similar for all flap deflections, there being an increase in slope with increasing Mach number which was slightly greater for the higher flap deflections.

Examination of the pitching-moment curves (figs. 7 and 10) reveals a large negative moment shift associated with deflection of the flap. However, as noted in figures 17 and 18, there were only small changes in pitching-moment curve slope due to flap deflection throughout most of the Mach number range, the exception being at a Mach number of 0.90 where a flap deflection of  $10^\circ$  caused a 10-percent increase in stability at a lift coefficient of 0.5 for the model with the slat retracted (fig. 17).

Drag characteristics.- Deflection of the split flap with the slat retracted (fig. 9) and with the slat extended  $10^\circ$  (fig. 12) resulted in substantial increases in lift-drag ratio, particularly at the higher lift coefficients. As shown in figures 19 and 20, a decrease in maximum lift-drag ratio generally resulted from deflection of the split flap. However, slight improvements in maximum lift-drag ratio were evidenced at the higher Mach numbers and particularly for the condition of slat extended  $10^\circ$ .

In assessing the improvements afforded by these devices, it must be recognized that the measured lift-drag ratios are for an untrimmed condition. The split flap produces large negative pitching moments that must be balanced by the airplane longitudinal control. Estimates of the

effects of balancing the airplane, wherein it was assumed that the tail effectiveness is not reduced by flap deflection, have indicated that the improvements in lift-drag ratio due to flap deflection are approximately the same for both the trimmed and untrimmed conditions.

#### CONCLUSIONS

The effects of a leading-edge slat and of a trailing-edge split flap on the aerodynamic characteristics of a model representing the wing-fuselage portion of an airplane having a nearly triangular wing of aspect ratio 2.9 and a sweepback of  $41.1^\circ$  were investigated at Mach numbers from 0.60 to 0.92. It was found that deflection of the slat resulted in increased lift at high angles of attack throughout the Mach number range. The slat was effective in promoting substantial increases in lift-drag ratio at high lift coefficients, although reductions in maximum lift-drag ratio occurred with all slat angles. The data indicated that on the basis of over-all gains in lift-drag ratio a slat angle of  $10^\circ$  was nearly optimum. In general, deflection of the slat also resulted in more nearly linear pitching-moment curves and in shifting the region of abrupt stability change to higher lift coefficients.

Deflecting the split flap generally promoted no adverse effects on static longitudinal stability, but resulted in large negative moment shifts. Although slight increases in maximum lift-drag ratio were indicated at the highest Mach numbers, the primary effect of deflecting the flap was an increase in lift-drag ratio at high lift coefficients.

Ames Aeronautical Laboratory  
National Advisory Committee for Aeronautics  
Moffett Field, Calif., Aug. 19, 1957

#### REFERENCES

1. Runkel, Jack F., and Steinberg, Seymour: Effects of Leading-Edge Slats on the Aerodynamic Characteristics of a  $45^\circ$  Sweptback Wing-Fuselage Configuration at Mach Numbers of 0.4 to 1.03. NACA RM L53F23, 1953.
2. Sivells, James C., and Salmi, Rachel M.: Jet-Boundary Corrections for Complete and Semispan Swept Wings in Closed Circular Wind Tunnels. NACA TN 2454, 1951.
3. Herriot, John G.: Blockage Corrections for Three-Dimensional-Flow Closed-Throat Wind Tunnels, With Consideration of the Effect of Compressibility. NACA Rep. 995, 1950. (Supersedes NACA RM A7B28)

~~CONFIDENTIAL~~

TABLE I.- GEOMETRIC PROPERTIES OF THE MODEL

Wing	
Aspect ratio . . . . .	2.91
Taper ratio . . . . .	0.226
Sweepback (leading edge), deg . . . . .	41.1
Twist . . . . .	0
Dihedral (trailing edge), deg . . . . .	2.67
Incidence at root chord . . . . .	0
Airfoil section (parallel to plane of symmetry)	
Root . . . . .	NACA 0008 (mod)
Tip . . . . .	NACA 0005 (mod)
Area (semispan model), sq ft . . . . .	6.292
Mean aerodynamic chord, ft . . . . .	2.376
Semispan, ft . . . . .	3.025
Wing leading-edge slat	
Area, sq ft . . . . .	0.469
Span (perpendicular to plane of symmetry), ft . . . . .	1.651
Wing trailing-edge flap	
Type . . . . .	Split
Chord, ft . . . . .	0.458
Average span (perpendicular to plane of symmetry), ft . . . . .	1.332

TABLE II.- WING COORDINATES

[Stations and ordinates given in percent of airfoil chord.]

Root, NACA 0008 (mod)			
Upper Surface		Lower Surface	
Station	Ordinate	Station	Ordinate
0	0	0	0
1.07	1.50	1.43	-1.14
2.29	2.19	2.71	-1.53
4.79	3.15	5.21	-2.00
7.34	3.80	7.66	-2.31
9.90	4.25	10.10	-2.54
15.00	4.72	15.00	-2.88
20.04	4.85	19.96	-3.08
25.04	4.83	24.96	-3.17
30.04	4.75	29.96	-3.20
40.04	4.46	39.96	-3.13
50.04	4.01	49.96	-2.90
60.03	3.41	59.97	-2.53
70.03	2.70	69.97	-2.04
80.02	1.89	79.98	-1.45
90.01	.99	89.99	-.77
95.00	.52	95.00	-.41
100.00	0	100.00	0

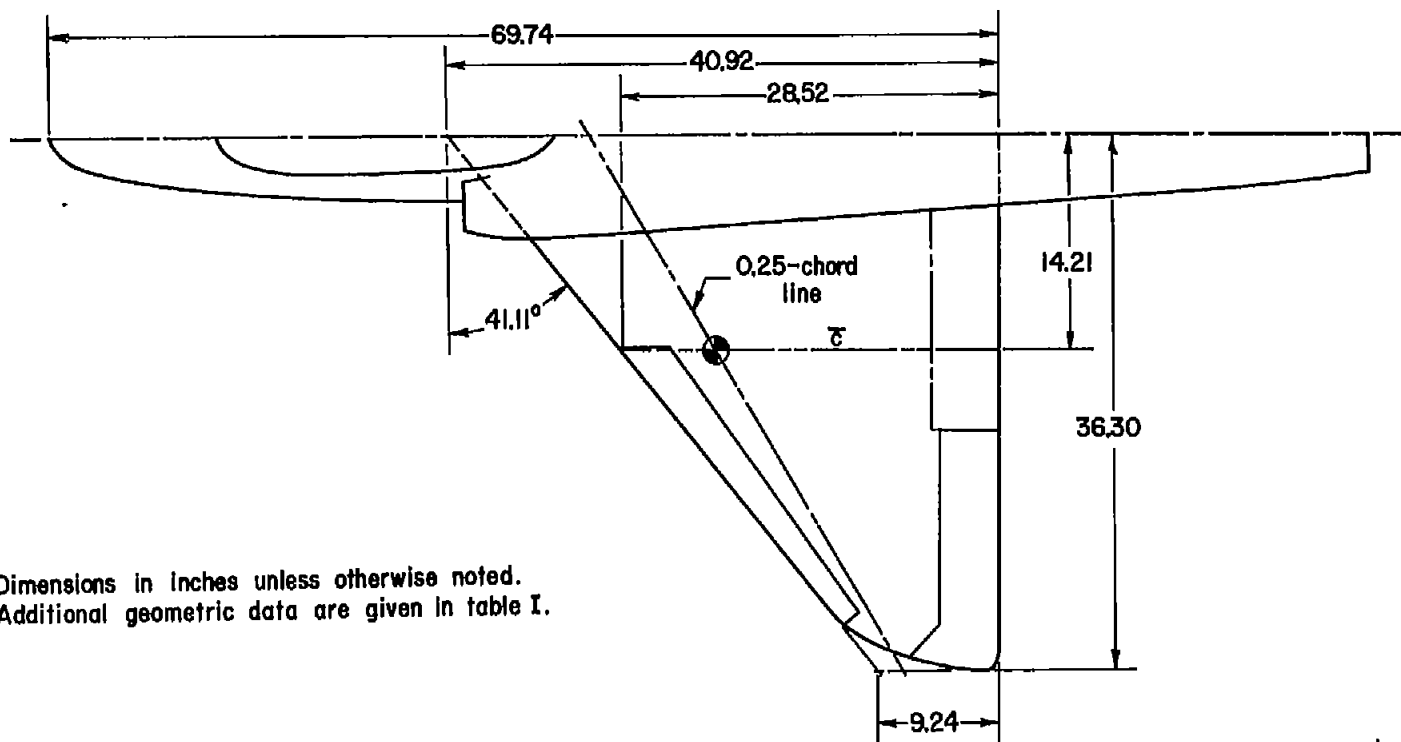
Leading edge radius: 0.704

Tip, NACA 0005 (mod)			
Upper Surface		Lower Surface	
Station	Ordinate	Station	Ordinate
0	0	0	0
1.16	.83	1.34	-.47
2.40	1.22	2.60	-.55
4.90	1.77	5.10	-.61
7.43	2.15	7.58	-.65
9.95	2.41	10.05	-.71
15.00	2.73	15.00	-.90
20.02	2.89	19.98	-1.12
25.02	2.98	24.98	-1.33
30.03	3.05	29.98	-1.50
40.03	3.10	39.97	-1.78
50.03	3.05	49.98	-1.95
60.03	2.86	59.98	-1.98
70.03	2.47	69.98	-1.81
80.02	1.85	79.98	-1.41
90.01	1.04	89.99	-.82
95.01	.59	94.99	-.48
100.00	0	100.00	0

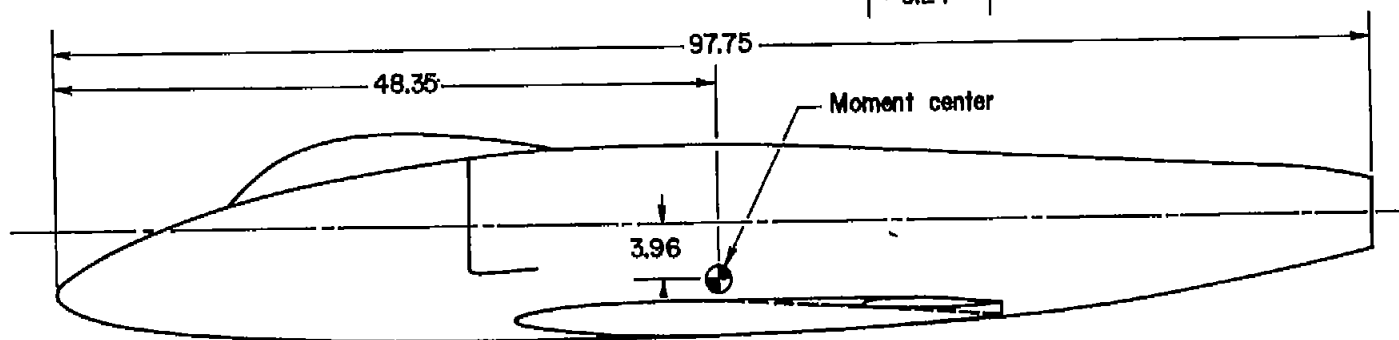
Leading edge radius: 0.207

~~CONFIDENTIAL~~

~~CONFIDENTIAL~~



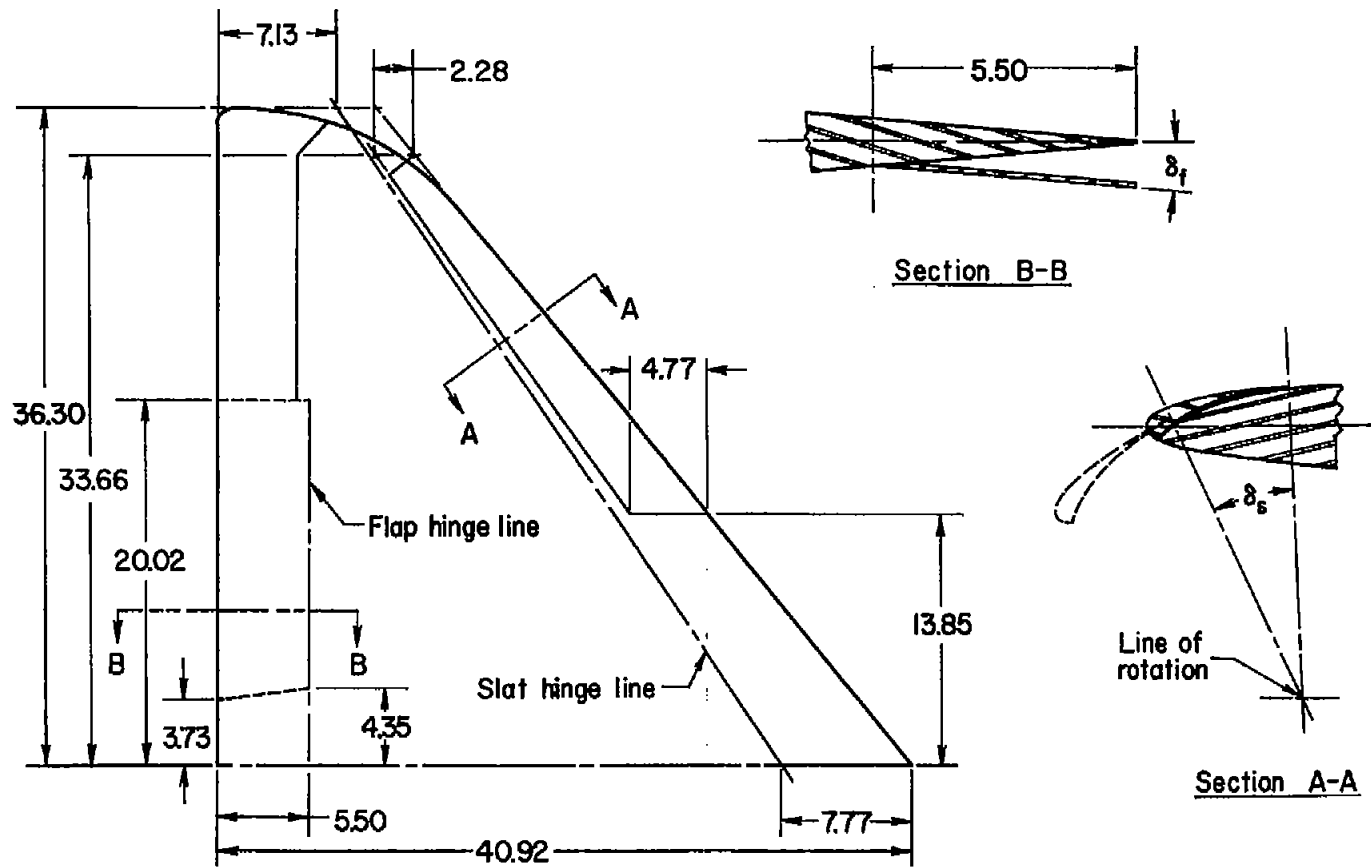
Dimensions in inches unless otherwise noted.  
Additional geometric data are given in table I.



(a) Dimensions.

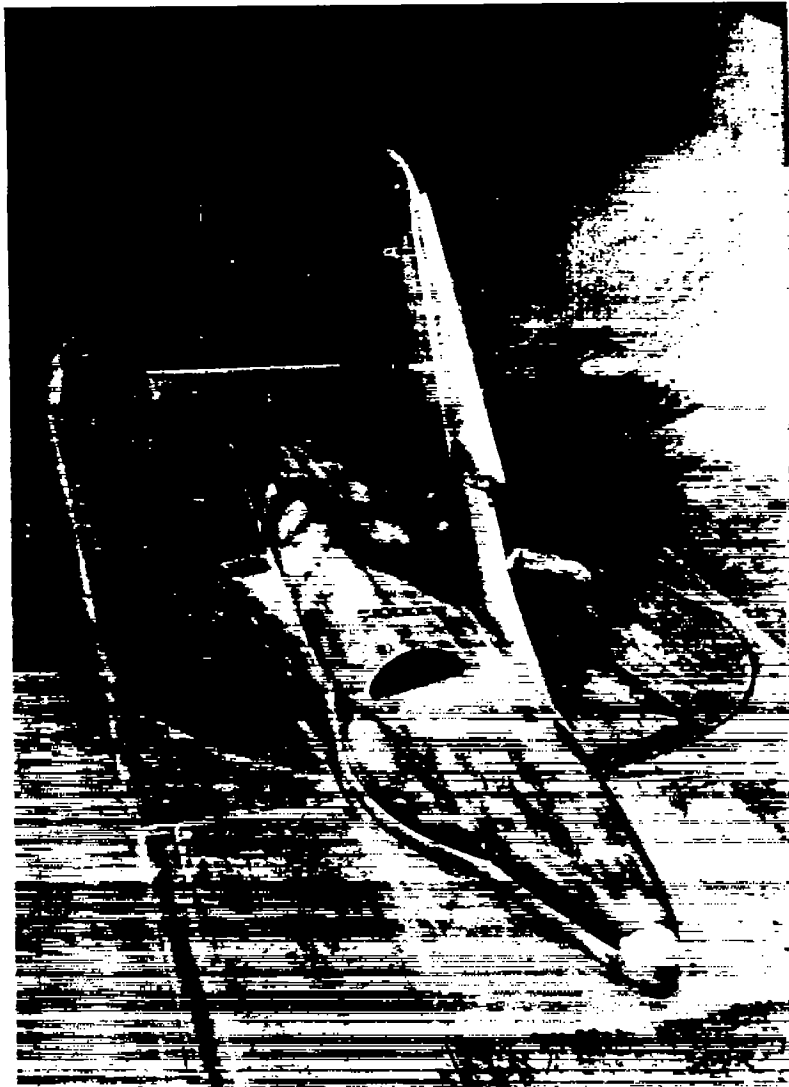
Figure 1.- Geometric characteristics of the model.

Dimensions in inches unless otherwise noted.



(b) Flap and slat details.

Figure 1.- Concluded.



(a) Three-quarter front view.

A-22221

Figure 2.- Photographs of the model mounted in the wind tunnel.





A-22222

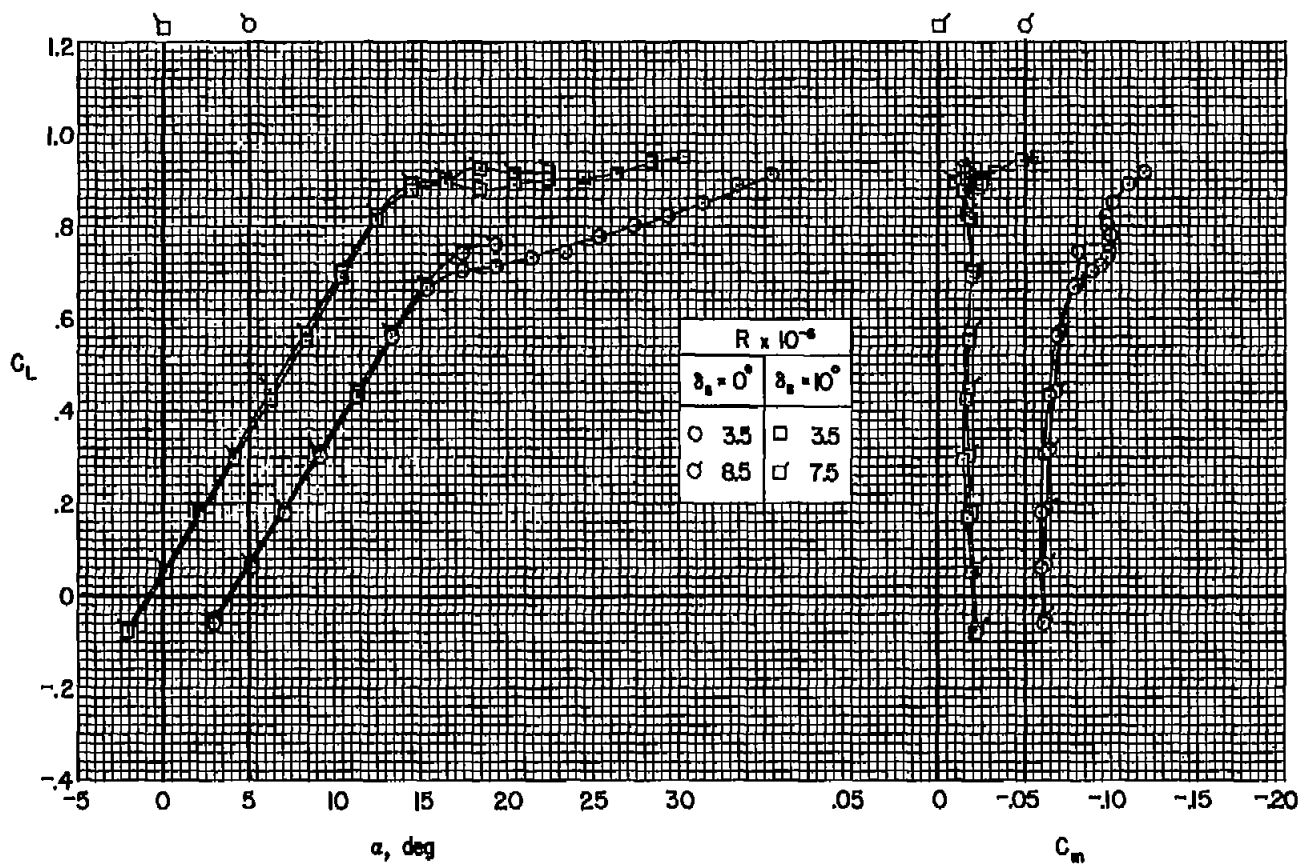
(b) Detail of slat.



A-22223

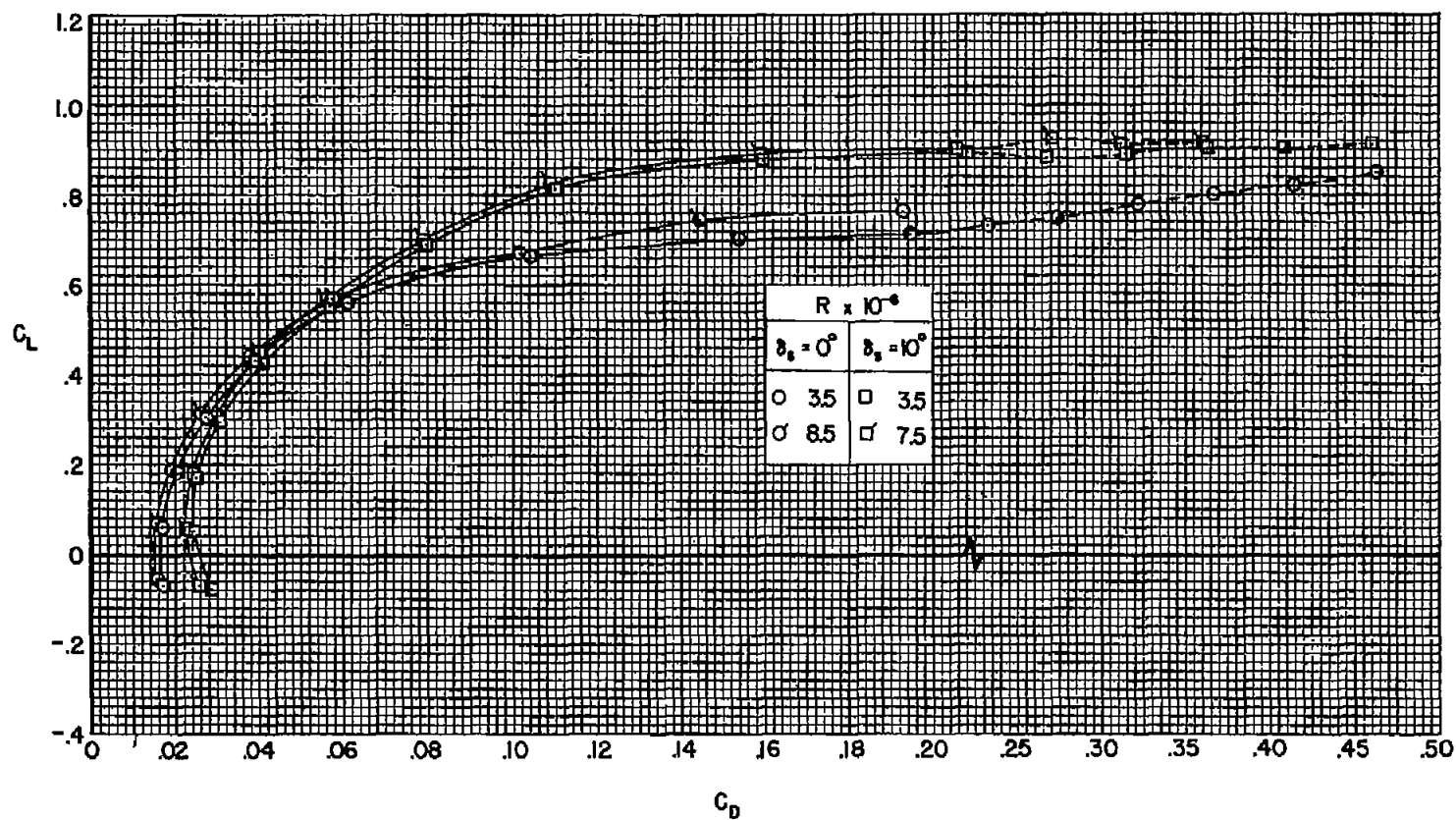
(c) Detail of split flap.

Figure 2.- Concluded.



(a) Lift and pitching-moment coefficient.

Figure 3.- The effect of Reynolds number on the aerodynamic characteristics of the model;  
 $M = 0.60$ .



(b) Drag coefficient.

Figure 3.- Concluded.

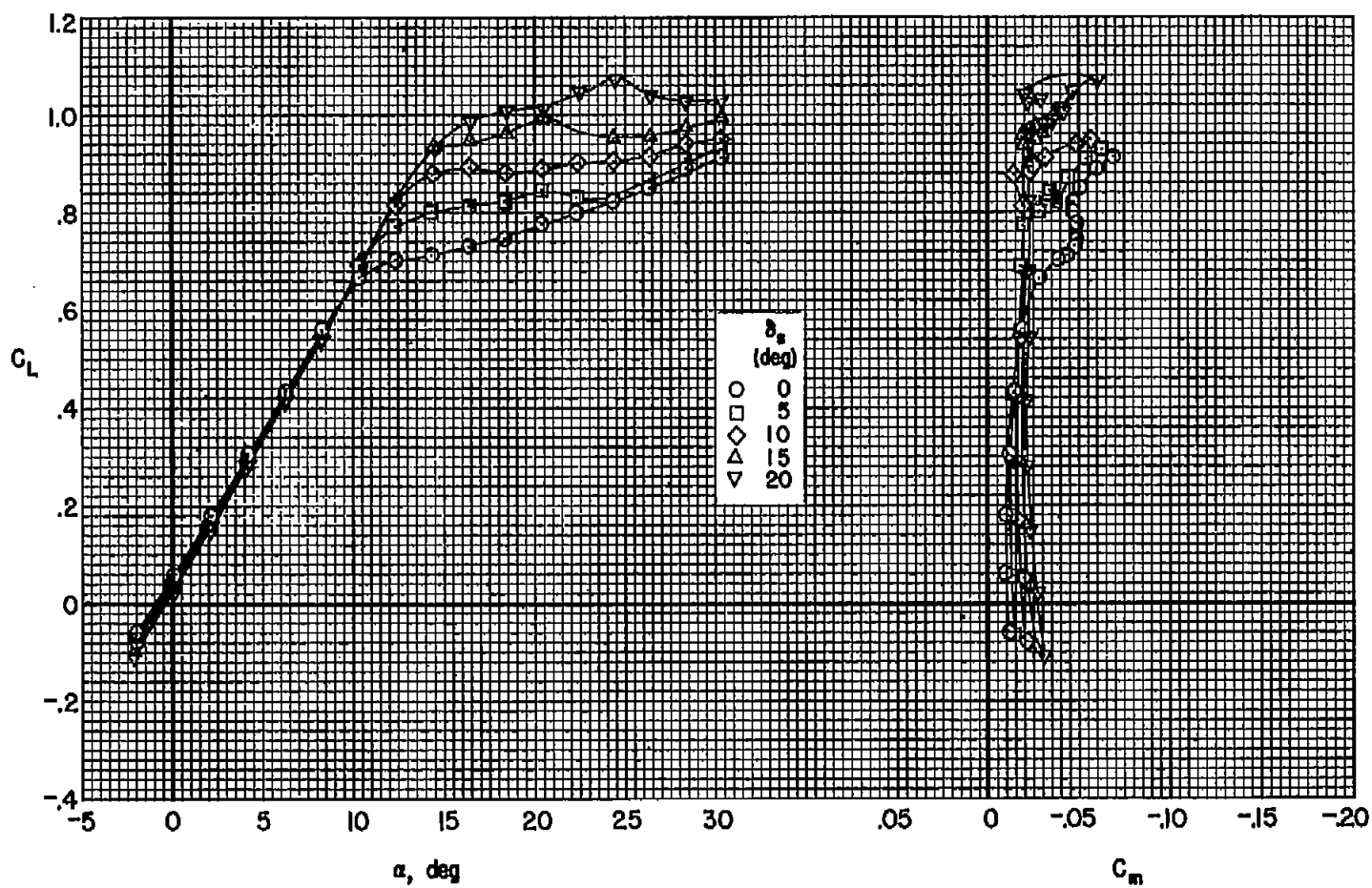
(a)  $M = 0.60$ 

Figure 4.- The effect of slat deflection on the lift and pitching-moment coefficients of the model;  $R \approx 3.5 \times 10^6$ ,  $\delta_p = 0^\circ$ .

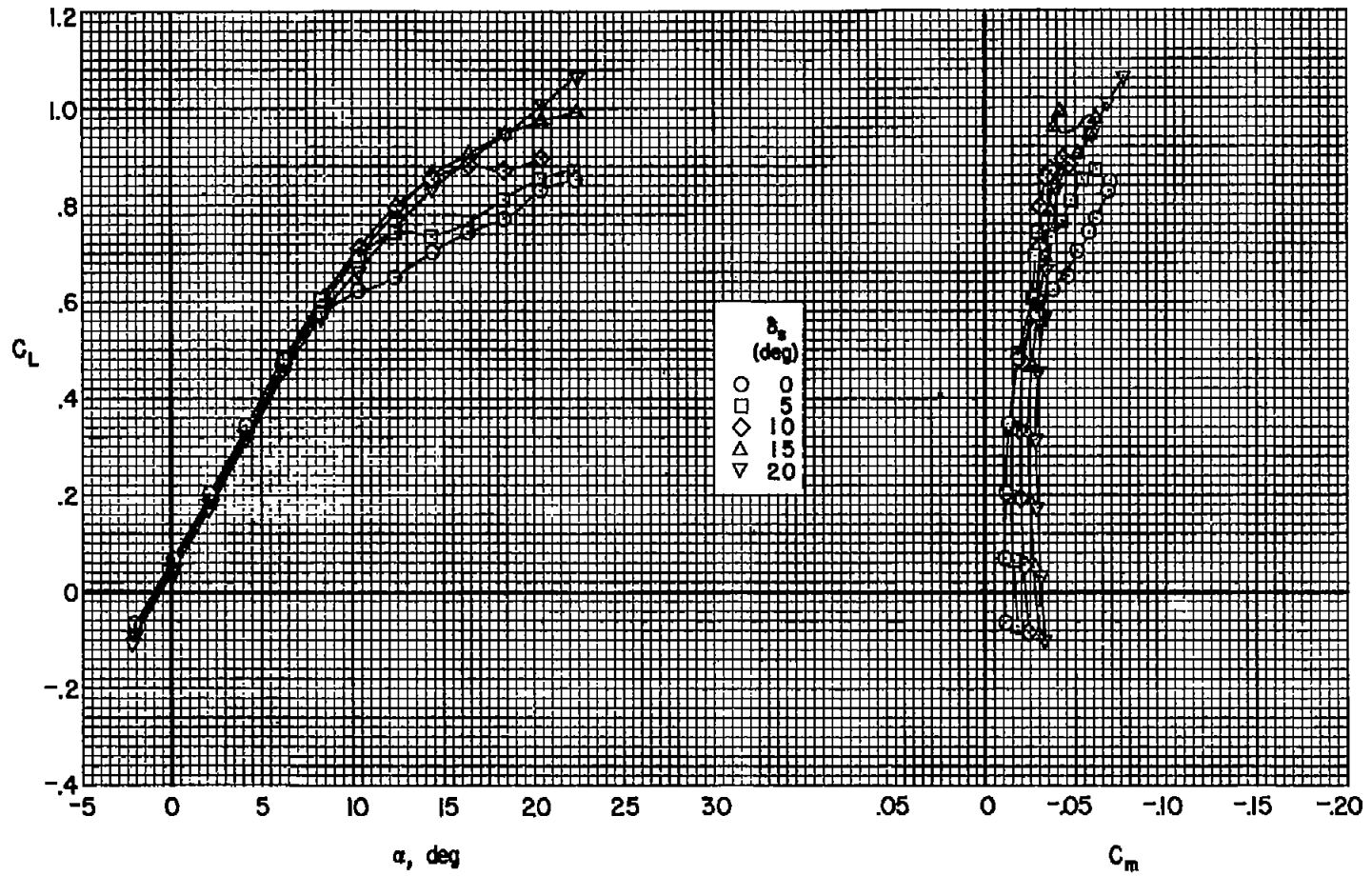
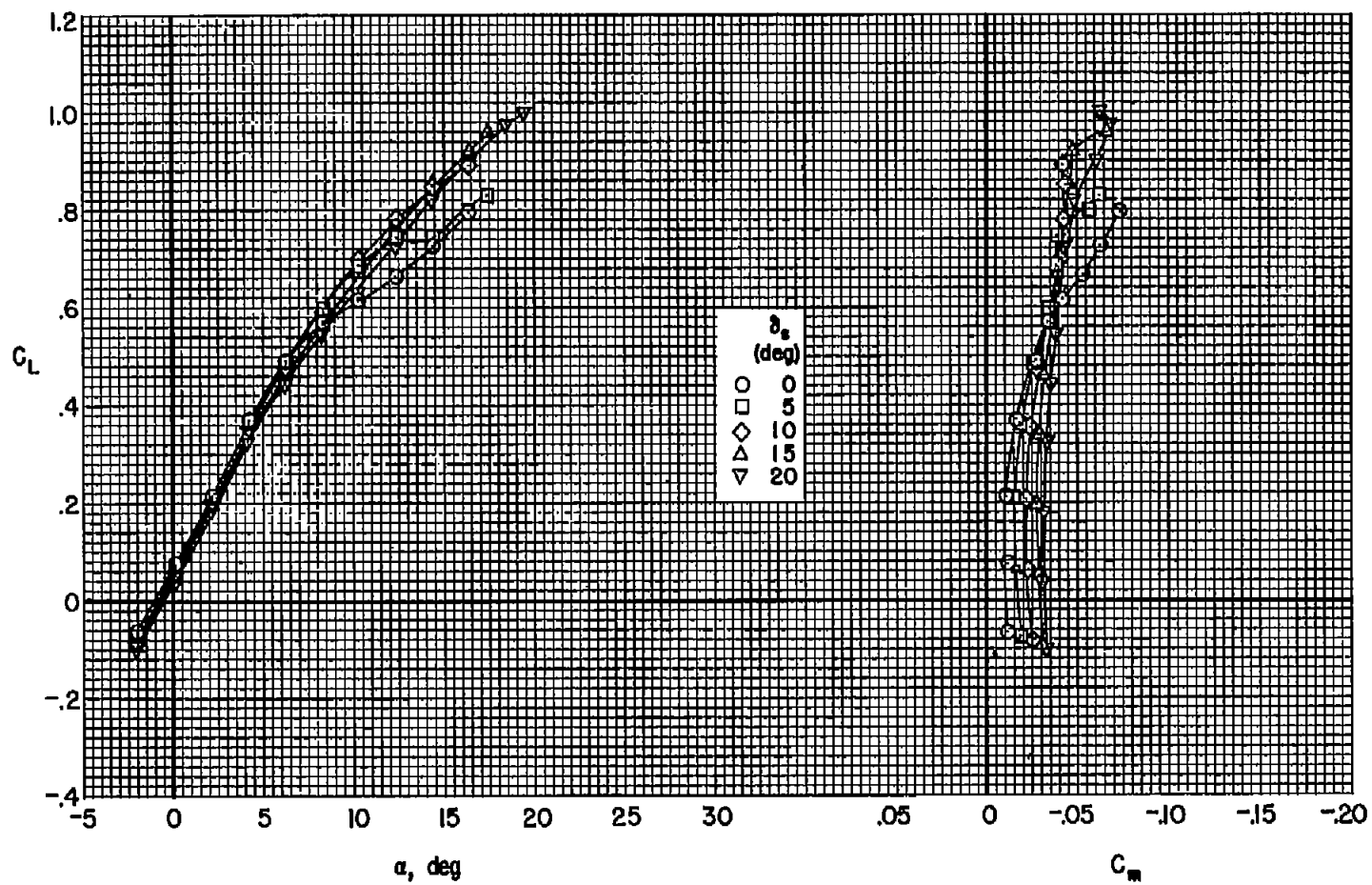
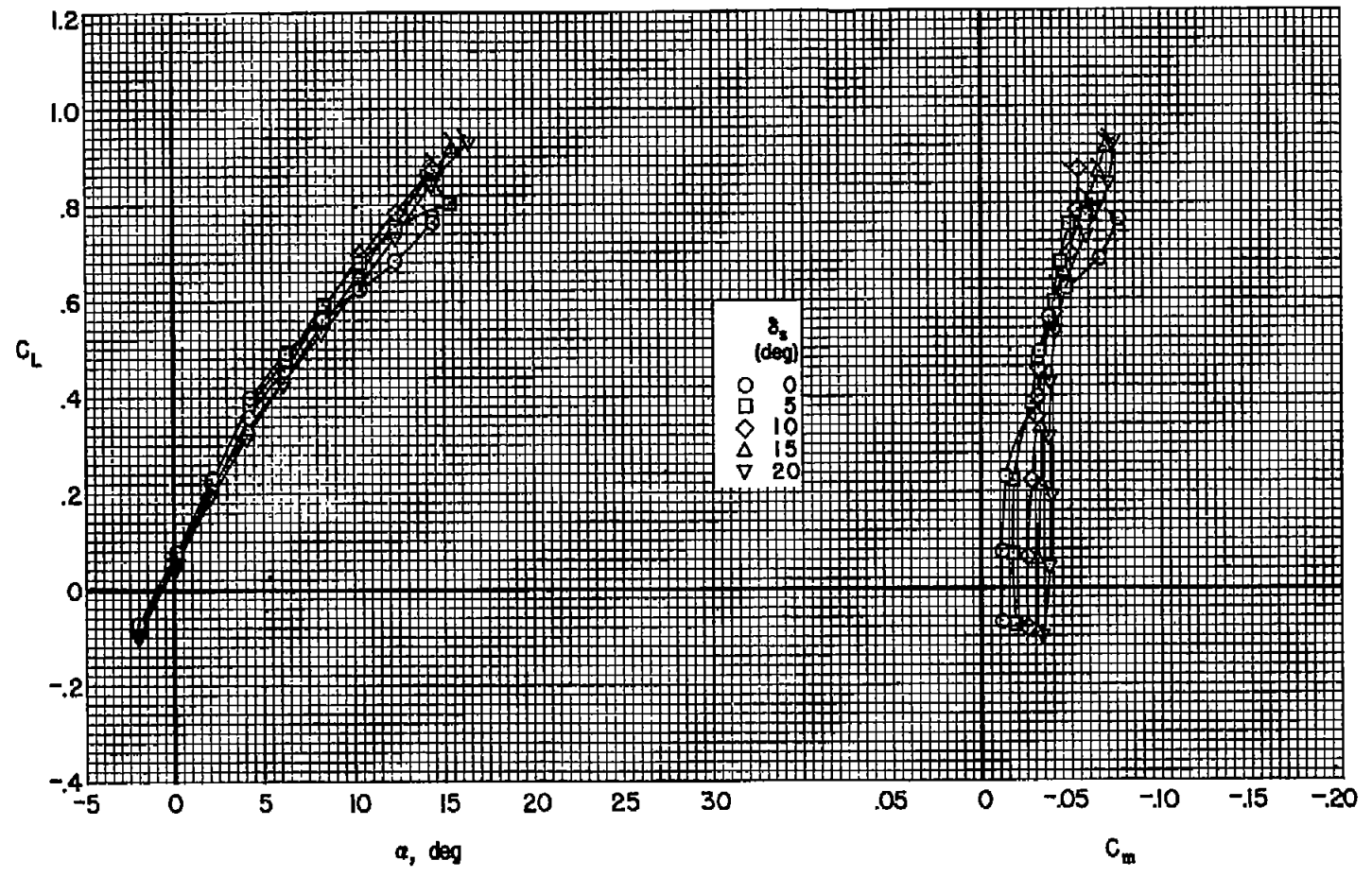
(b)  $M = 0.80$ 

Figure 4.- Continued.



(c)  $M = 0.85$

Figure 4.- Continued.

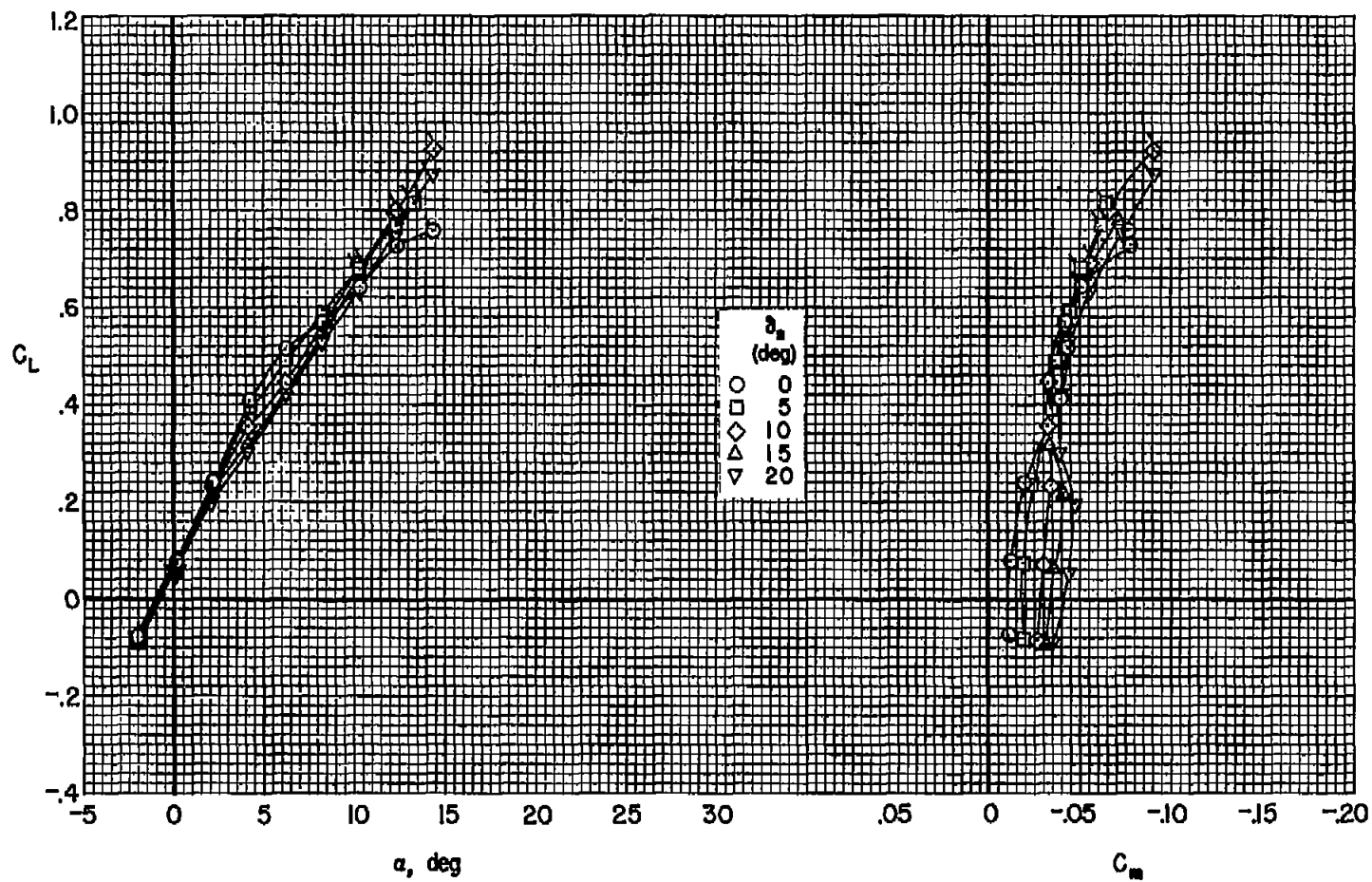


(d)  $M = 0.88$

Figure 4.- Continued.

$C_L$

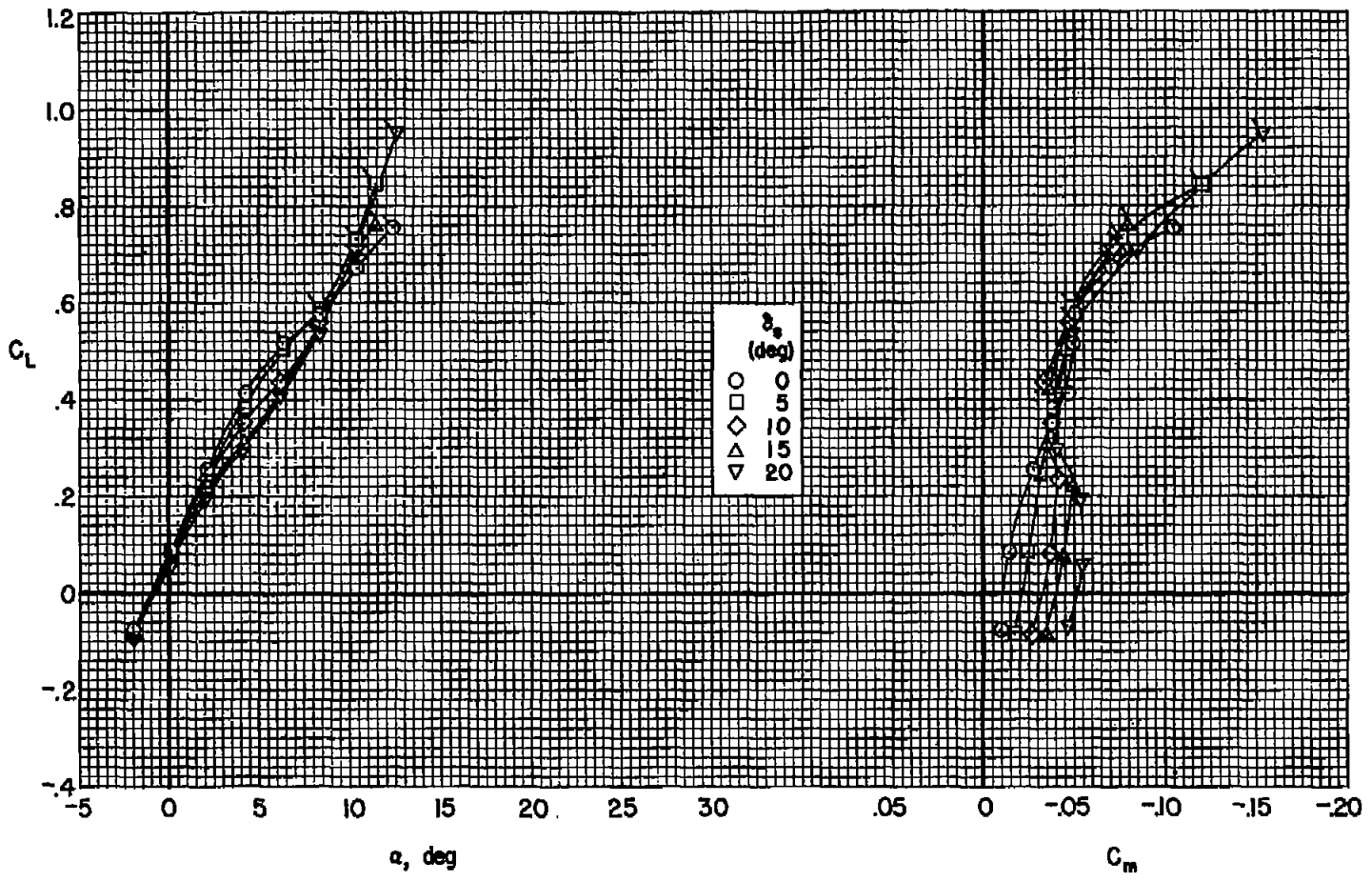
NACA RM A57E19



(e)  $M = 0.90$

Figure 4.- Continued.





(f)  $M = 0.92$

Figure 4.- Concluded.

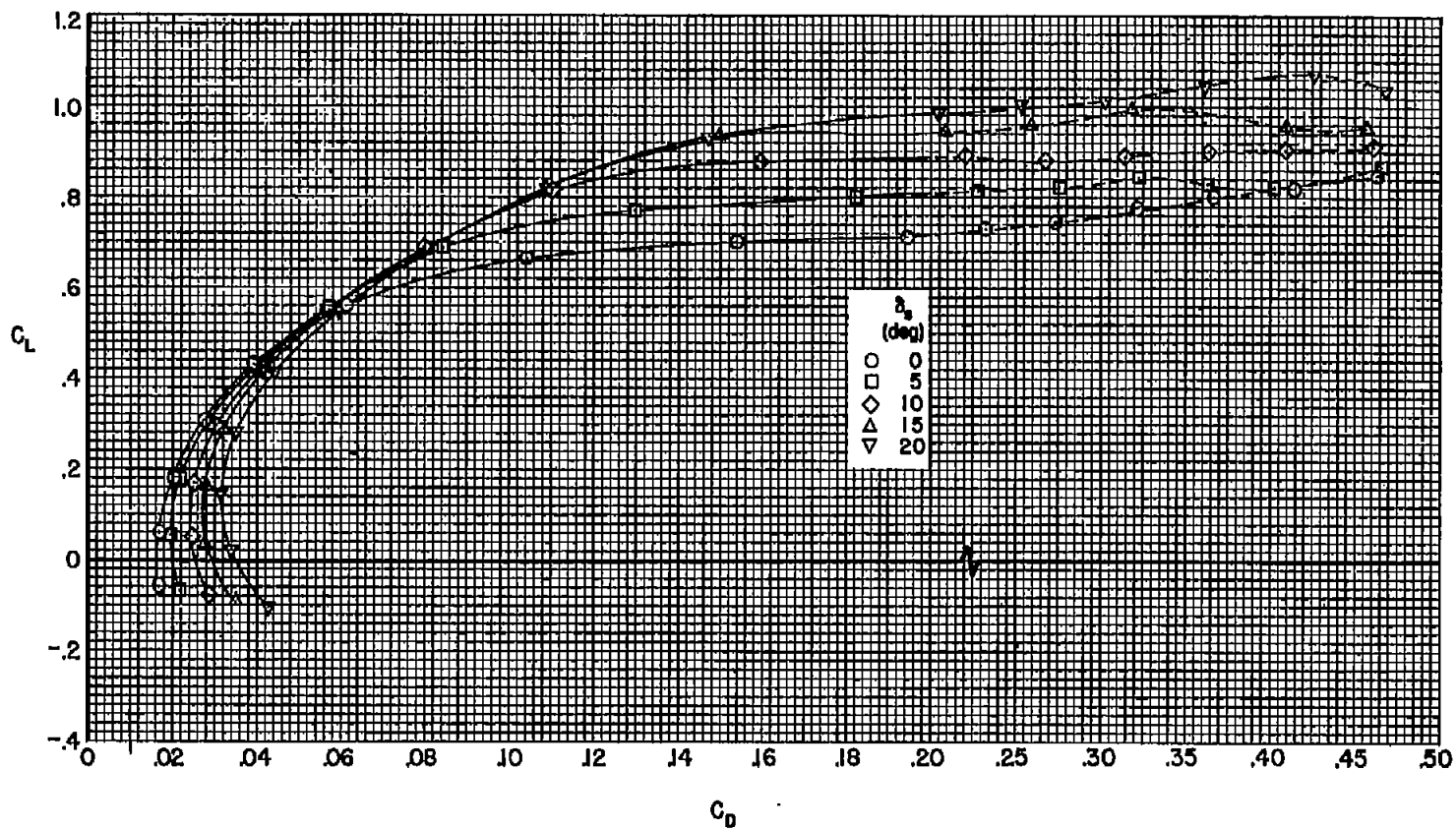
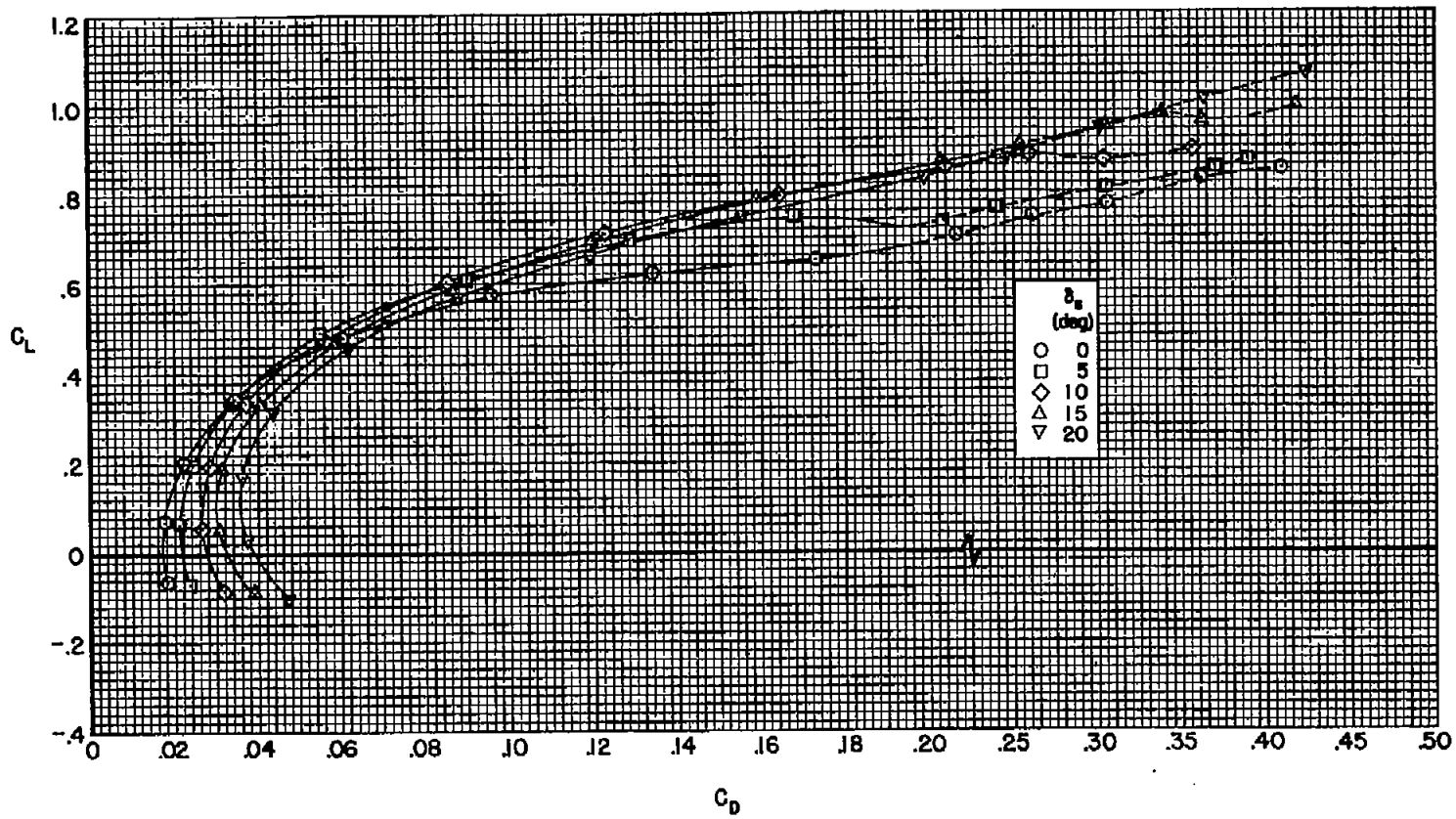
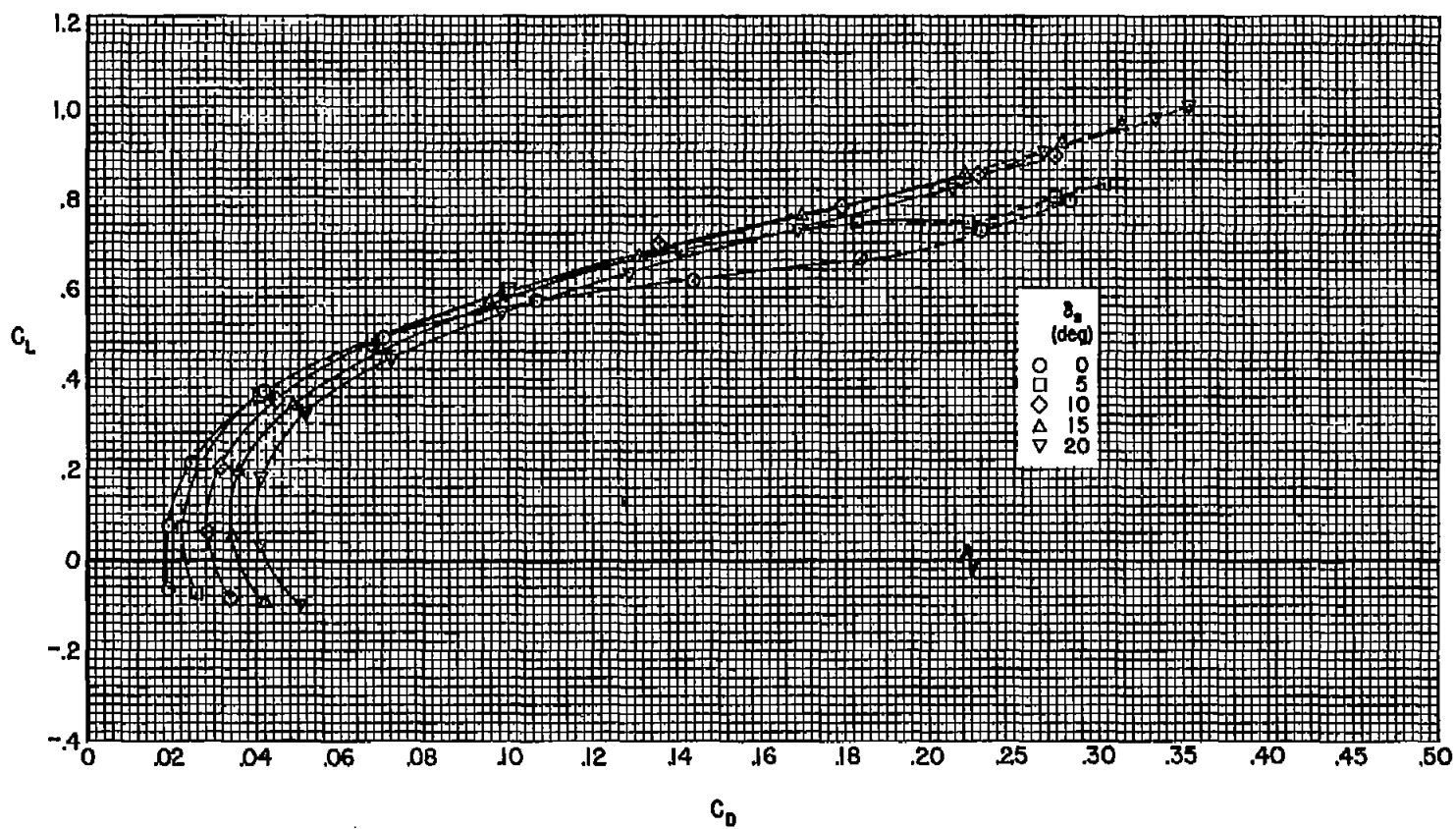
(a)  $M = 0.60$ 

Figure 5.- The effect of slat deflection on the drag coefficient of the model;  
 $R \approx 3.5 \times 10^6$ ,  $\delta_f = 0^\circ$ .



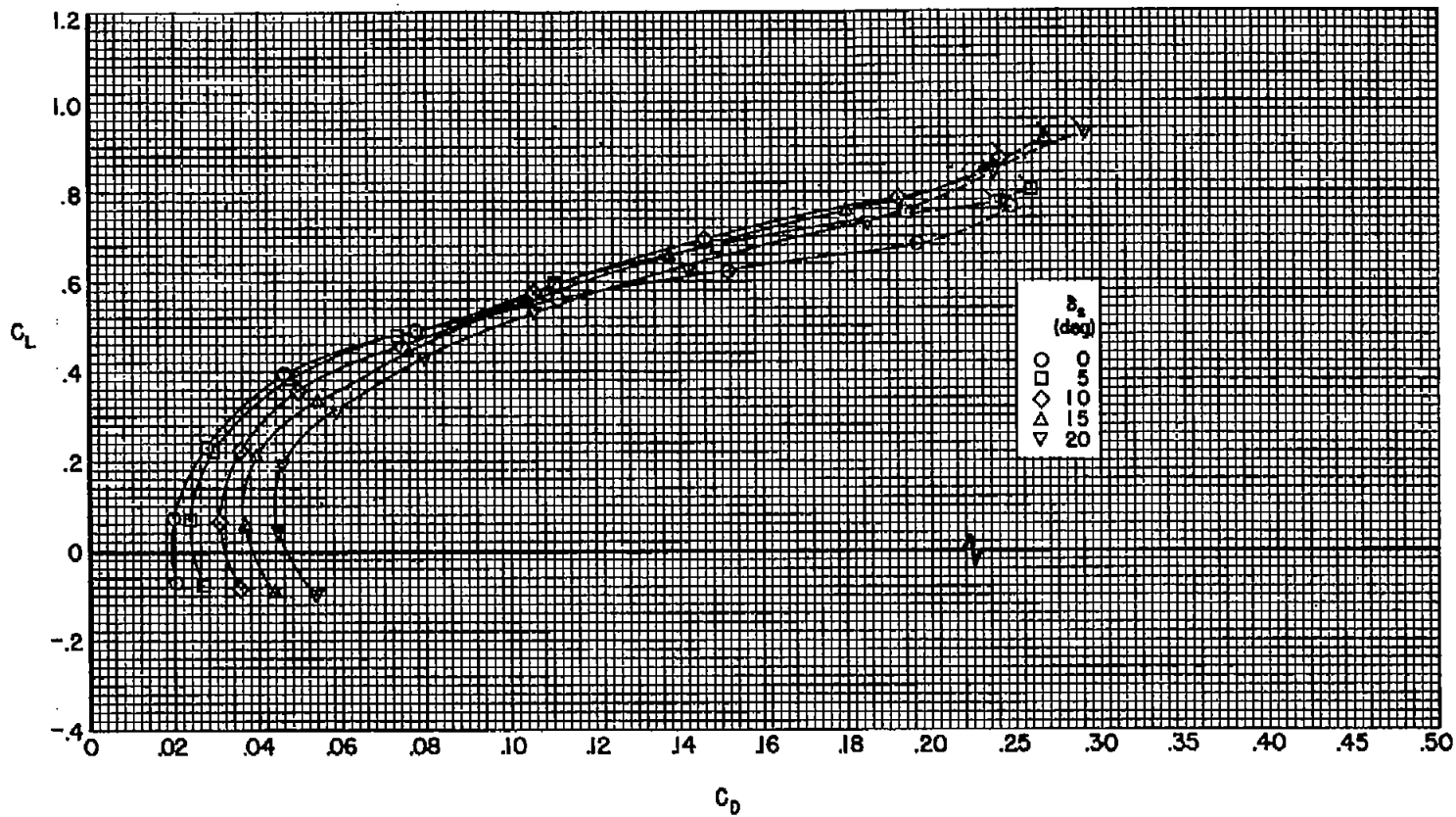
(b)  $M = 0.80$

Figure 5.- Continued.



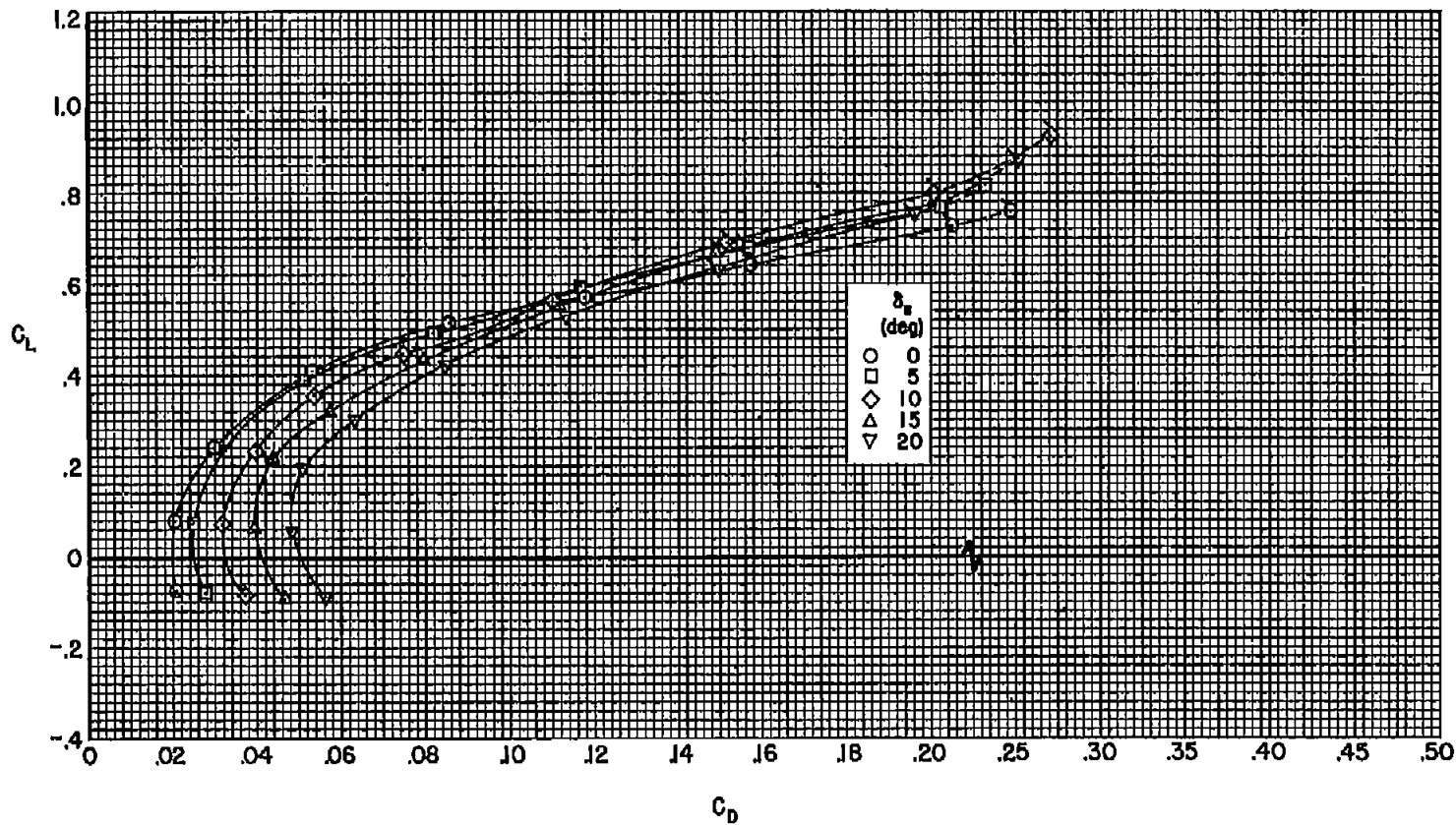
(c)  $M = 0.85$

Figure 5.- Continued.



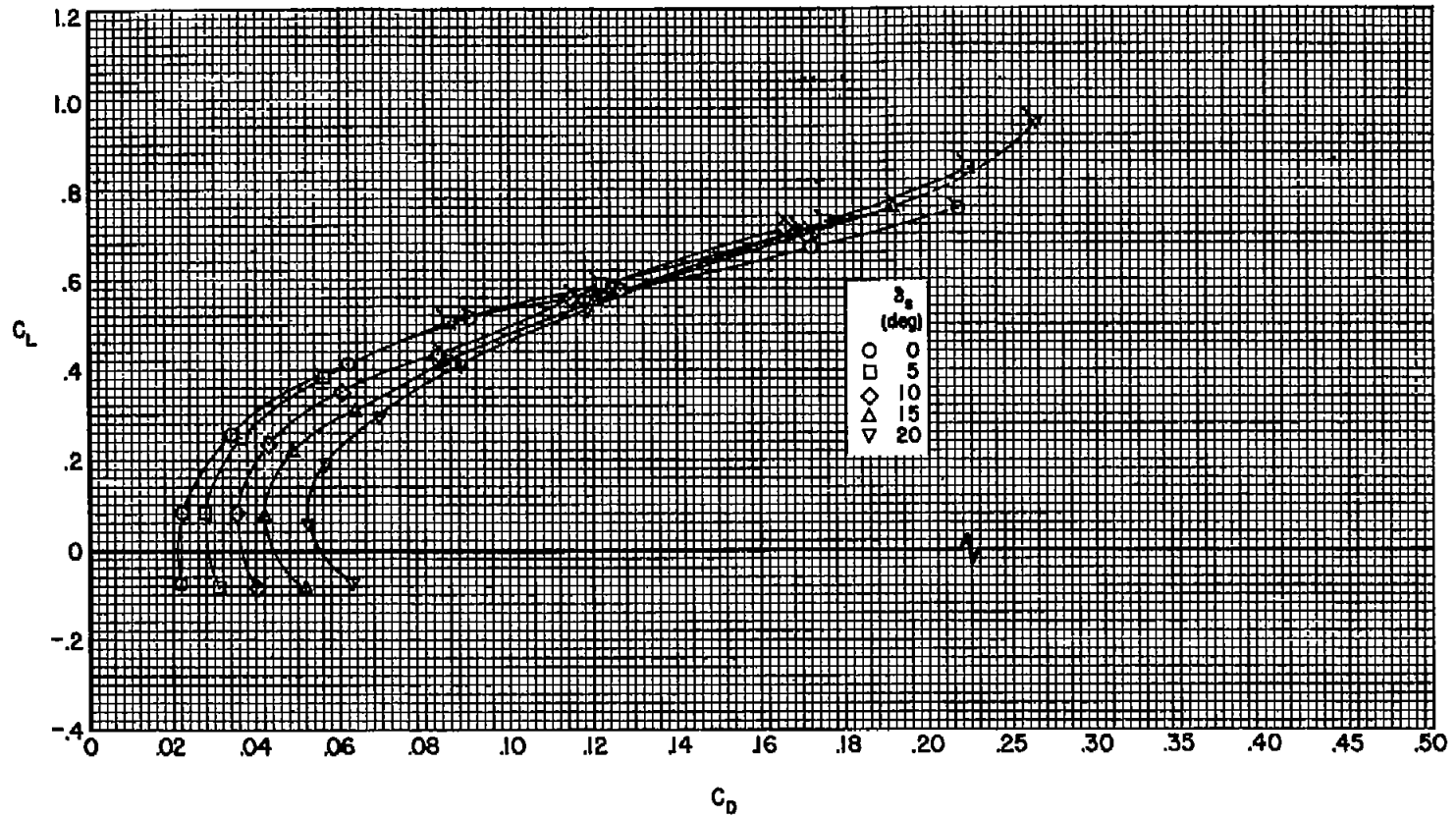
(d)  $M = 0.88$

Figure 5.- Continued.



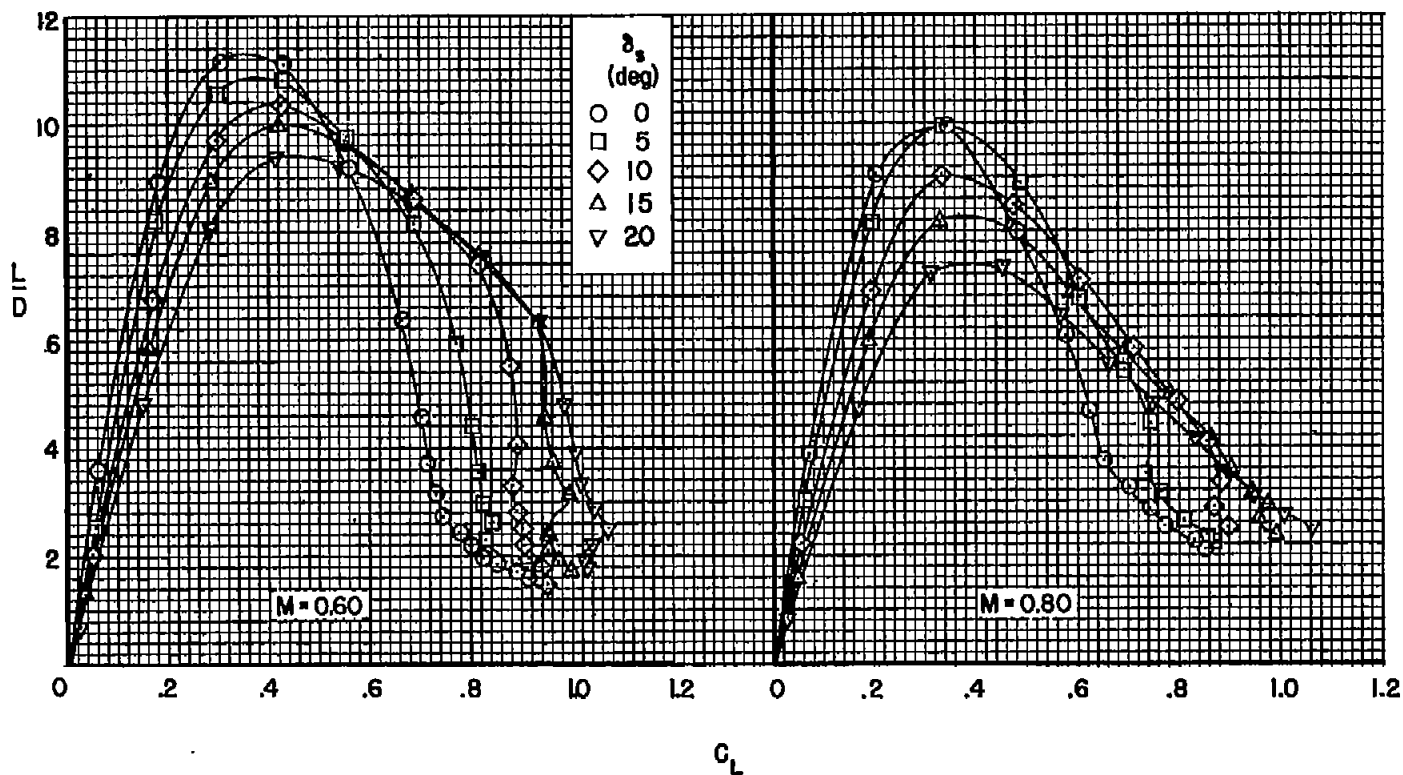
(e)  $M = 0.90$

Figure 5.- Continued.



(f)  $M = 0.92$

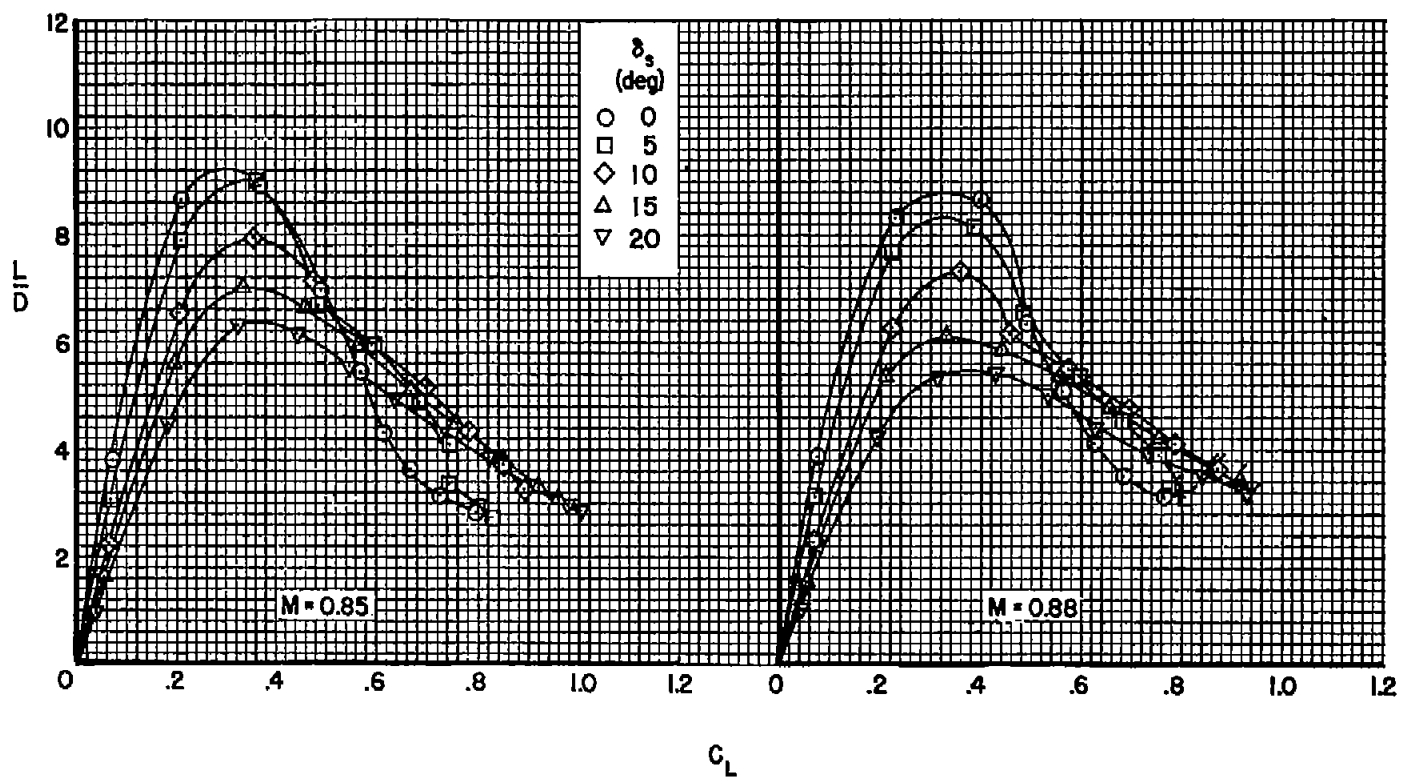
Figure 5.- Concluded.



(a)  $M = 0.60, 0.80$

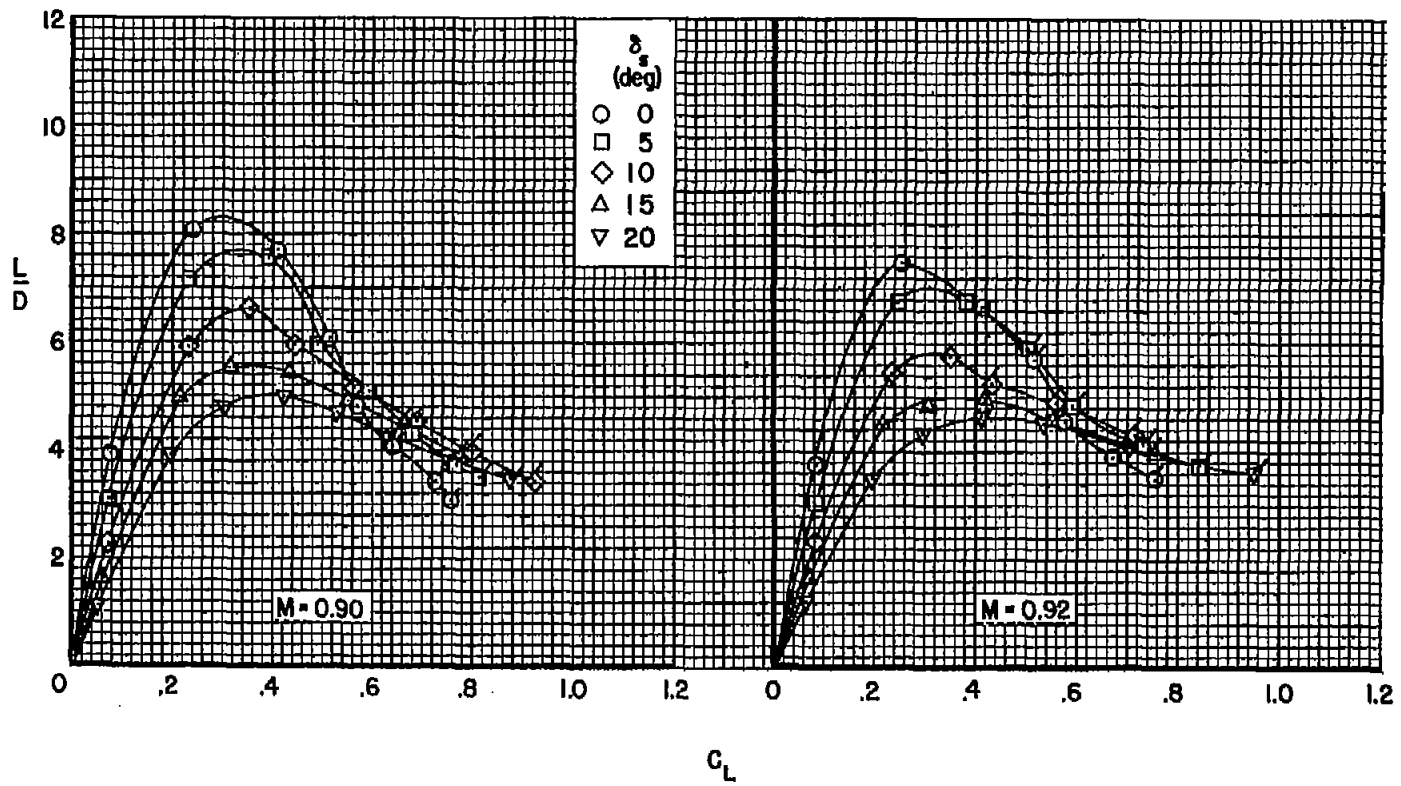
Figure 6.- The effect of slat deflection on the lift-drag ratio of the model;  
 $R \approx 3.5 \times 10^6$ ,  $\delta_P = 0^\circ$ .





(b)  $M = 0.85, 0.88$

Figure 6.- Continued.



(c)  $M = 0.90, 0.92$

Figure 6.- Concluded.

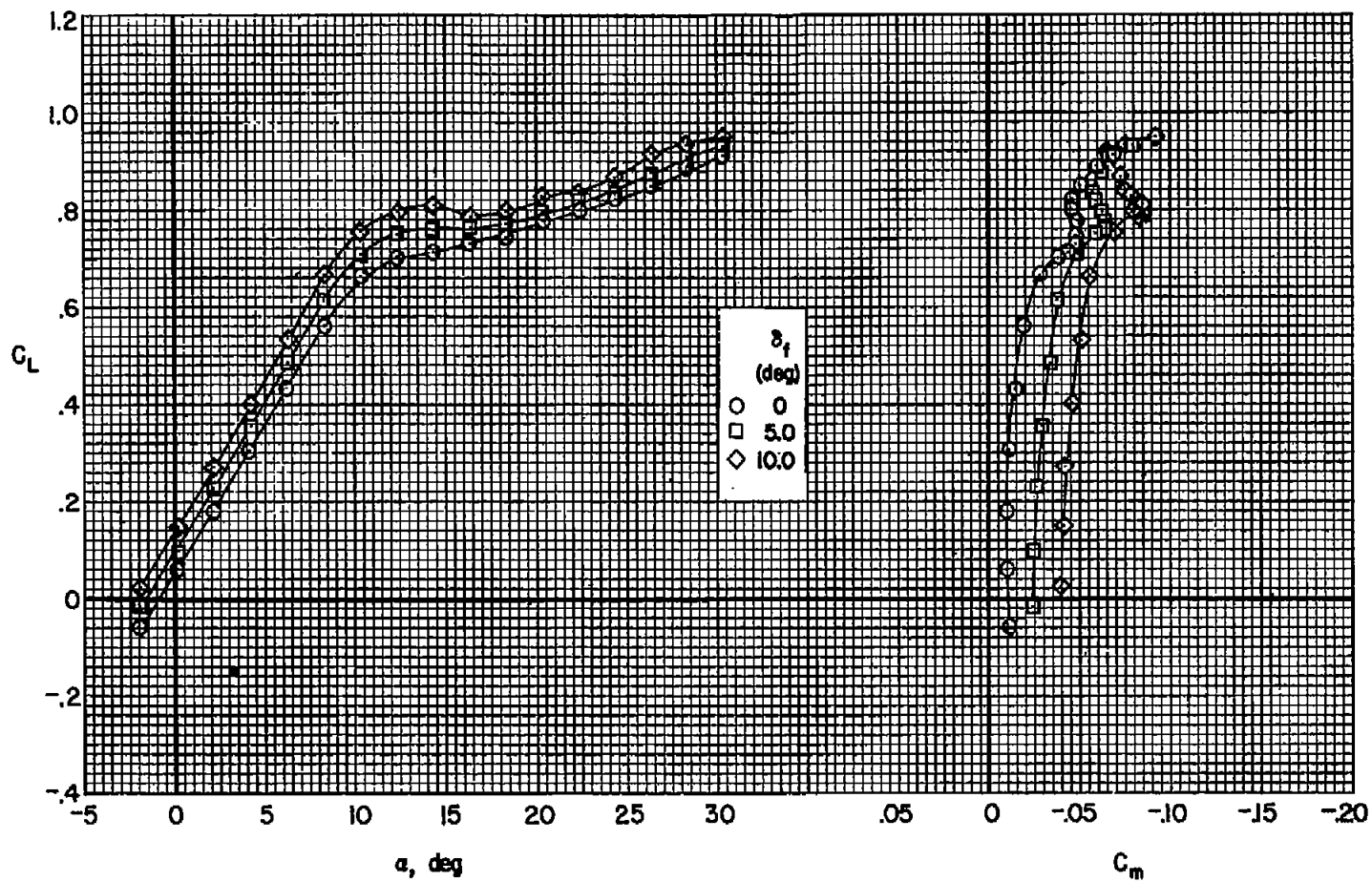
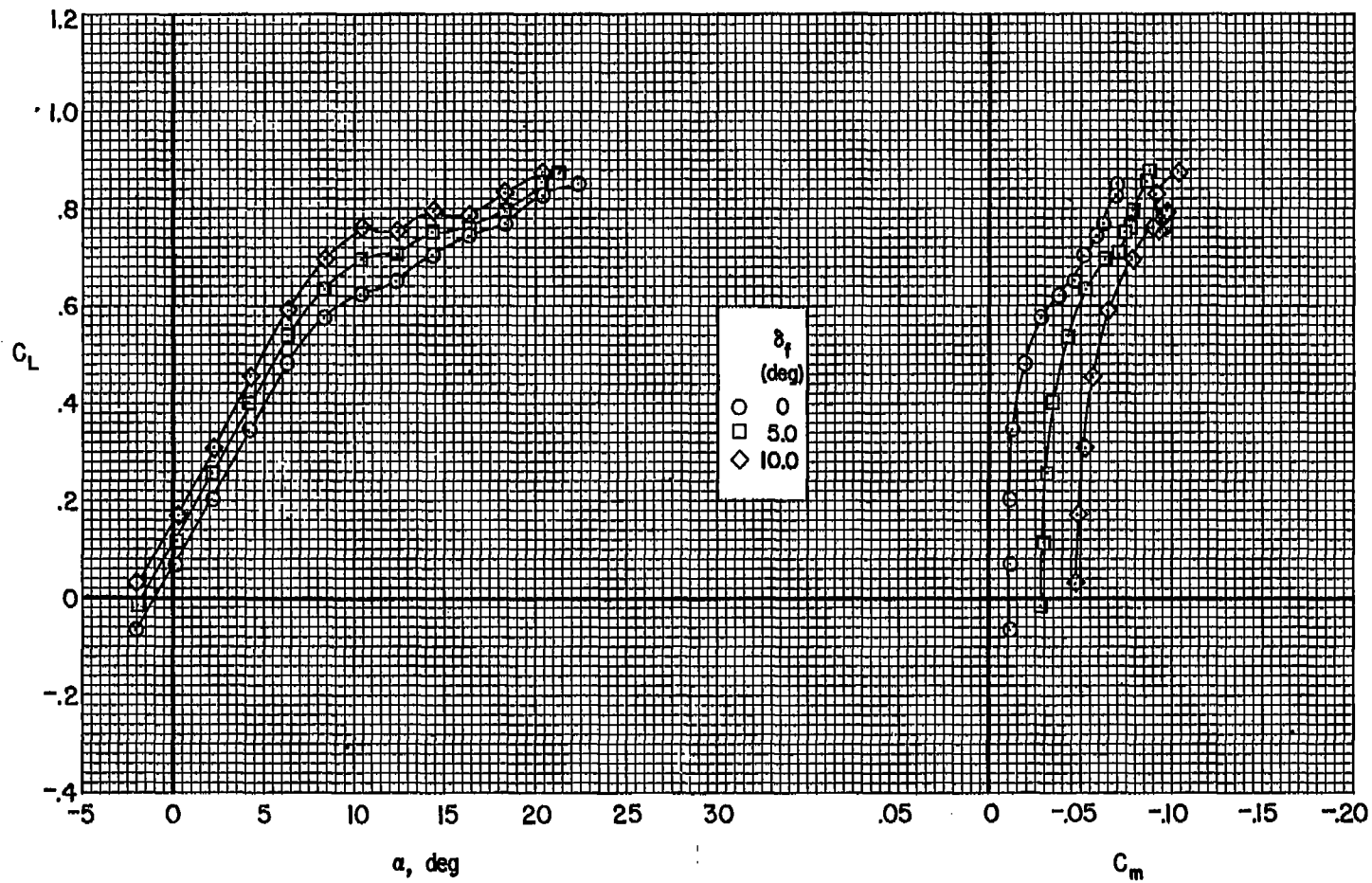
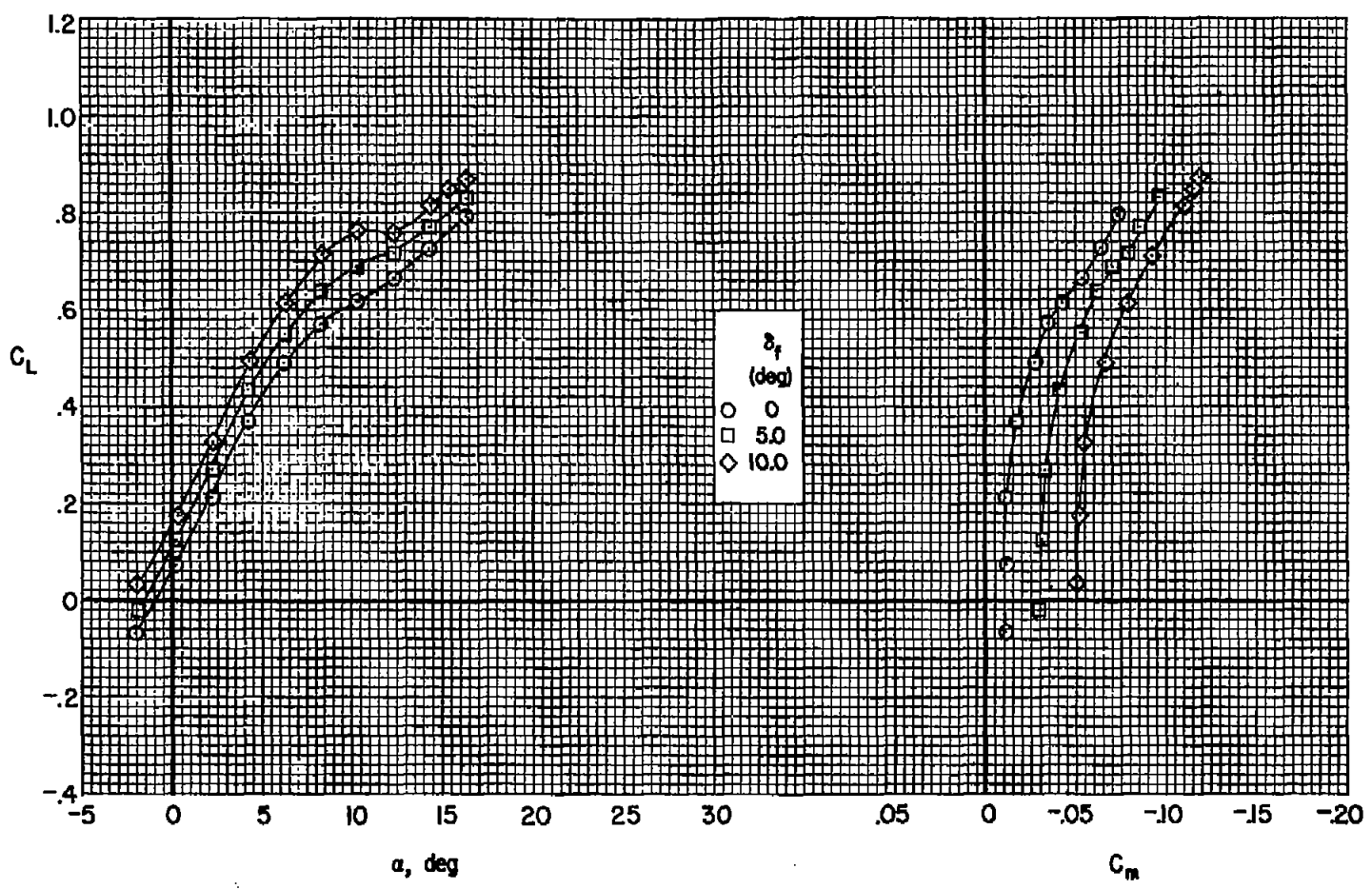
(a)  $M = 0.60$ 

Figure 7.- The effect of flap deflection on the lift and pitching-moment coefficients of the model;  $R \approx 3.6 \times 10^6$ ,  $\delta_B = 0^\circ$ .



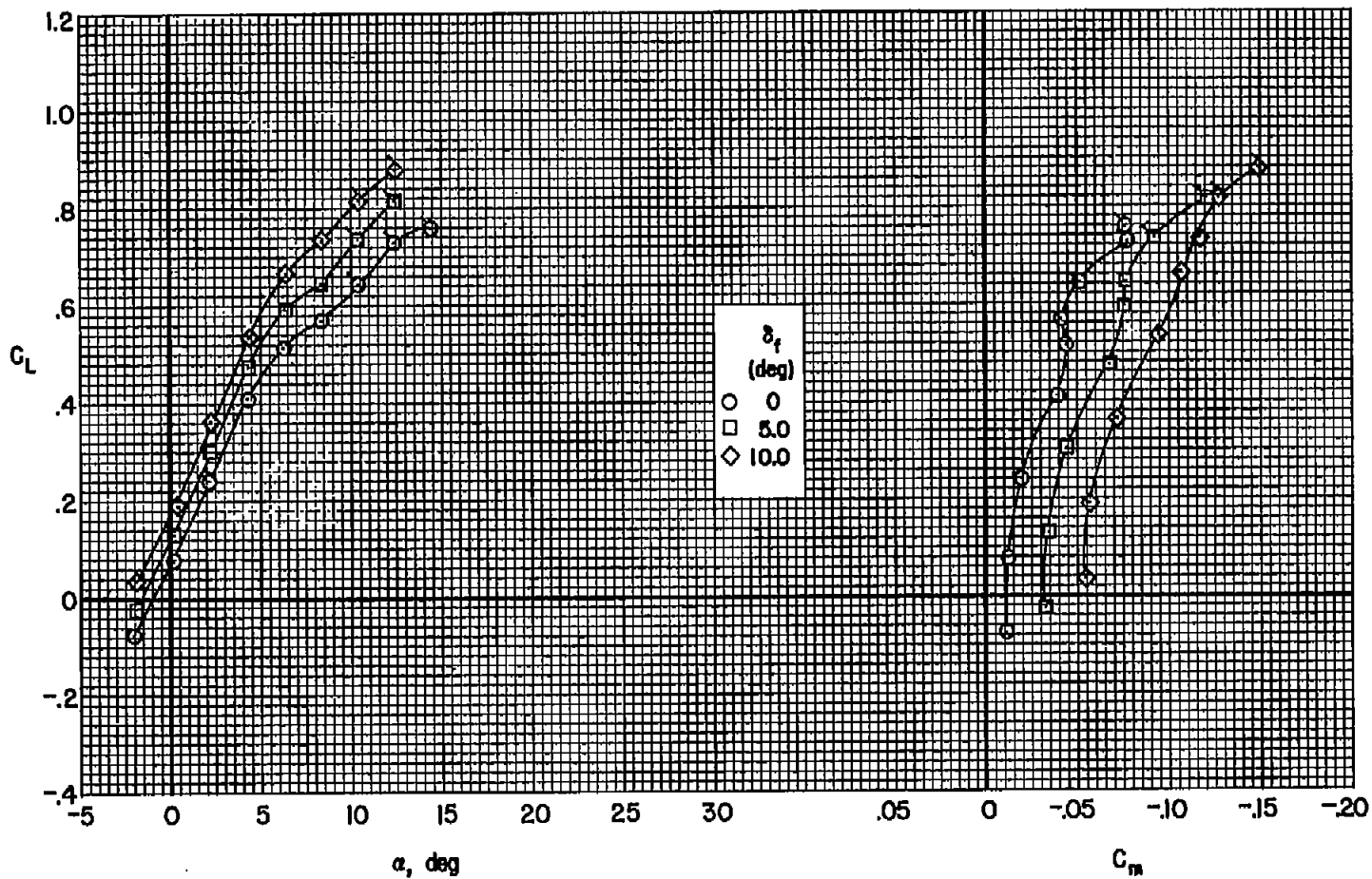
(b)  $M = 0.80$

Figure 7.- Continued.



(c)  $M = 0.85$

Figure 7.- Continued.



(d)  $M = 0.90$

Figure 7.- Concluded.

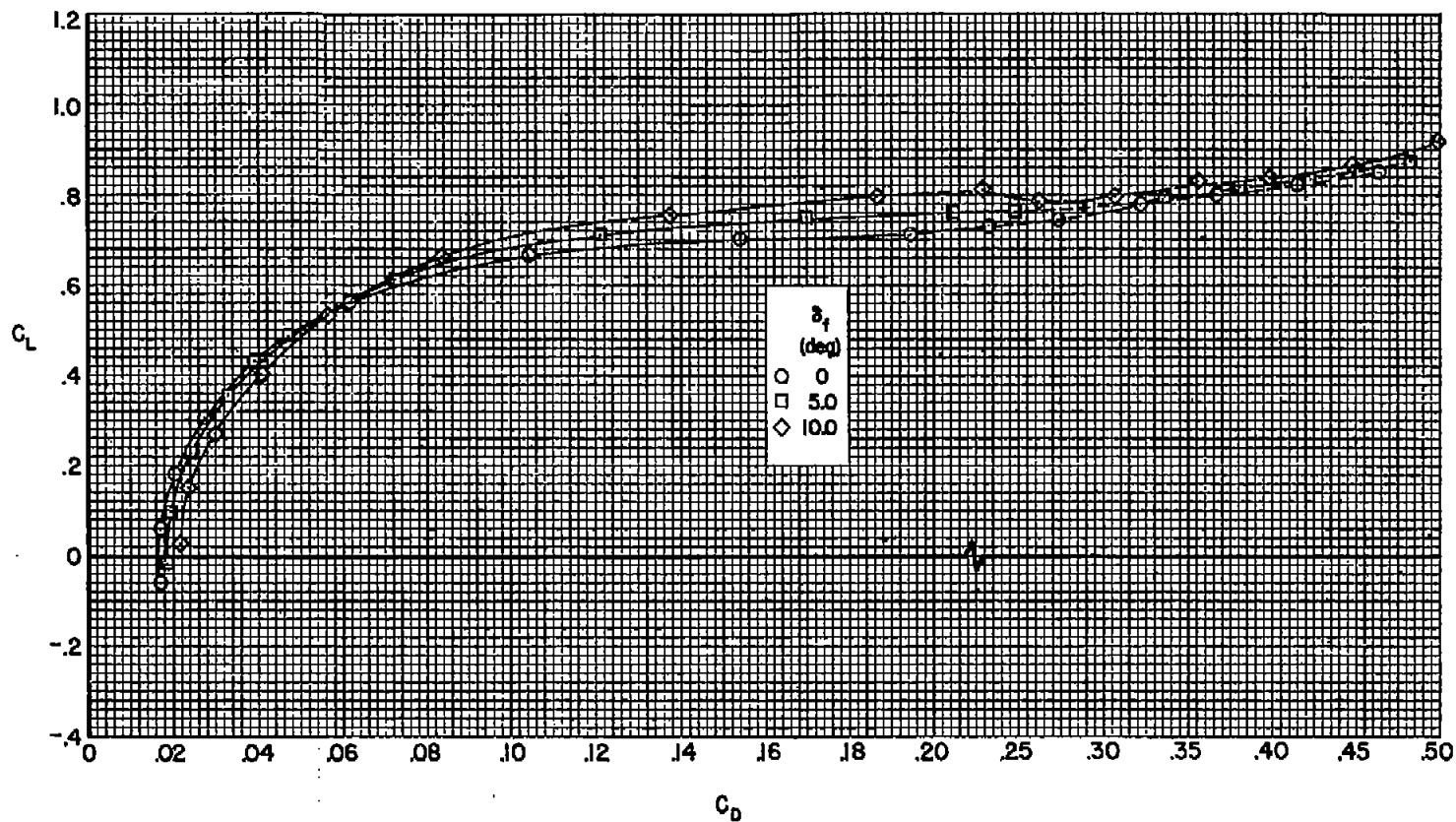
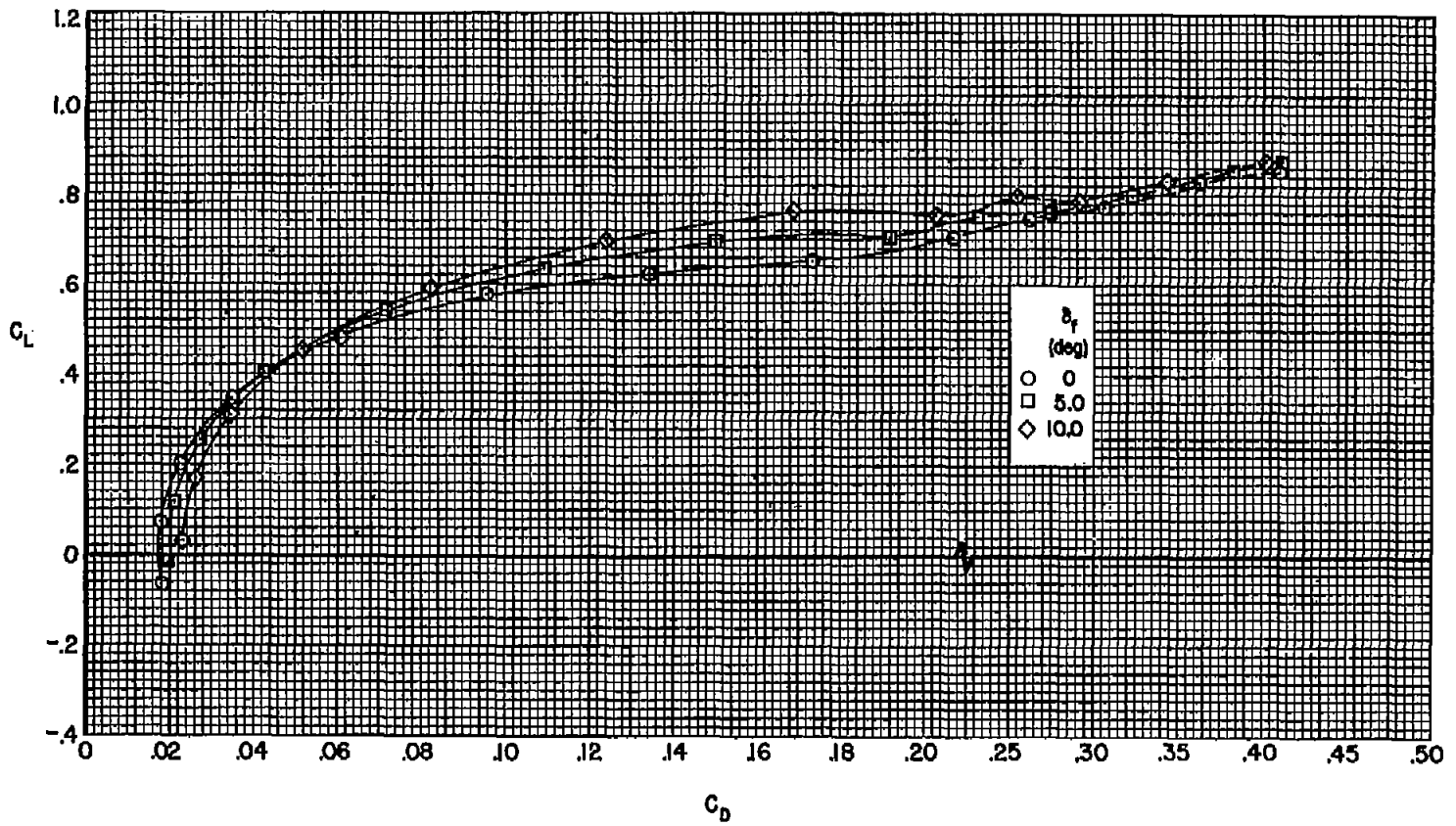
(a)  $M = 0.60$ 

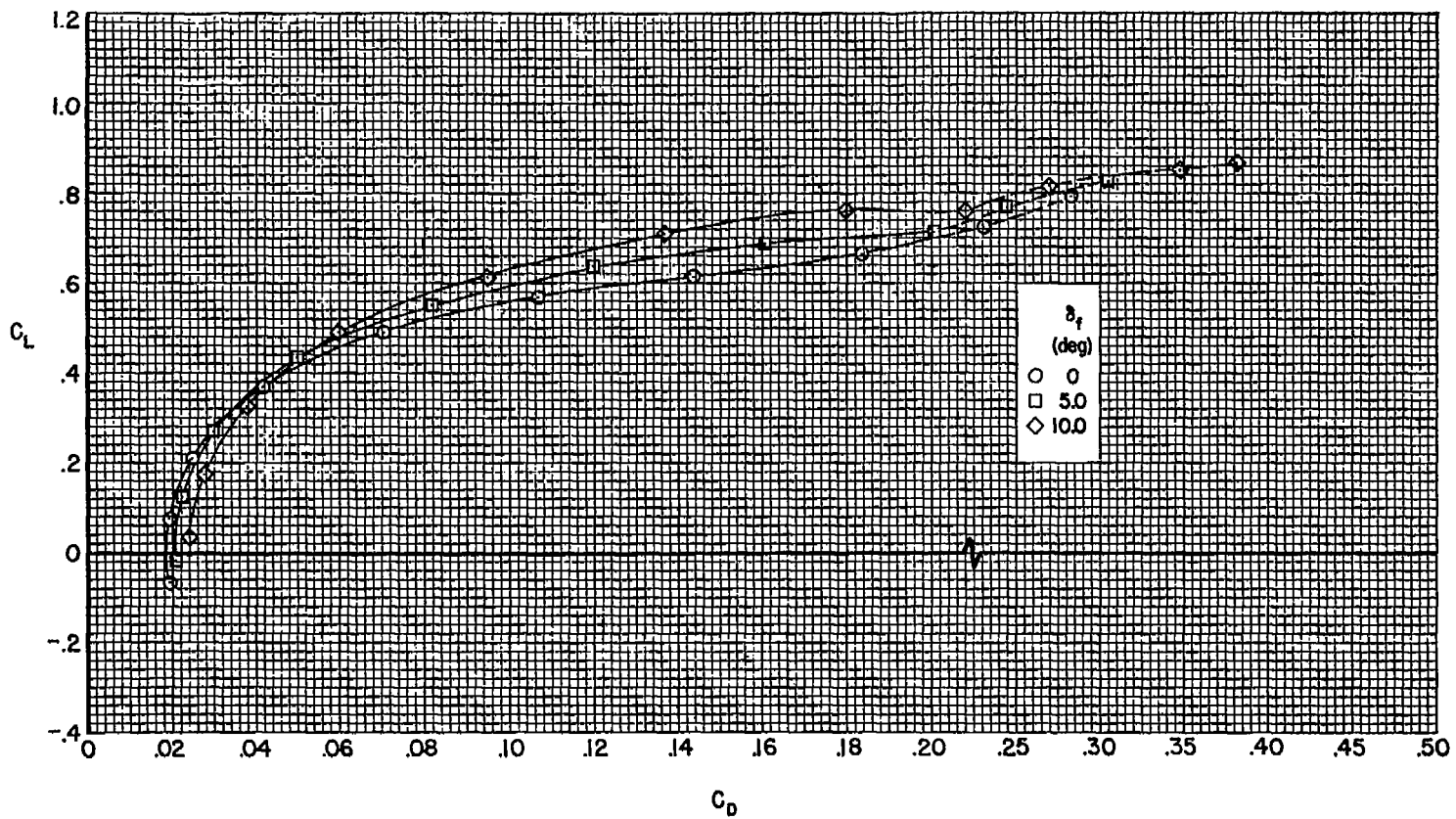
Figure 8.- The effect of flap deflection on the drag coefficient of the model;  
 $R \approx 3.6 \times 10^6$ ,  $\delta_S = 0^\circ$ .



(b)  $M = 0.80$

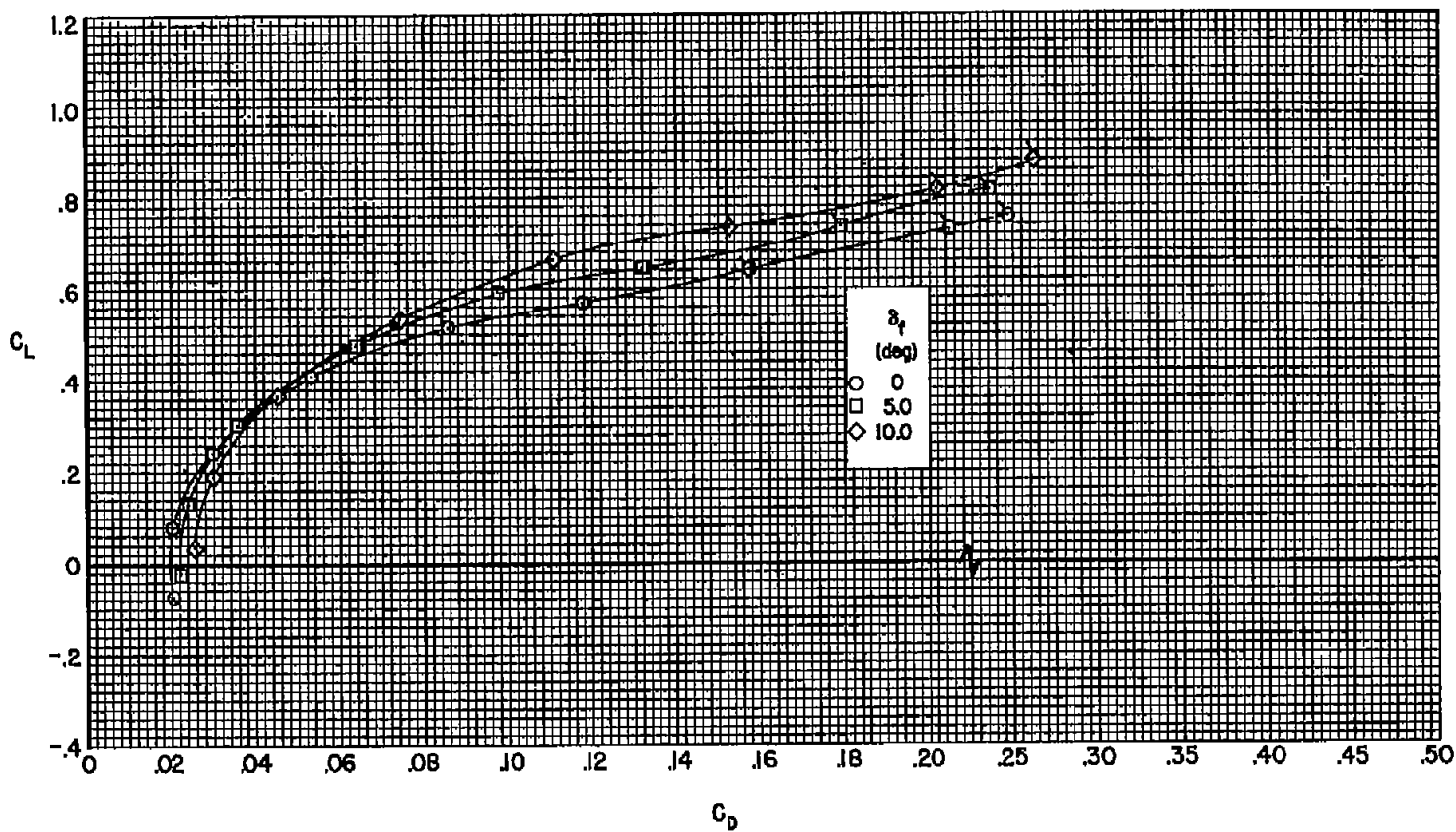
Figure 8.- Continued.





(c)  $M = 0.85$

Figure 8.- Continued.



(d)  $M = 0.90$

Figure 8.- Concluded.

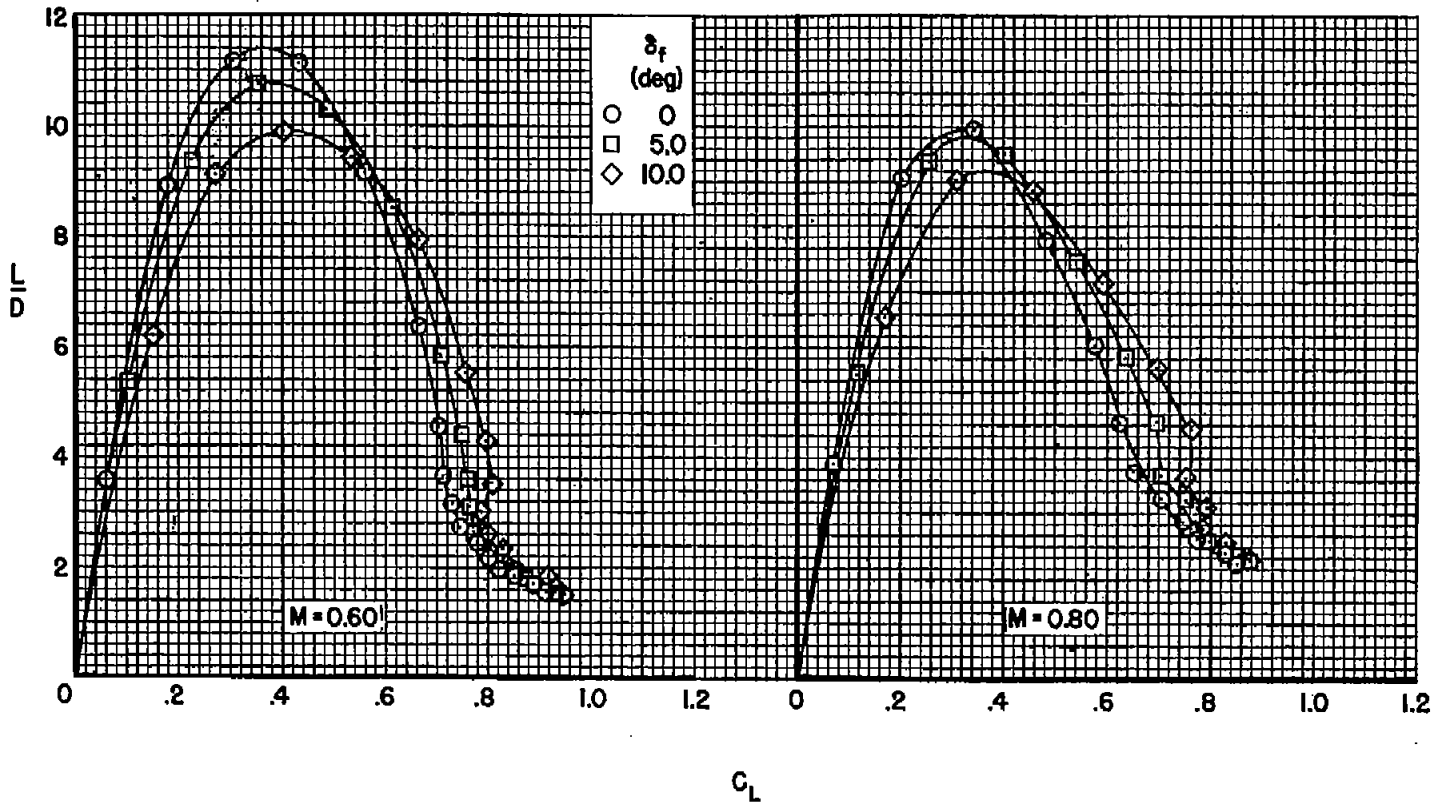
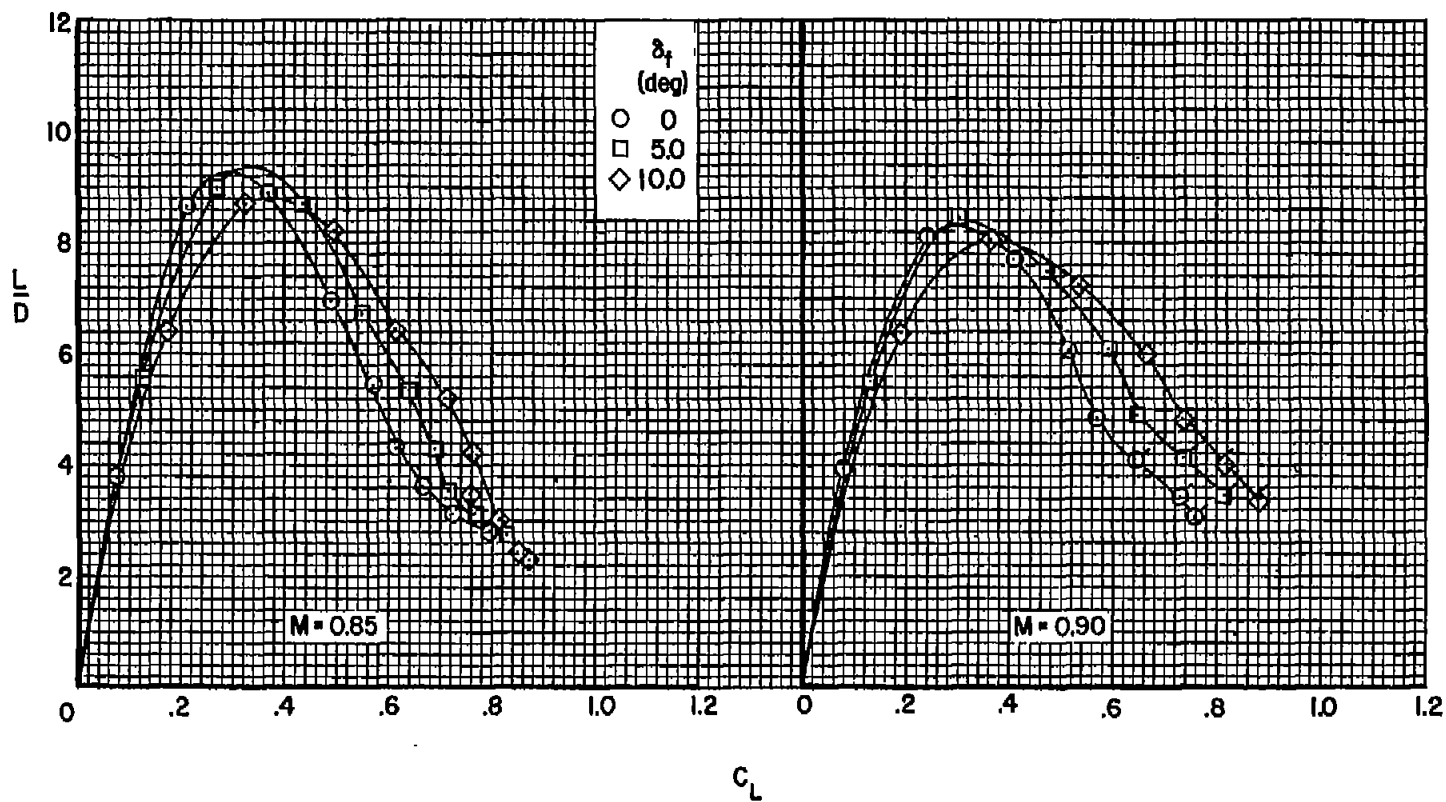
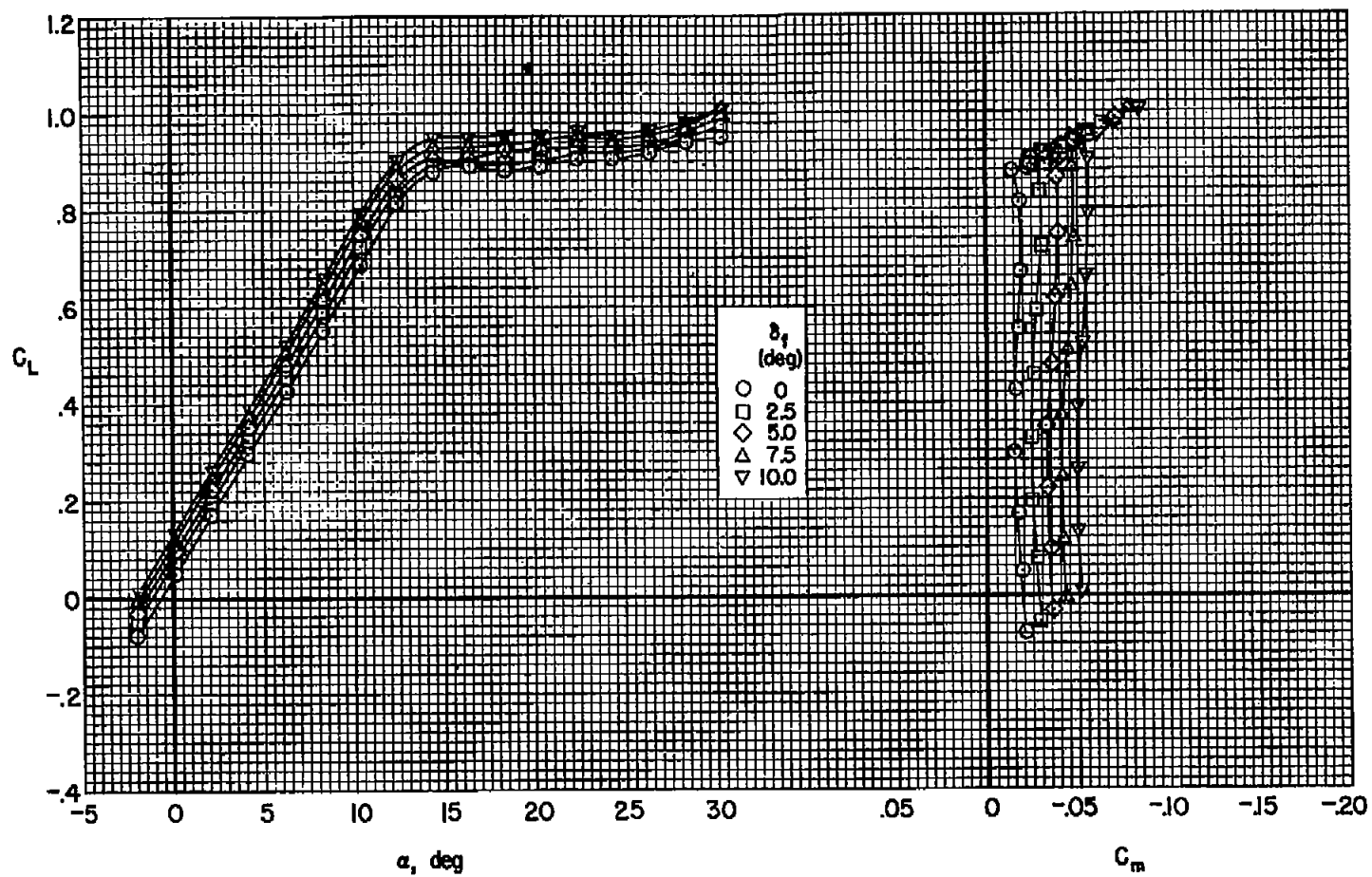
(a)  $M = 0.60, 0.80$ 

Figure 9.- The effect of flap deflection on the lift-drag ratio of the model;  
 $R \approx 3.6 \times 10^6$ ,  $\delta_B = 0^\circ$ .



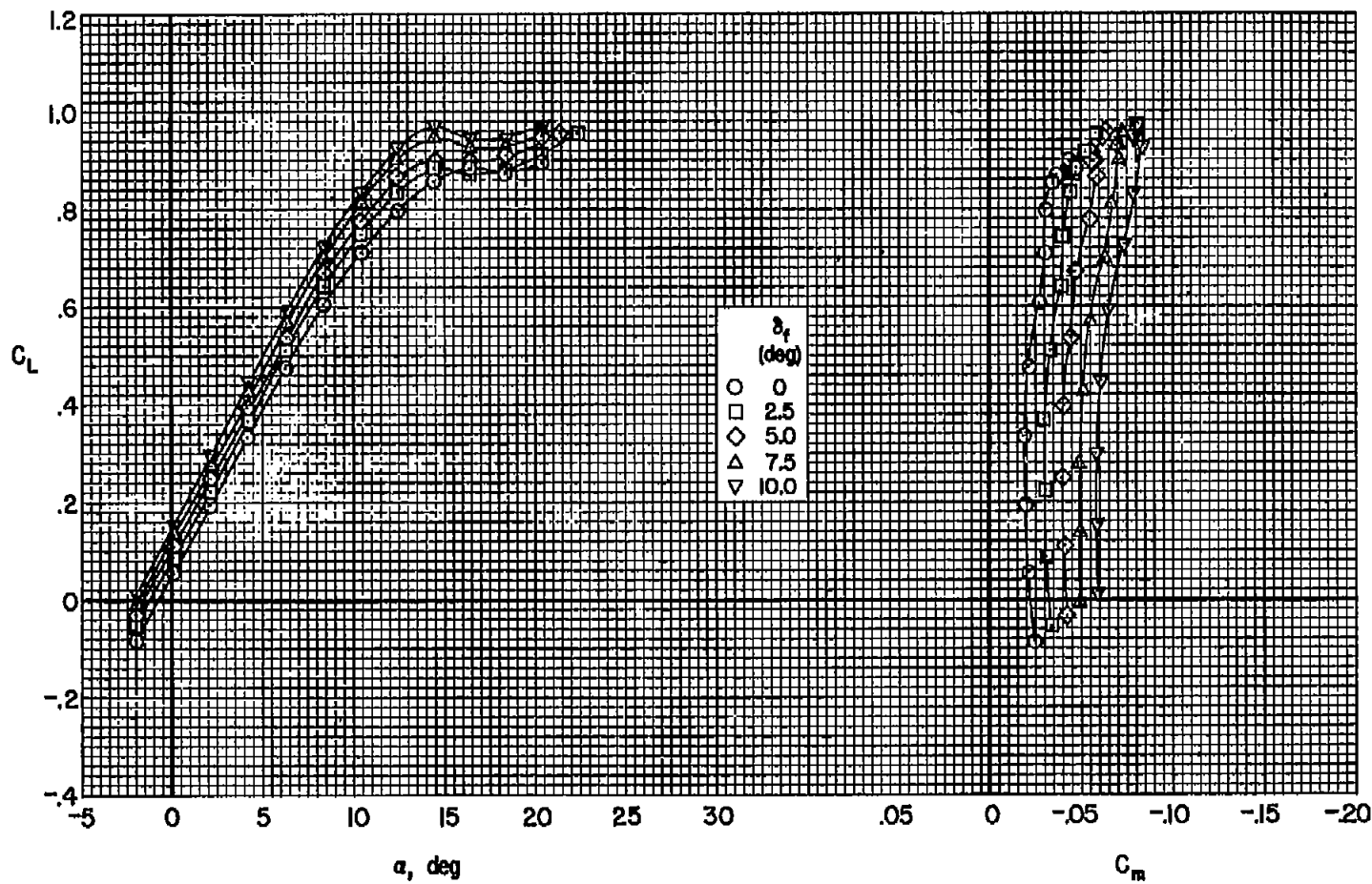
(b)  $M = 0.85, 0.90$

Figure 9.- Concluded.



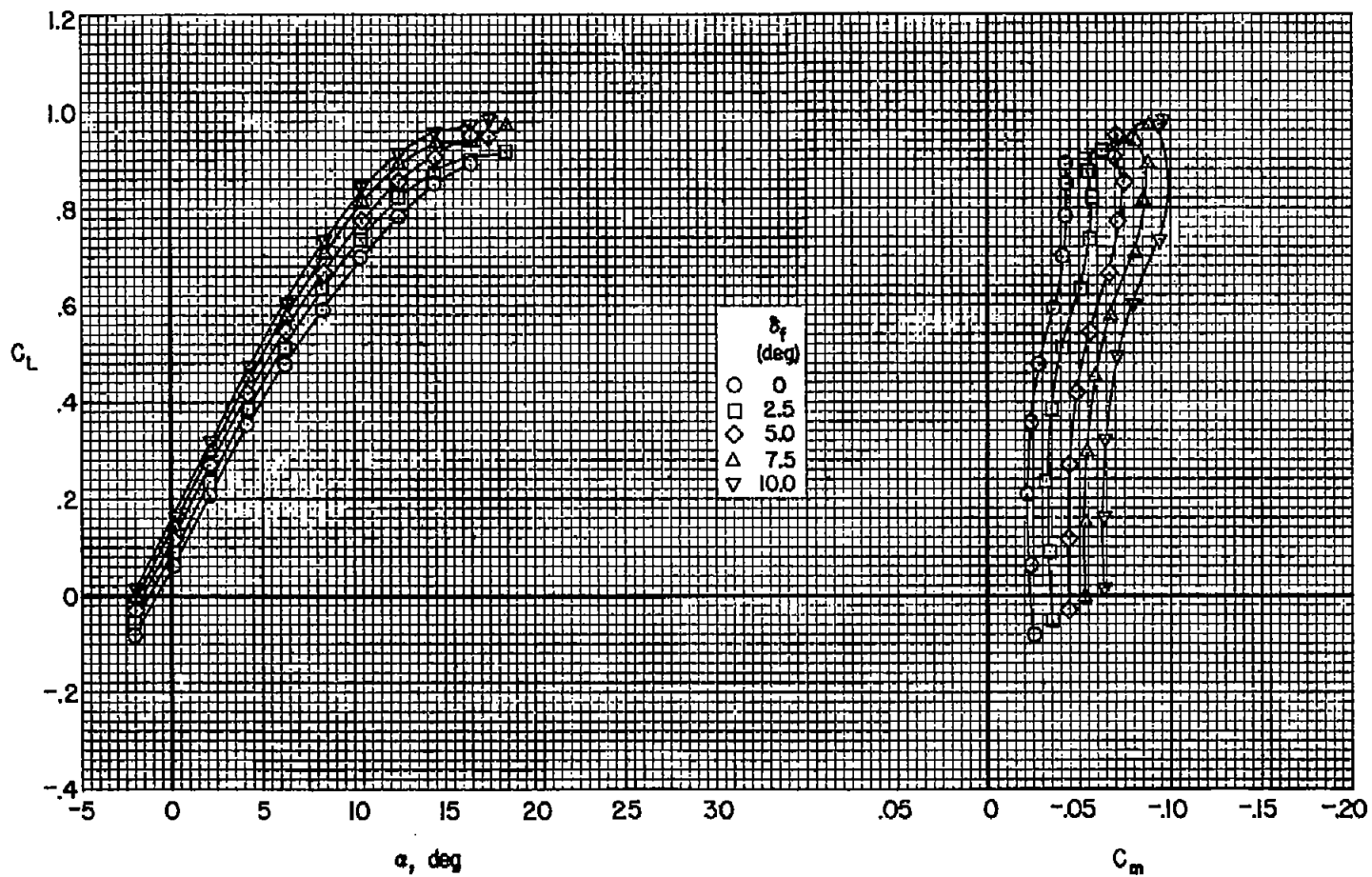
(a)  $M = 0.60$

Figure 10.- The effect of flap deflection on the lift and pitching-moment coefficients of the model;  $R \approx 3.6 \times 10^6$ ,  $\delta_B = 10^\circ$ .



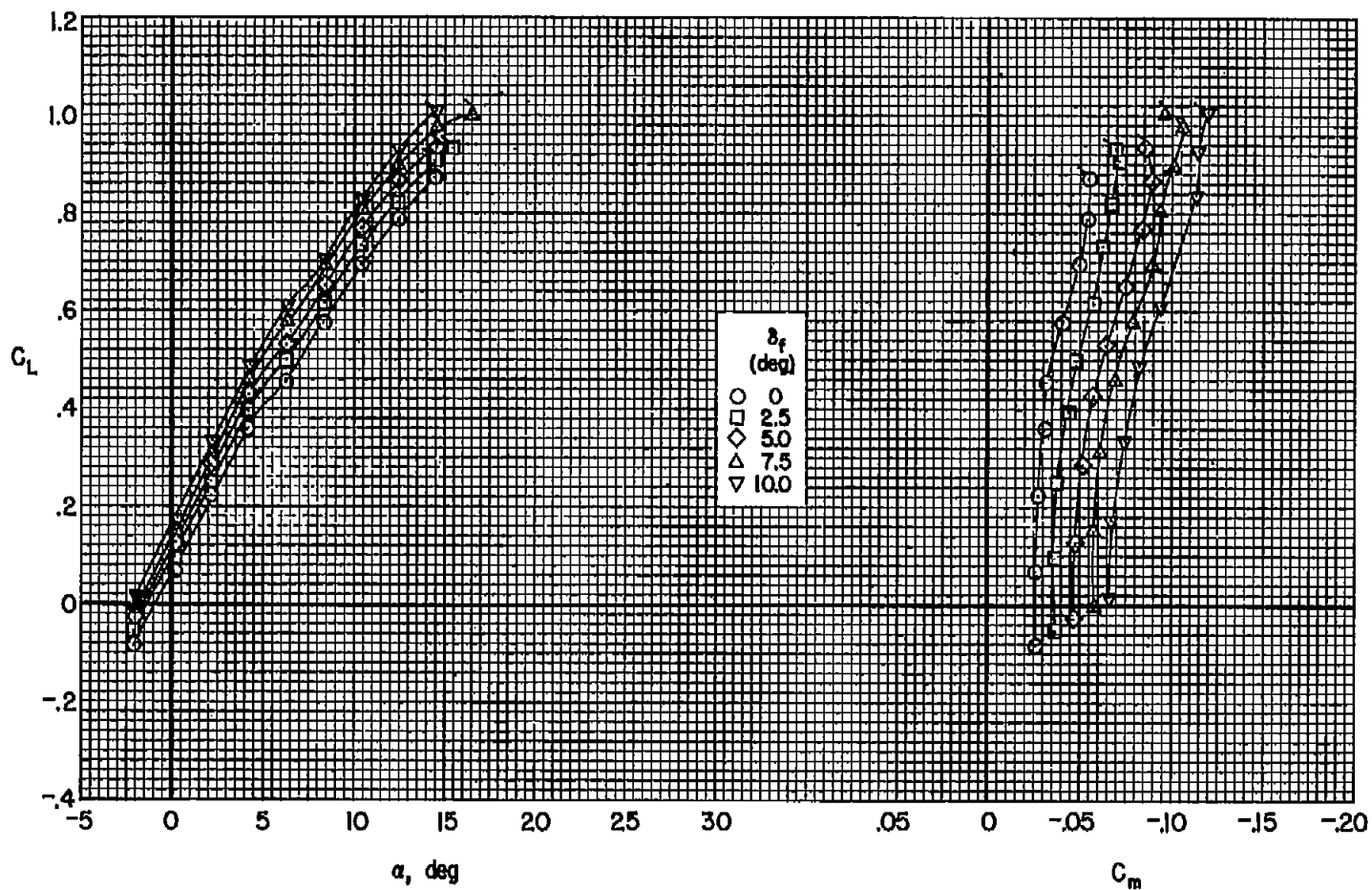
(b)  $M = 0.80$

Figure 10.- Continued.



(c)  $M = 0.85$

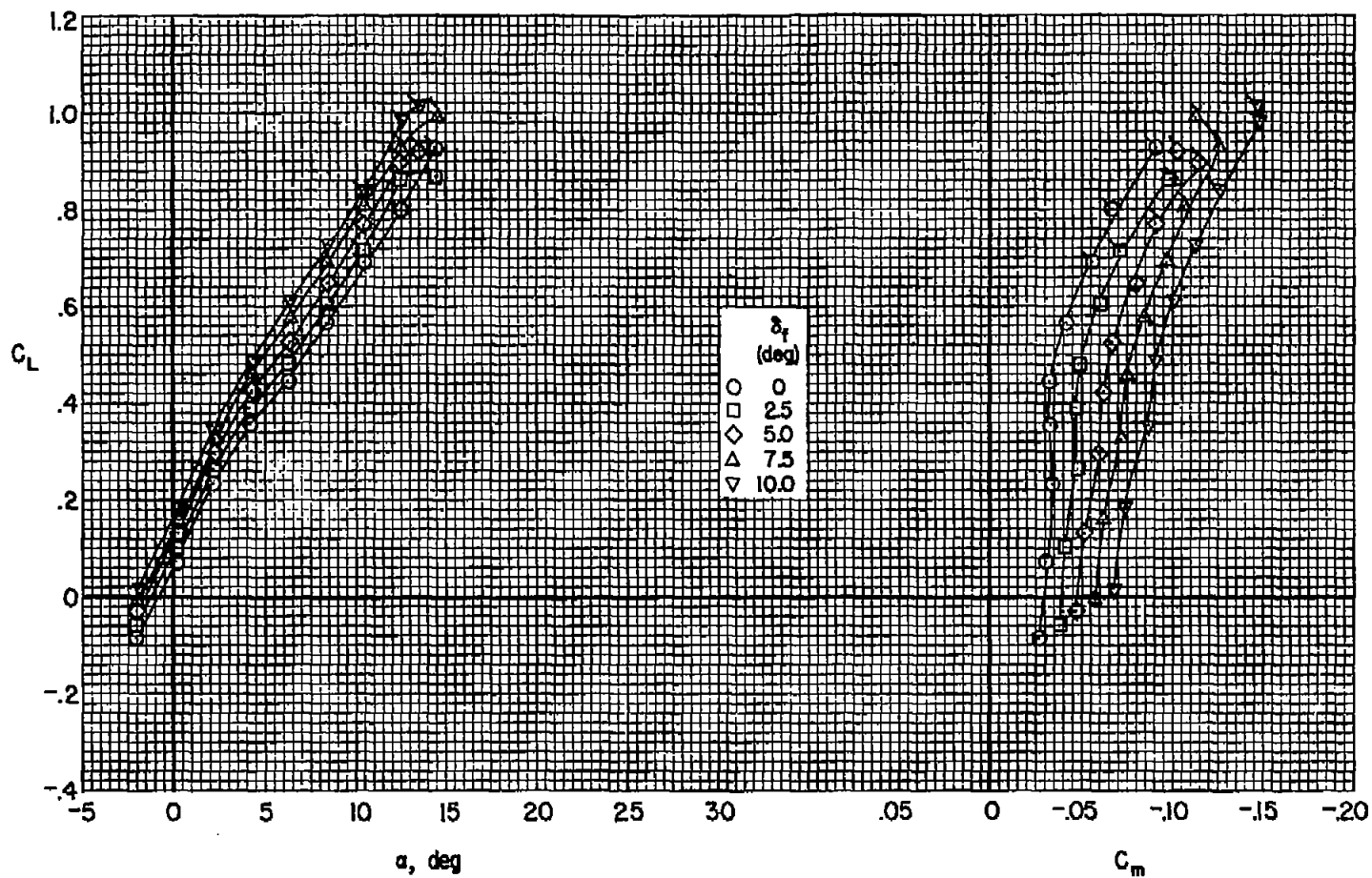
Figure 10.- Continued.



(a)  $M = 0.88$

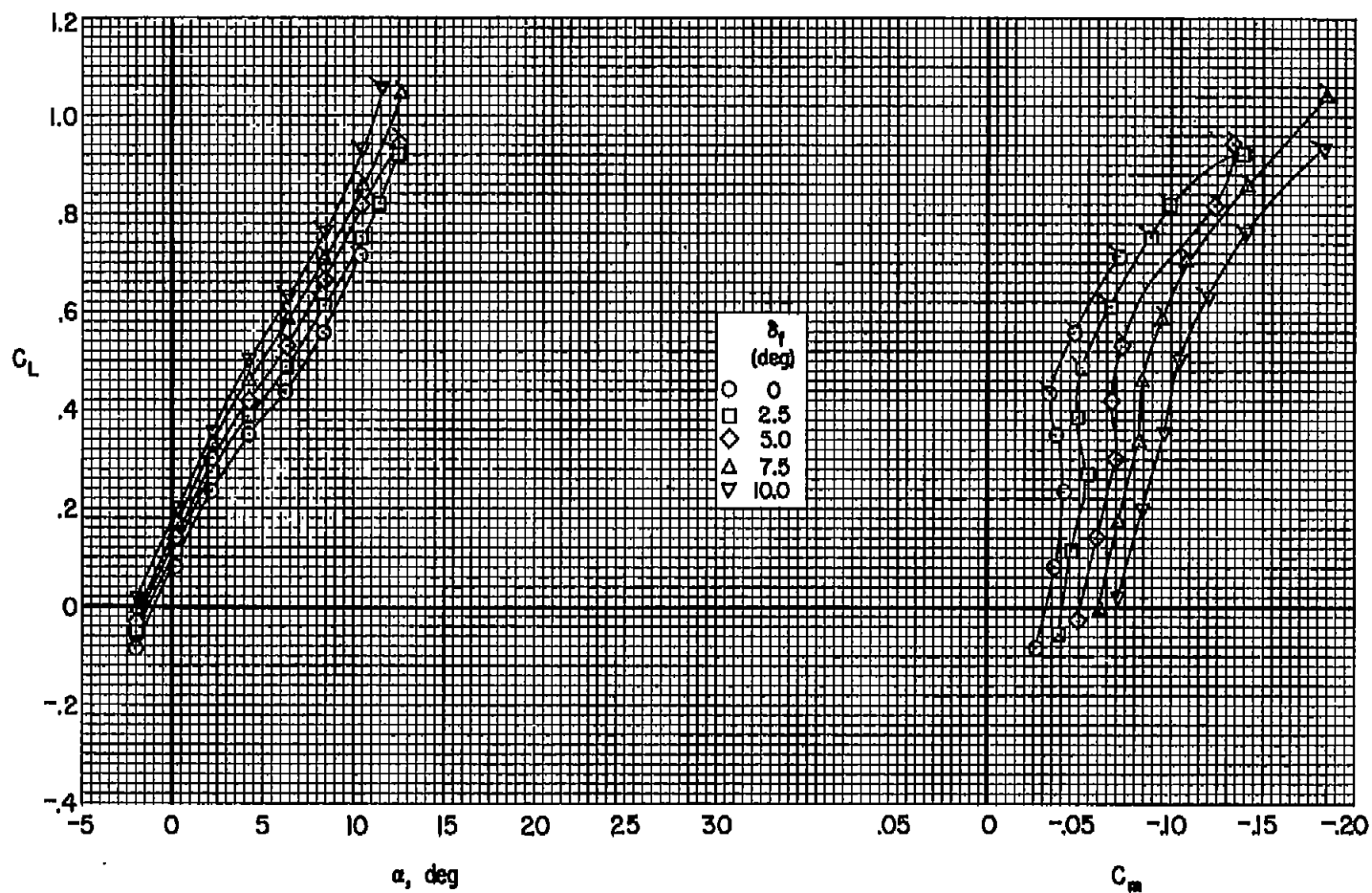
Figure 10.- Continued.





(e)  $M = 0.90$

Figure 10.- Continued.



(f)  $M = 0.92$

Figure 10.- Concluded.

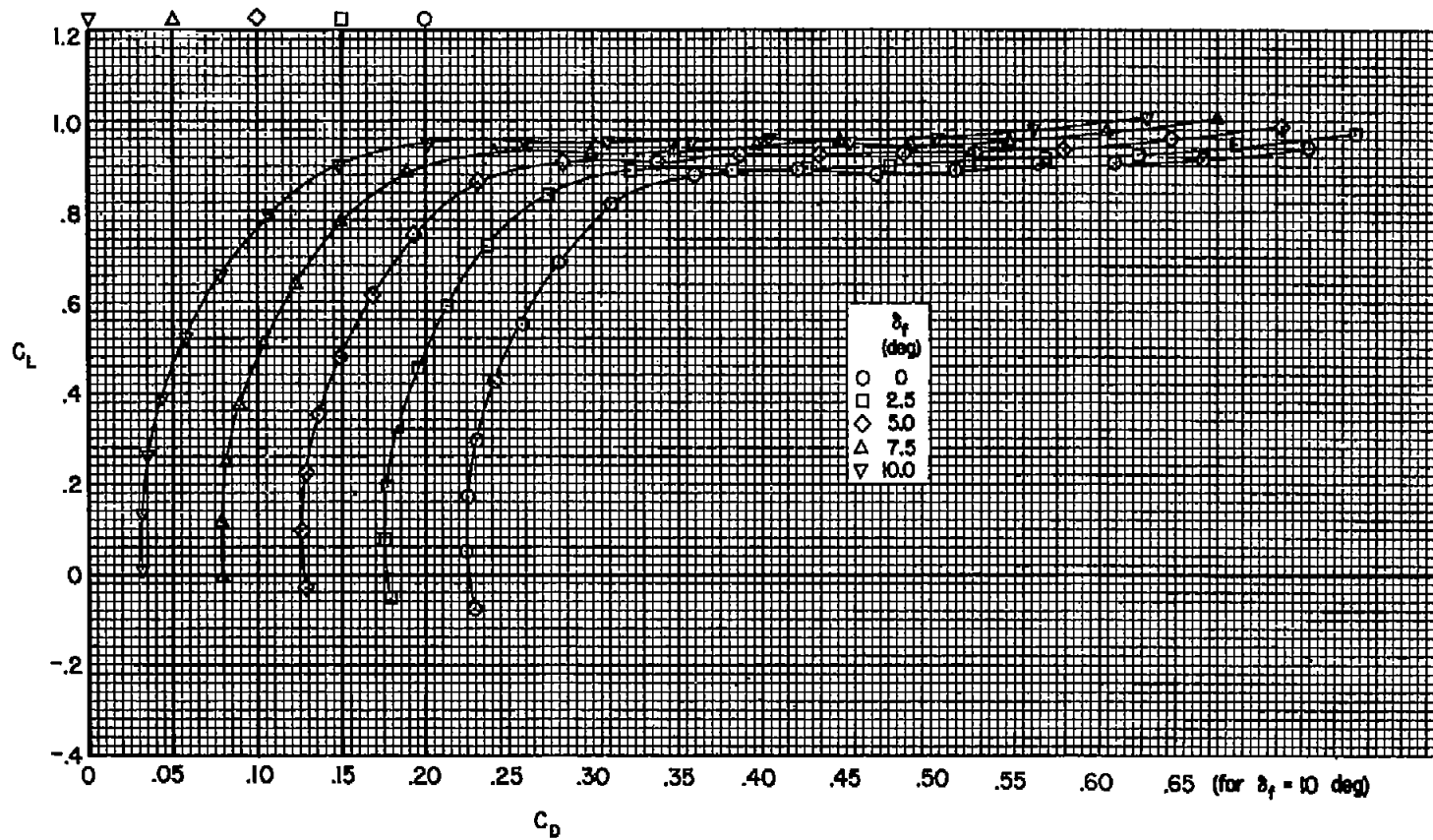
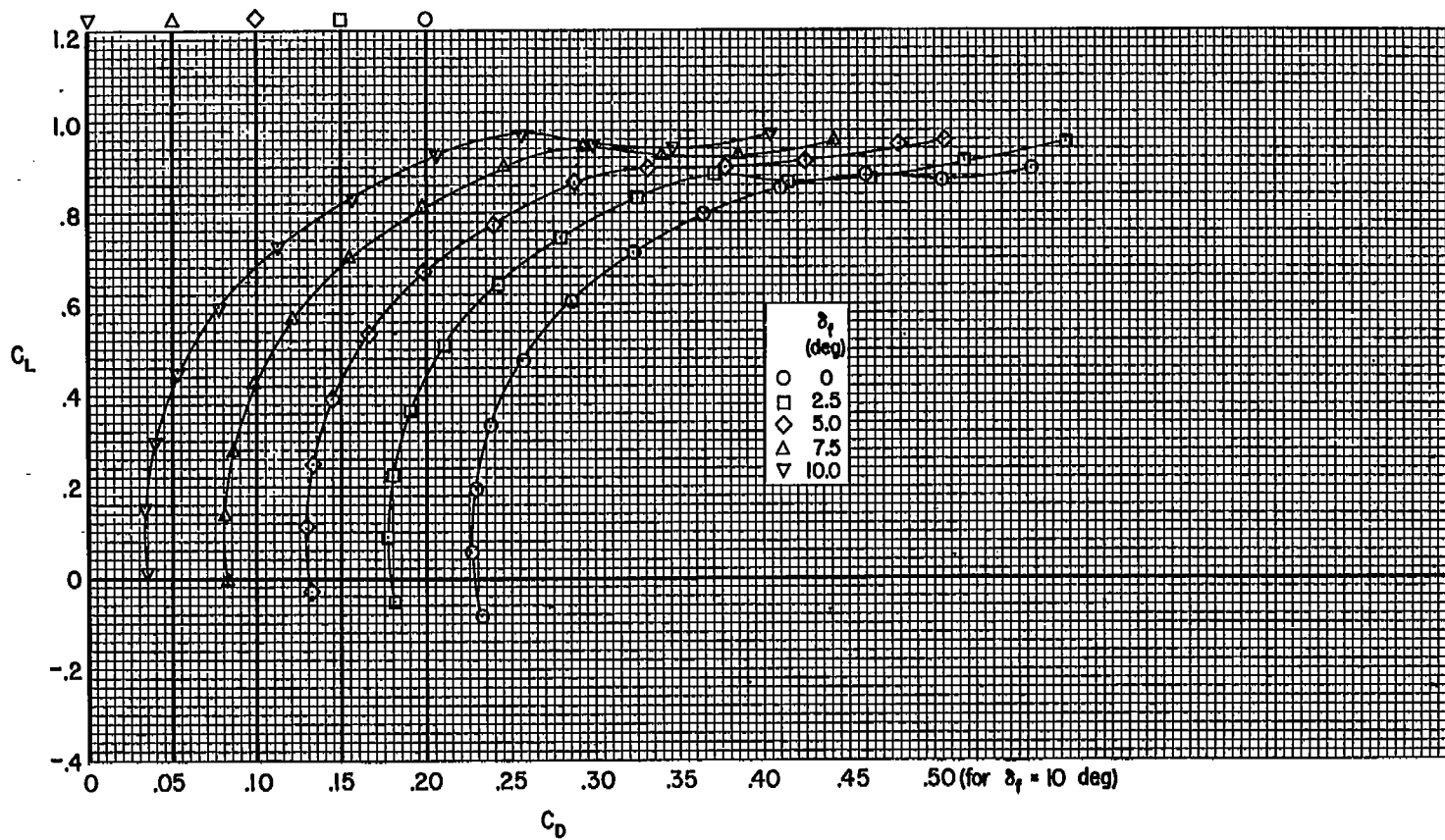
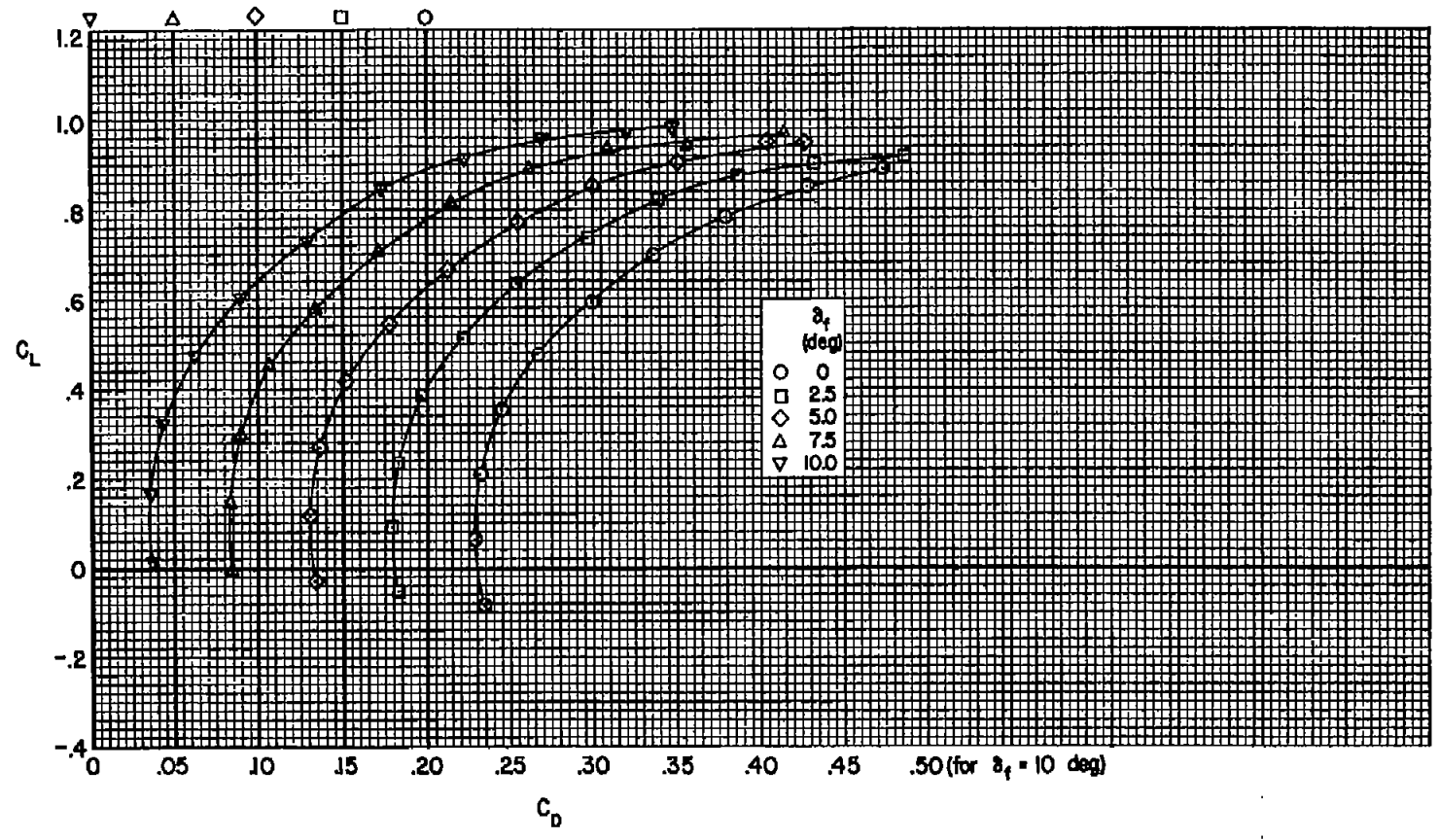
(a)  $M = 0.60$ 

Figure 11.- The effect of flap deflection on the drag coefficient of the model;  
 $R \approx 3.6 \times 10^6$ ,  $\delta_s = 10^\circ$ .



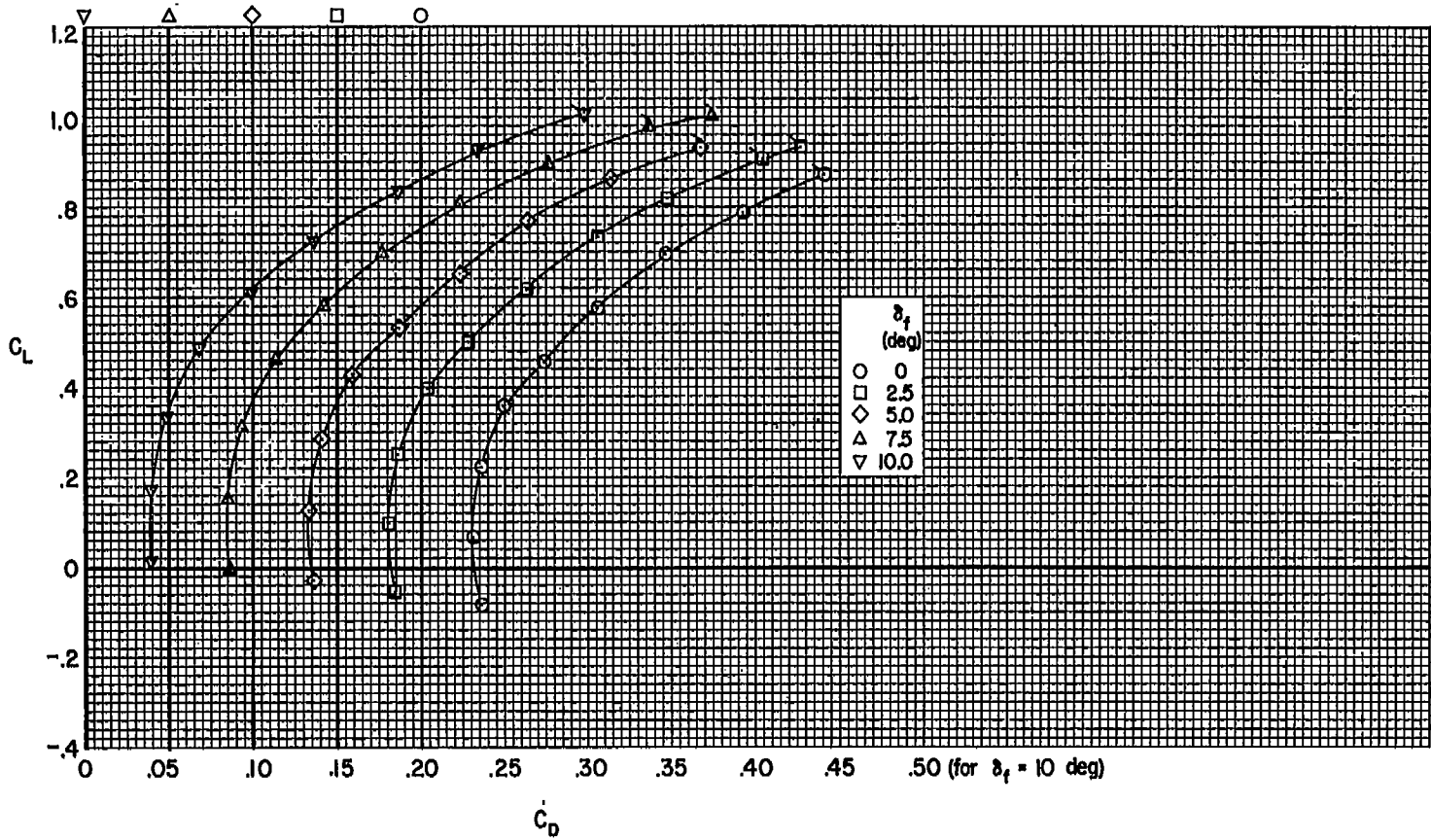
(b)  $M = 0.80$

Figure 11.- Continued.



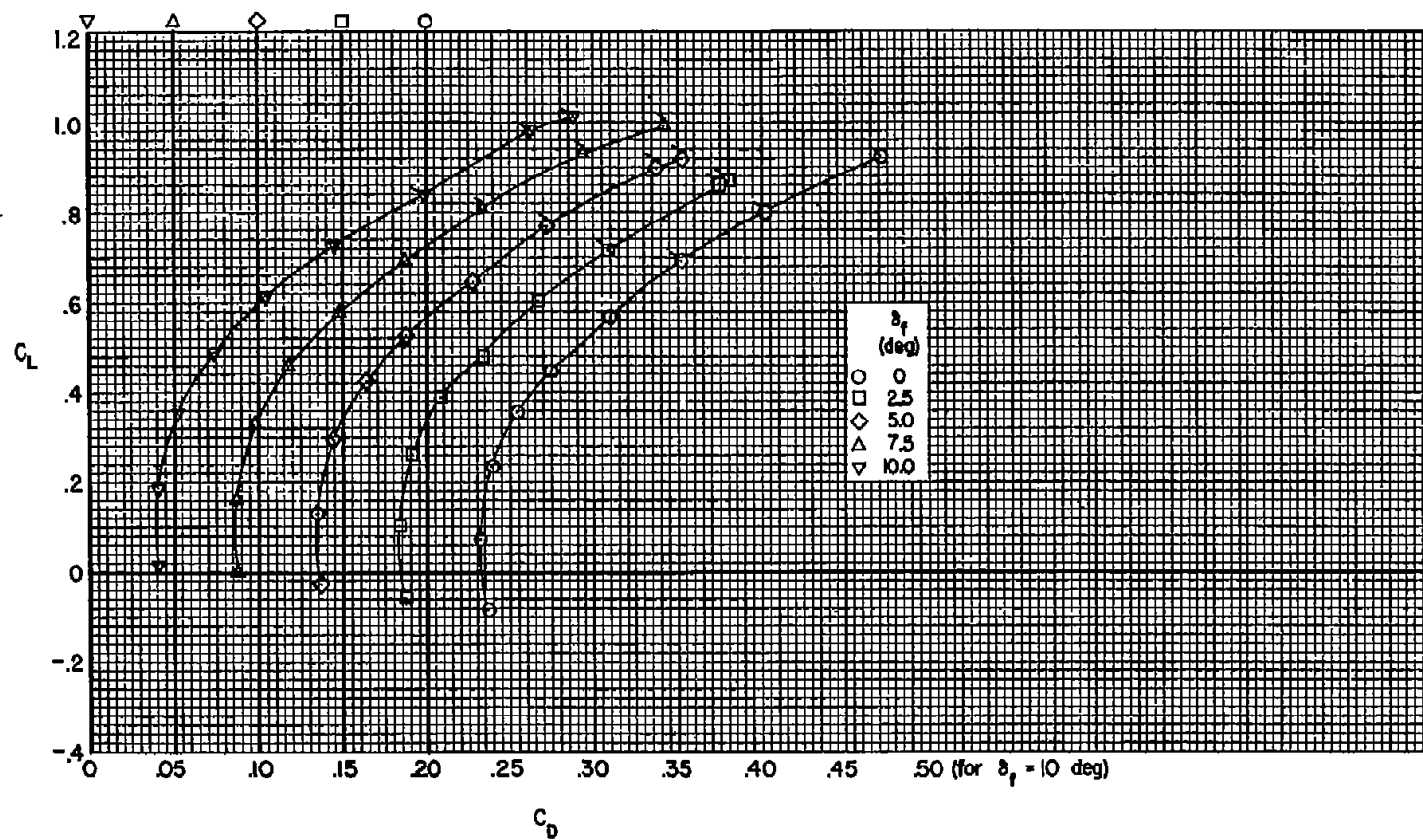
(c)  $M = 0.85$

Figure 11.- Continued.



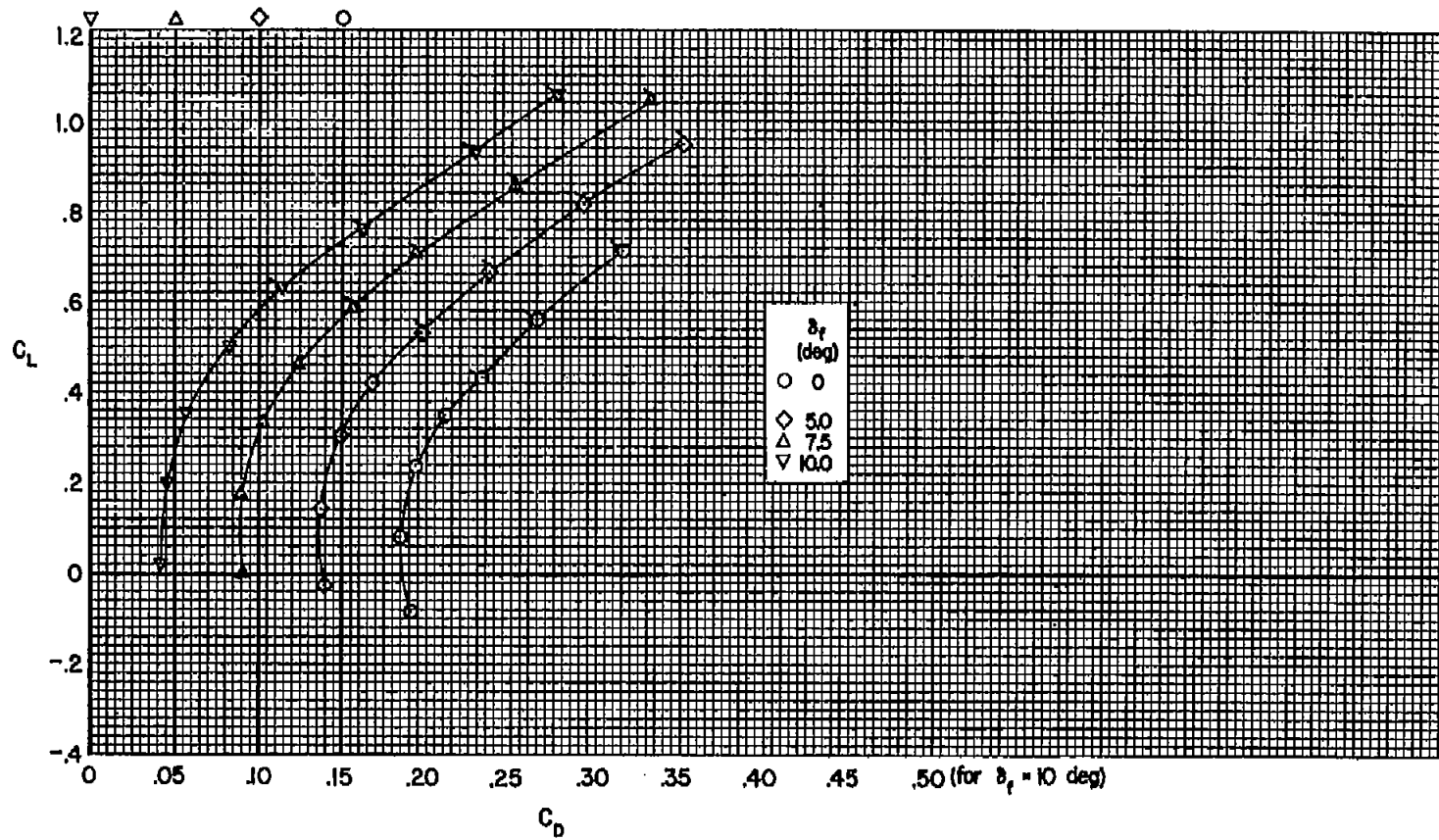
(d)  $M = 0.88$

Figure 11.- Continued.



(e)  $M = 0.90$

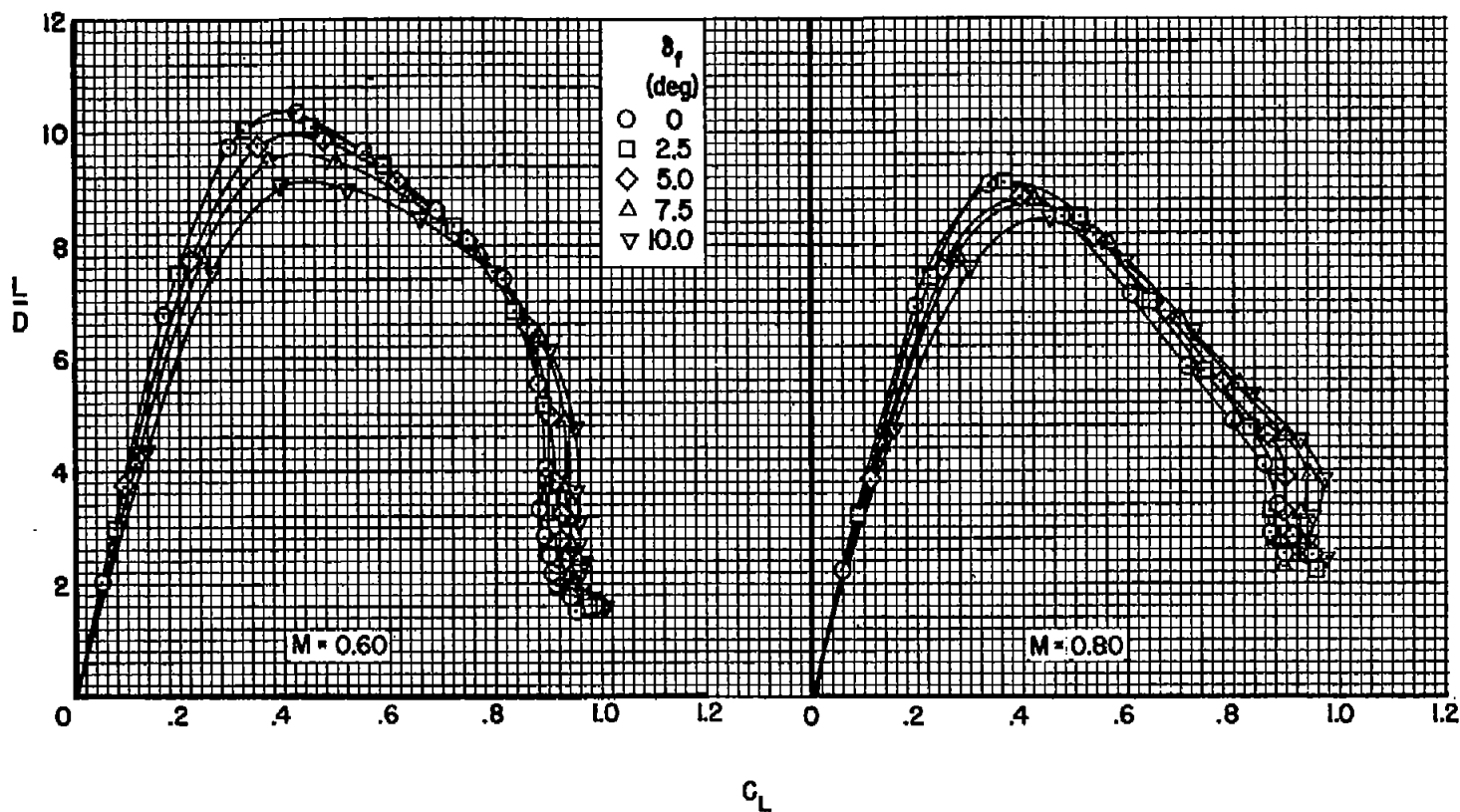
Figure 11.- Continued.



(f)  $M = 0.92$

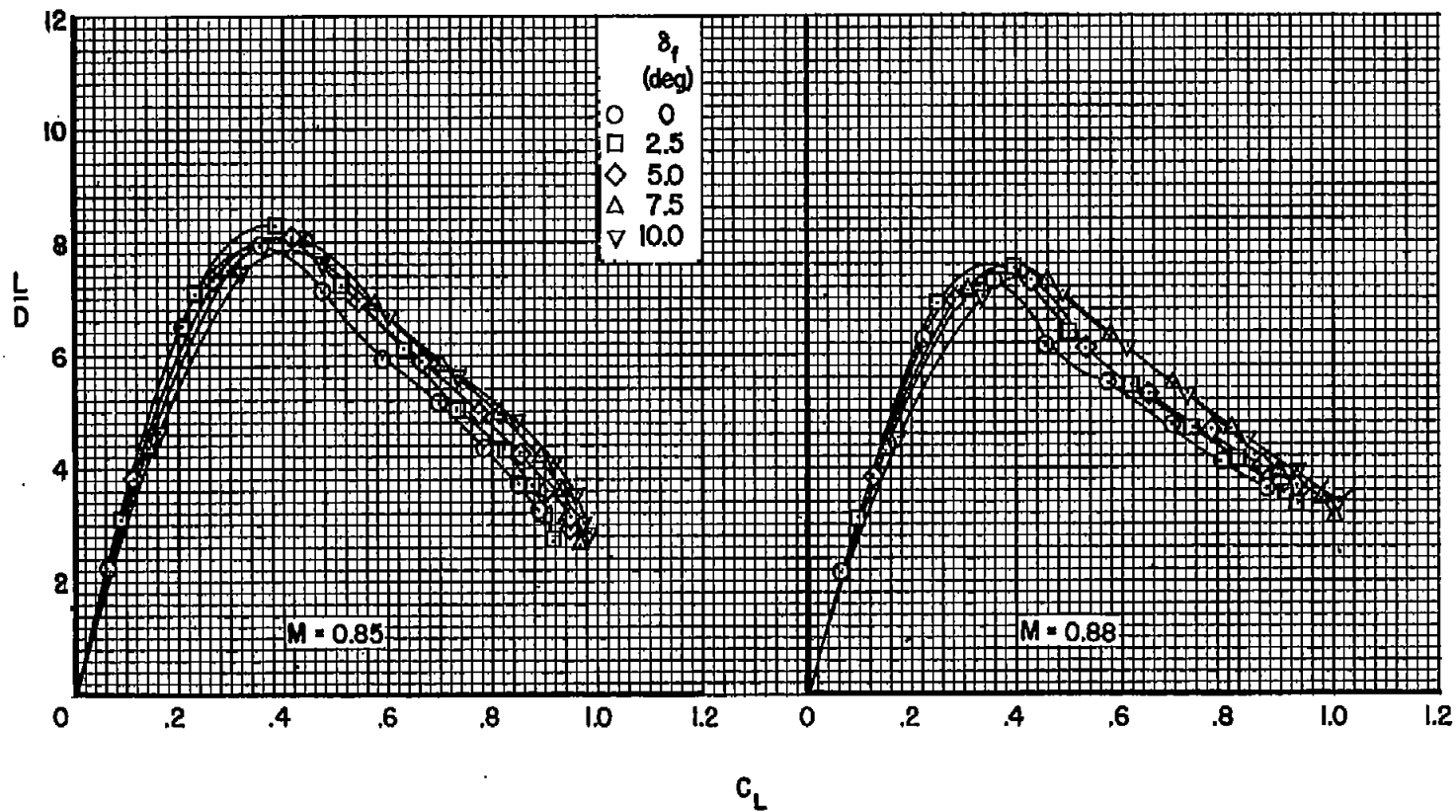
Figure 11.- Concluded.





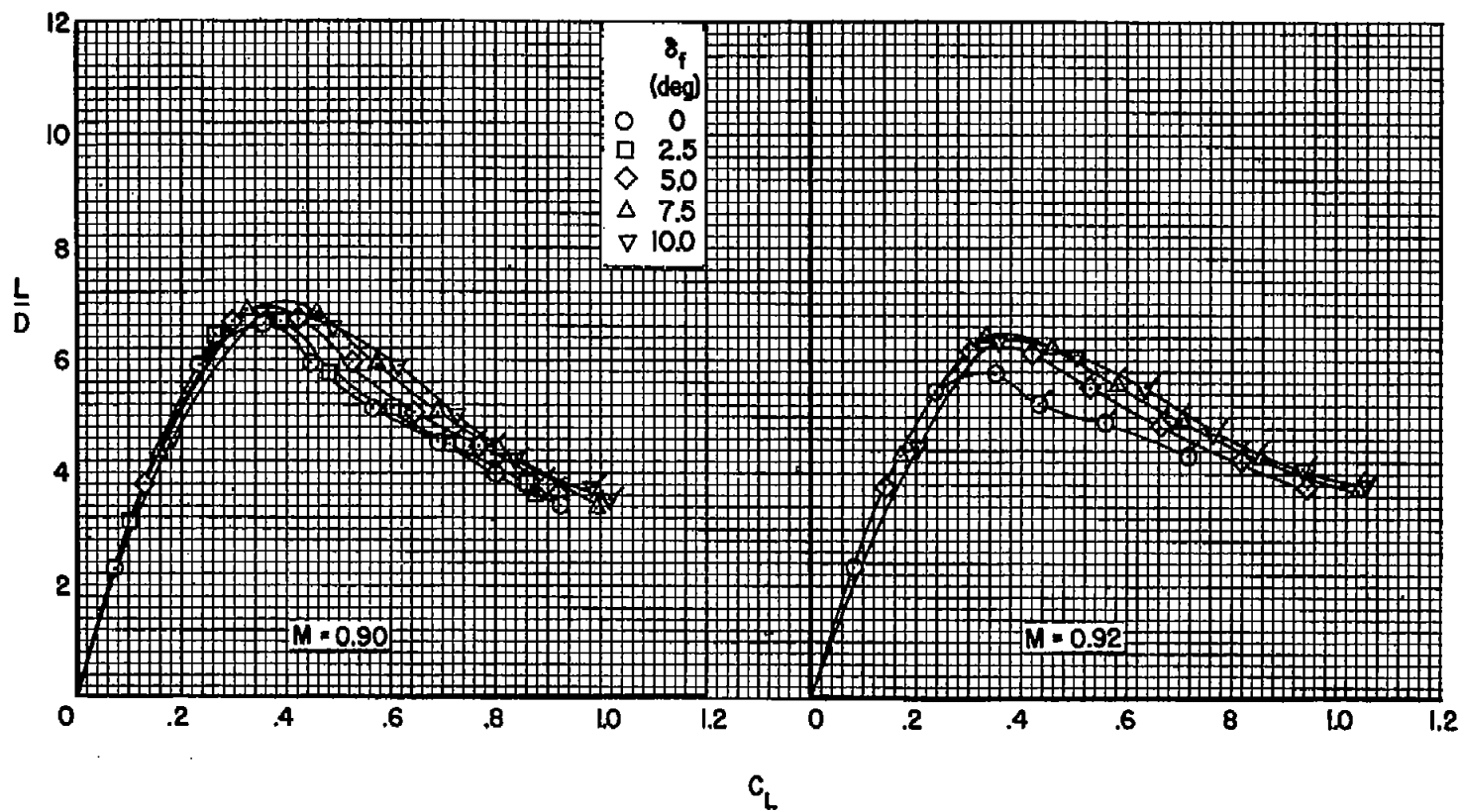
(a)  $M = 0.60, 0.80$

Figure 12.- The effect of flap deflection on the lift-drag ratio of the model;  
 $R \approx 3.6 \times 10^6$ ,  $\delta_g = 10^\circ$ .



(b)  $M = 0.85, 0.88$

Figure 12.- Continued.



(c)  $M = 0.90, 0.92$

Figure 12.- Concluded.

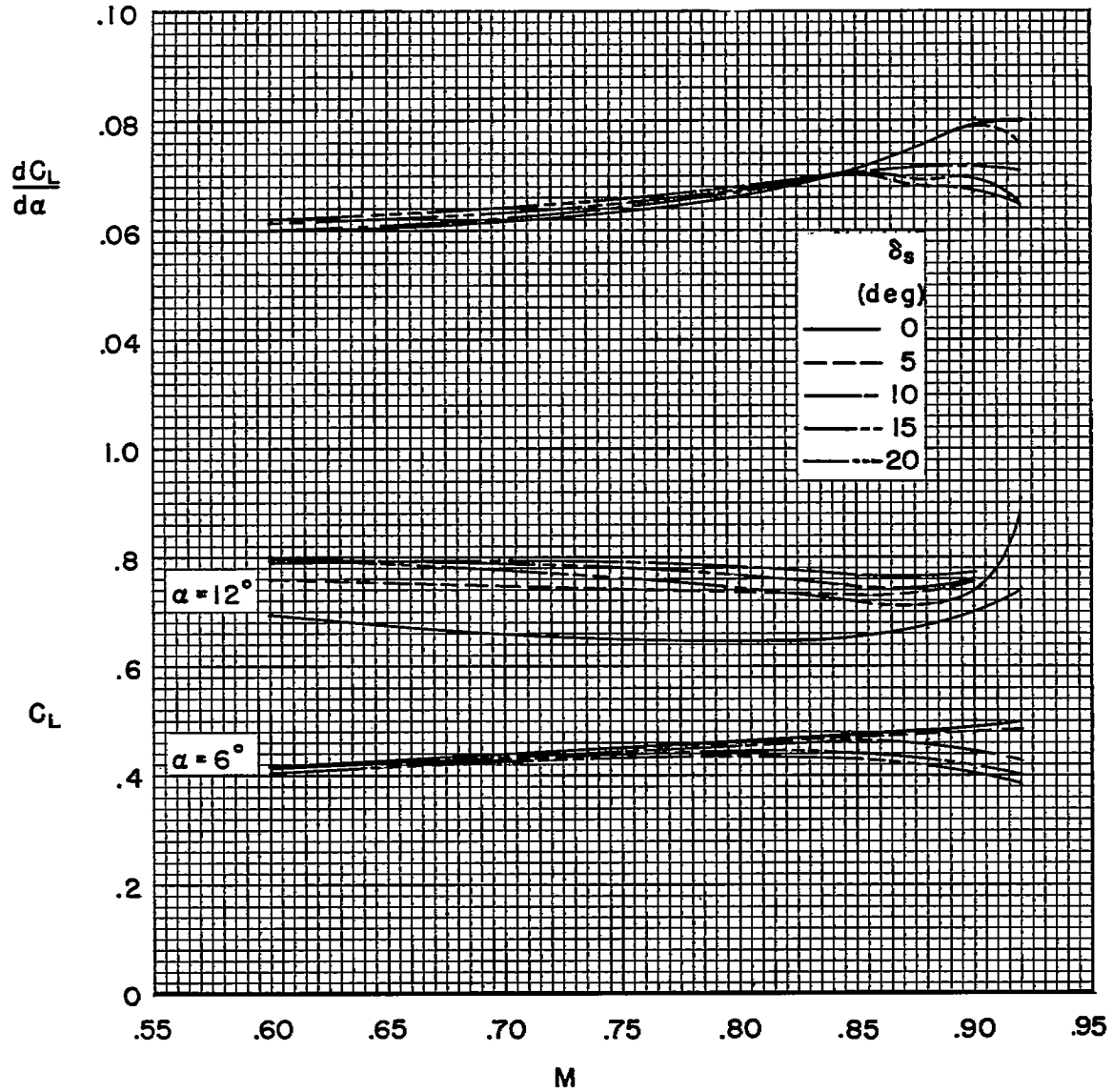


Figure 13.- The variation with Mach number of average lift-curve slope and lift coefficient for various slat deflections;  $R \approx 3.5 \times 10^6$ ,  $\delta_s = 0^\circ$ .

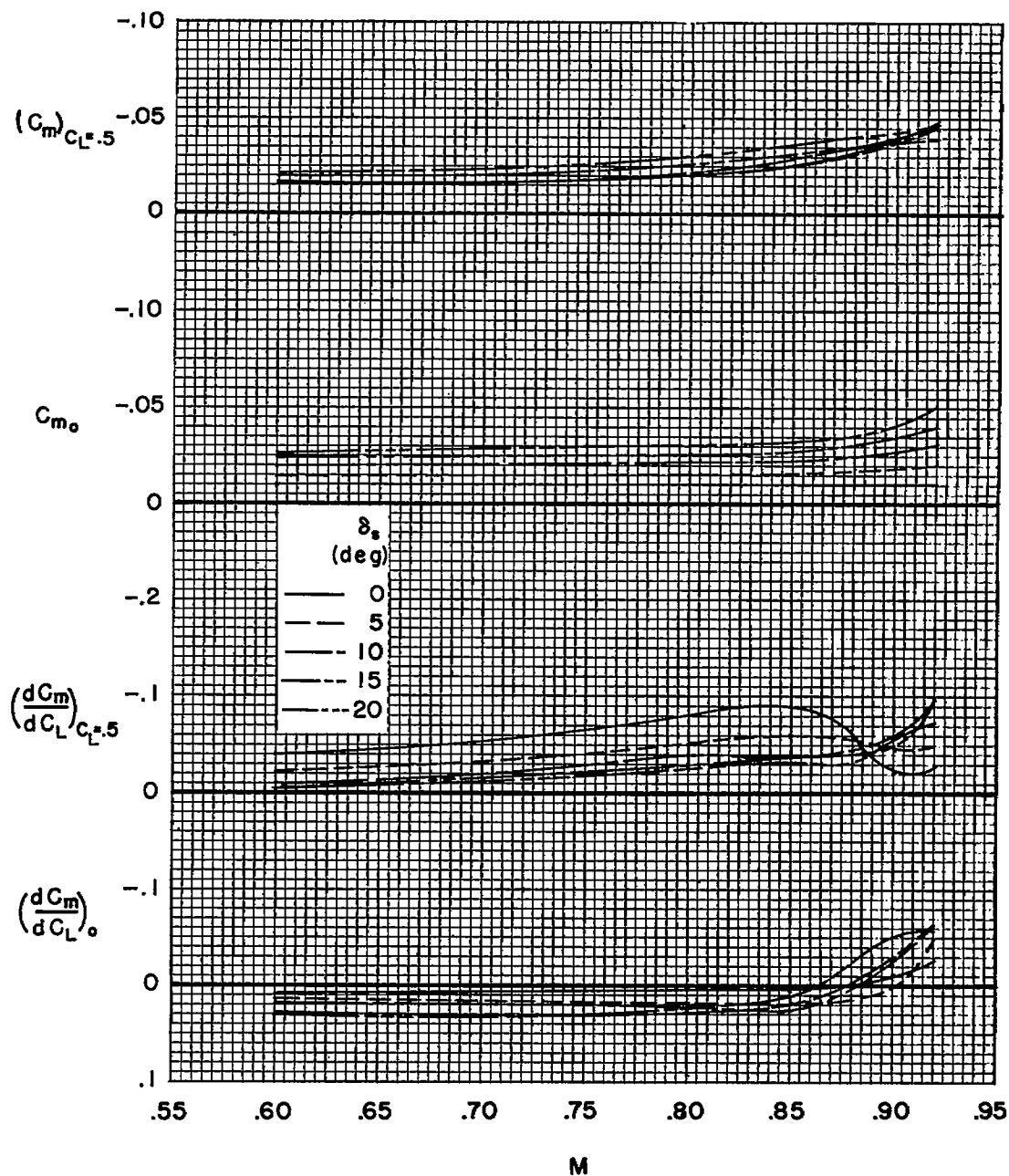


Figure 14.- The variation with Mach number of pitching-moment coefficient and pitching-moment curve slope for various slat deflections;  $R \approx 3.5 \times 10^6$ ,  $\delta_F = 0^\circ$ .

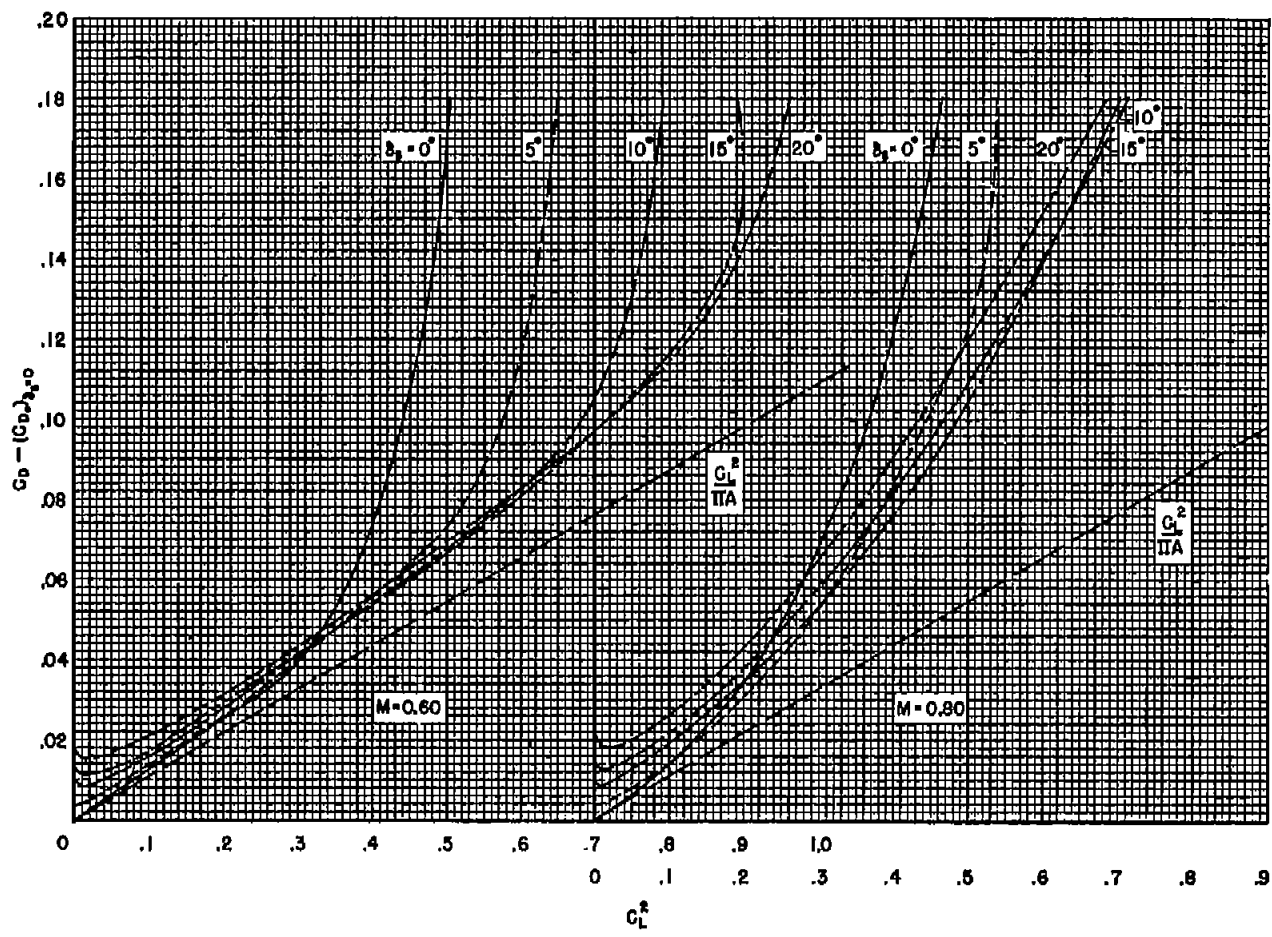


Figure 15.- The variation of  $C_D - (C_{D0})_{\delta_B=0}$  with lift coefficient squared for several slat deflections;  $R \approx 3.5 \times 10^8$ ,  $\delta_P = 0^\circ$ .

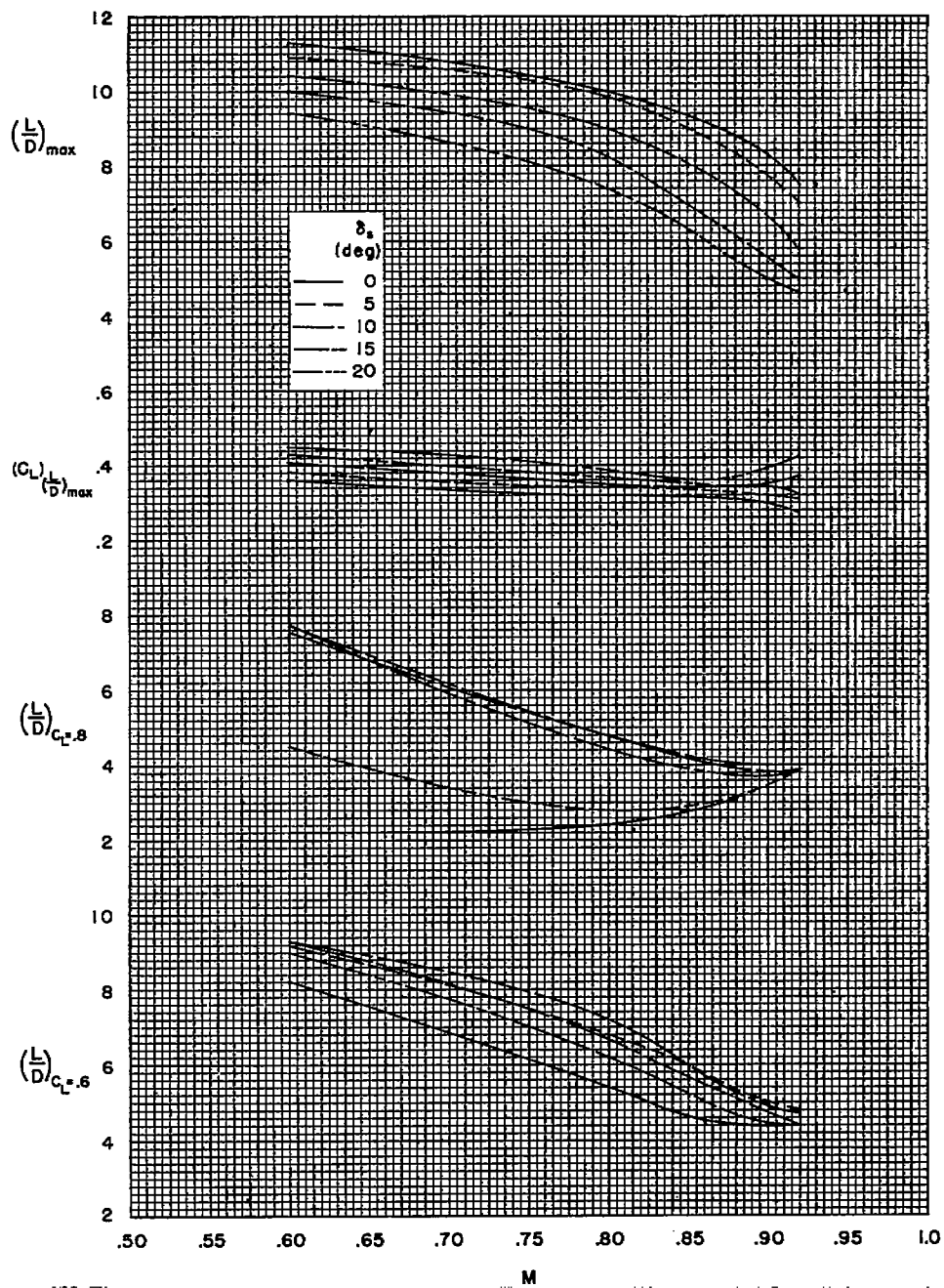


Figure 16.- The effect of Mach number on the lift-drag ratio characteristics of the model with the slat in various positions;  $R \cong 3.5 \times 10^6$ ,  $\delta_f = 0^\circ$ .

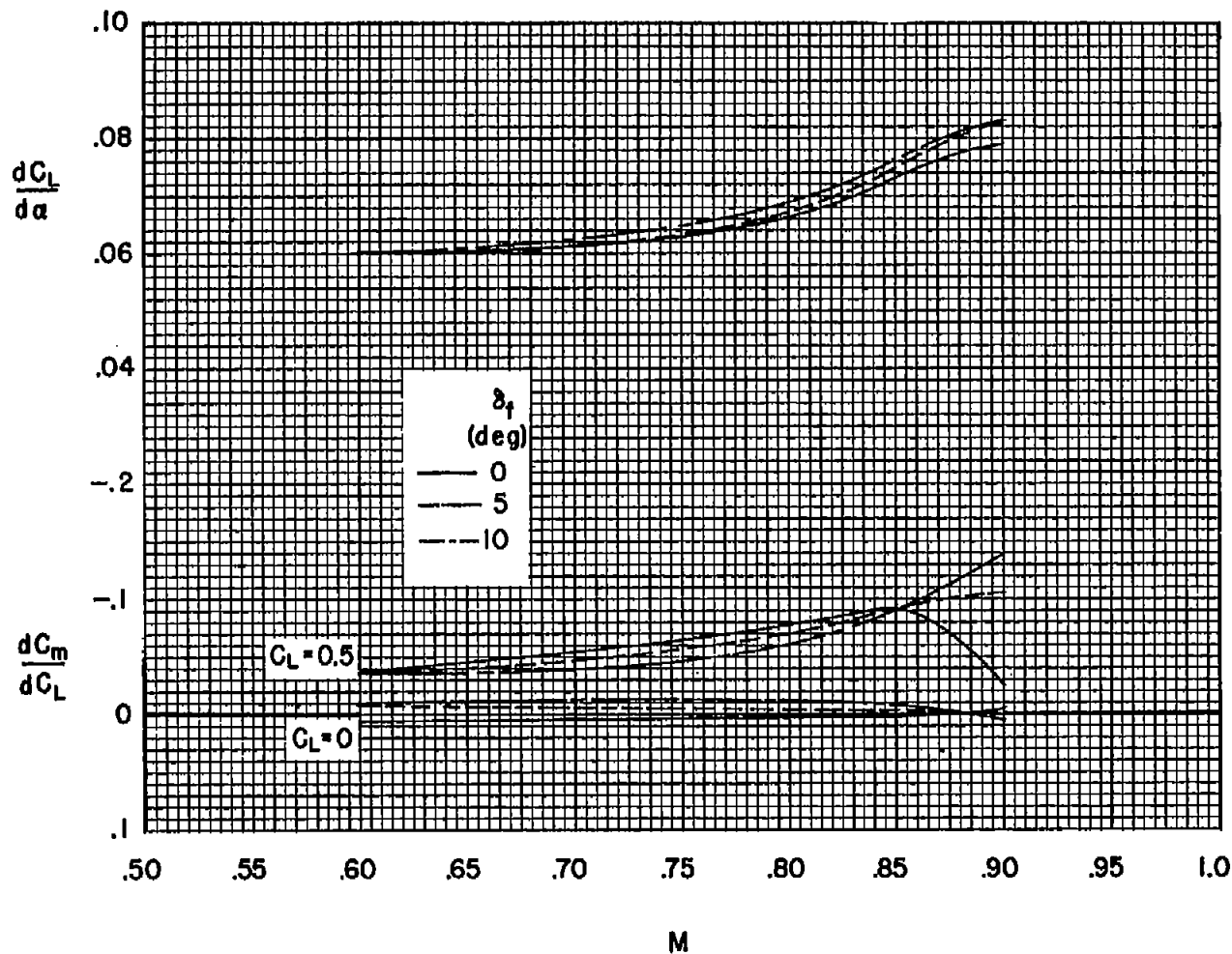


Figure 17.- The variation with Mach number of average lift-curve slope and pitching-moment curve slope for various flap deflections;  $R \approx 3.6 \times 10^6$ ,  $\delta_B = 0^\circ$ .



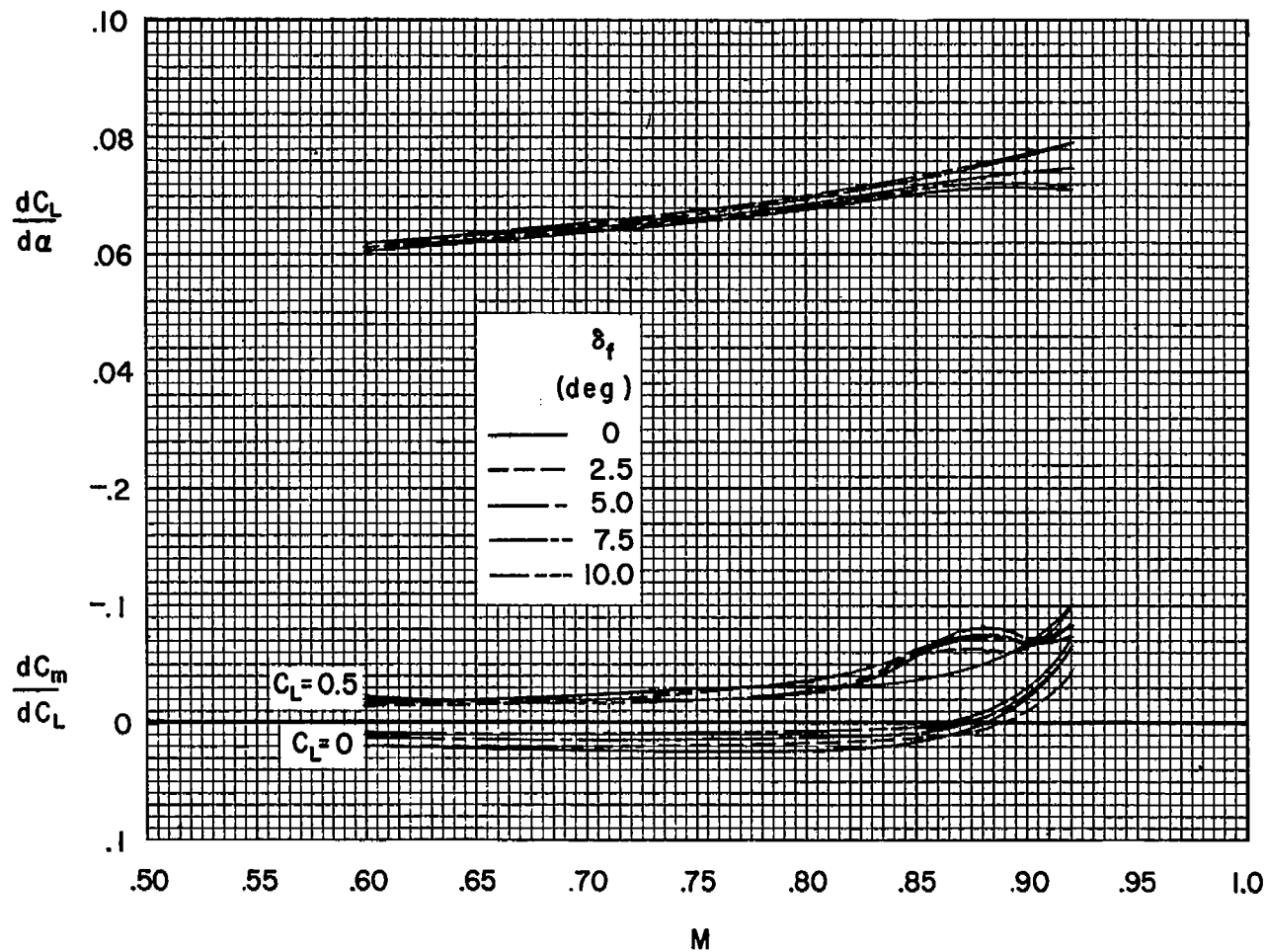


Figure 18.- The variation with Mach number of average lift-curve slope and pitching-moment curve slope for various flap deflections;  $R \approx 3.6 \times 10^6$ ,  $\delta_s = 10^\circ$ .

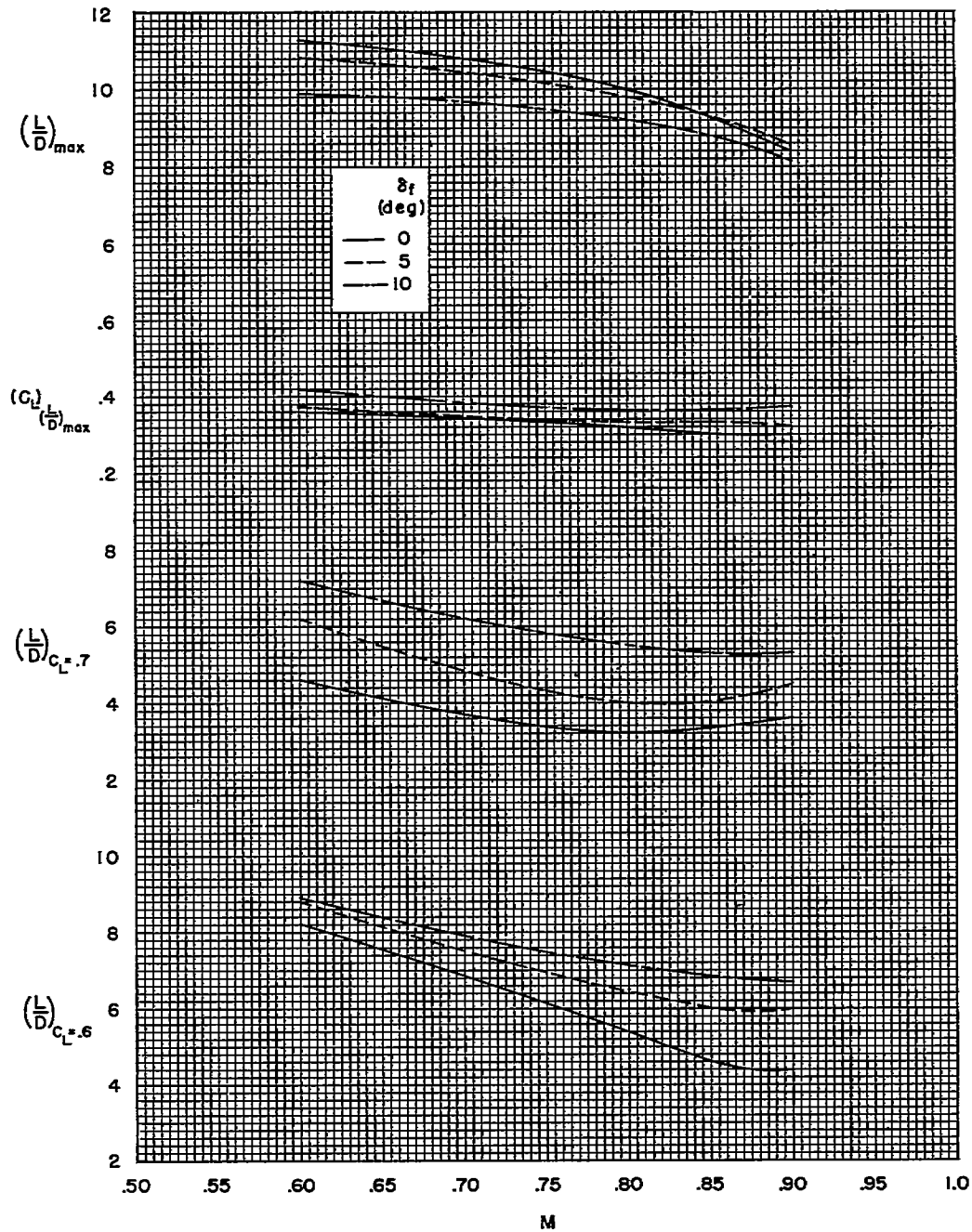


Figure 19.- The effect of Mach number on the lift-drag-ratio characteristics of the model with the flap in various positions;  $R \approx 3.6 \times 10^6$ ,  $\delta_s = 0^\circ$ .

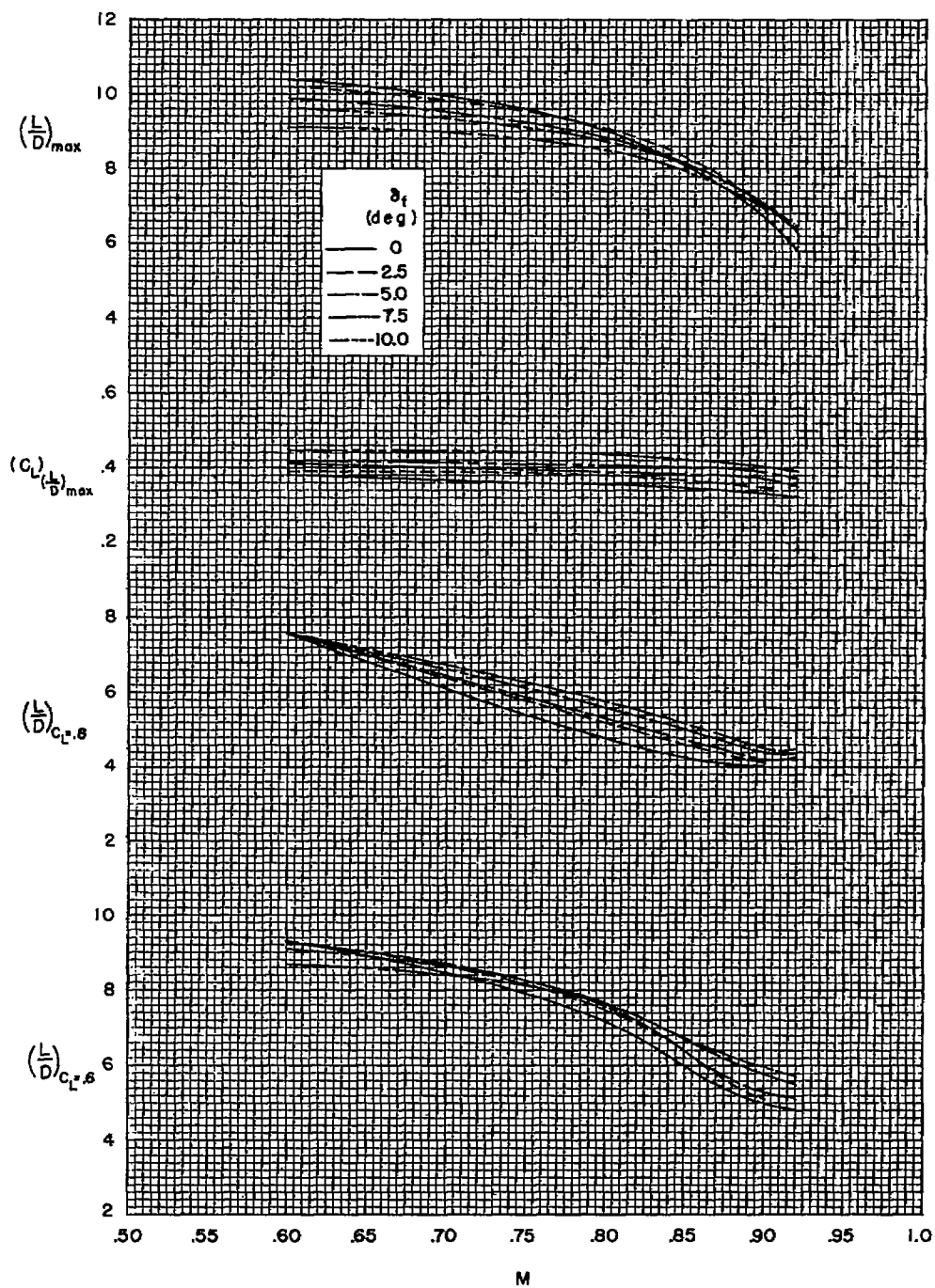


Figure 20.- The effect of Mach number on the lift-drag-ratio characteristics of the model with the flap in various positions;  $R \approx 3.6 \times 10^6$ ,  $\delta_B = 10^\circ$ .



3 1176 01434 9428

